中國醫藥大學中國醫學研究所博士論文

指 導 教 授：侯庭鏞 教 授

以新型功能性基因體平台分析中藥及其新穎致效成分在肝病效應之研究-以茵陳蒿湯為例

New functional genomics platform for analyzing the effects of Yin-Chen-Hao-Tang and its novel effective components in liver disease

研究生：李佳橙

中華民國一百零一年七月十一日

中國醫藥大學博士班研究生
論文指導教授推薦書

中醫學系博士班，李　佳　橙君所提之論文以新型功能性基因體平台分析中藥及其新穎致效成分在肝病效應之研究-以茵陳蒿湯為例（題目），係由本人指導撰述，同意提付審查。

指導教授 [signature]（簽章）

中華民國 101 年 6 月 16 日

中國醫藥大學博士班研究生

論文口試委員審定書

中醫學系博士班，李　佳　橙君所提之論文以新型功能性基因體平台分析中藥及其新穎致效成分在肝病效應之研究-以茵陳蒿湯為例(題目)，經本委員會審議，認為符合博士資格標準。

論文口試委員會　　委員 ________（簽章）

主任 ________

中華民國 101 年 6 月 26 日

目錄

圖目錄

表目錄

以新型功能性基因體平台分析中藥及其新穎致效成分在肝病效應之研究-以茵陳蒿湯為例

中國醫藥大學 中國醫學研究所

指導教授：侯庭鏞

學生：李佳橙

肝病在全世界已成為健康與醫療重要的問題之一，慢性肝病是典型的肝組織受到傷害造成持續性發炎。而 NF-κB 活性又與發炎反應息息相關。因此，我們構築 NF-κB 基因轉殖鼠，以四氯化碳誘發慢性肝炎建構一個即時性活體影像的疾病動物模式。並以 H&E、天狼星紅及免疫組織化學染色觀察肝組織病變。隨後利用 microarray 分析藥物作用機轉。前趨測試以 silymarin 進行治療，活體影像顯示 silymarin 下降肝臟 NF-κB 活性。利用 H&E 及天狼星染色可觀察到 silymarin 明顯改善肝組織傷害及纖維化程度。microarray 分析發現 silymarin 可透過調控粒線體電子傳遞鏈變化進而改善肝纖維化。證實此疾病動物模式及實驗平台可行後，我們分別驗證茵陳蒿湯及其單味藥在肝纖維化的效應。茵陳蒿湯是中醫及漢方醫學經常用來治療肝炎的方劑，茵陳蒿湯組成單味藥為茵陳蒿、梔子、大黃三種。從研究中也顯示，梔子調控活體影像肝臟的 NF-κB 活性或是組織切片染色 H&E 的細胞完整度上來看都有很明顯的效果，另外利用天狼星紅染色觀察肝纖維化程度，在梔子組與 CCl_4 組比較也有很明顯的勝出，而且梔子活性成份 genipin 在相同模式下，以 10 mg/kg 劑量連續投予 4 週後在抗肝臟發炎及纖維化也有明顯的改善。進一步為了探討 genepin 在體內抗發炎的機轉，我們利用 LPS 當作誘發劑，透過細胞模式、即時性活體冷光照影、組織切片化學染色和 microarray 分析，發現 genipin 透過下調 chemokine ligand，chemokine receptor 及

IFN-induced protein productions 的新穎機制抑制發炎。這些結果表明，新型的功能性基因平台可以即時性及有效率的分析茵陳蒿湯在肝病效應，並且推導出其中一個有效成份 genipin 可用來治療肝炎及全身炎症反應的候選藥物。

第一章 前言

1.1 研究動機

慢性肝炎在東方或西方國家人民健康與醫療問題上佔有相當大的比例，慢性肝病是典型的重複肝細胞傷害造成持續性發炎 (1) 。慢性肝炎可能由 hepatotropic 病毒的慢性病毒感染 (主要為 B 型和 C 型肝炎病毒) 、自體免疫、代謝性疾病、毒性物質或者藥物所引起。而這些各種因素造成的肝組織發炎最終會造會肝臟纖維化的病理現象(2-5) 。而發炎反應是由各種 cytokines 所調控，例如 interleukin-1β (IL1β) ，Tumor necrosis factor-α (TNF-α)和 Interferon-γ (IFN-γ) 等。進一步，cytokine 的生合成是由轉錄因子 NFκB 所控制的 (6)。NF-κB 最早是由 Baltimore 於 1986 年發現，NF-κB 是由 p50、p52、p65 (Rel A) 、Rel B 及 c-Rel 組成的雙倍體轉錄因子 (7) 。NF-κB 為誘發型的轉錄因子，在發炎反應、免疫反應、腫瘤細胞惡化中扮演重要角色。在正常情況下，NF-κB 與其抑制蛋白質 IκB 結合而存在於細胞質當中，但是如果細胞受到傷害，IKK 會將 IκB 磷酸化，接下來 β-TrCP 與磷酸化的 IκB 結合，將其送到 26S proteosome 分解，IκB 與 NF-κB 解離之後，使 NF-κB 次單位 p50 及 p65 蛋白質的 nuclear localization signals 暴露出來，而使得 p50/p65 heterodimer 送到細胞核內。活化態的 heterodimer 會進一步與基因啟動子上的特定序列結合，而導致下游基因的表現 (8, 9) 。此外，控制 NF-κB 的活化已成為藥物的目標，特別是在慢性炎症性疾病 (10) 。

1.2 研究目的

中醫藥在肝病治療上有很長的一個歷史,最早記載於《黃帝內經》,這也暗示著中醫藥於西元前 475 年已經開始用於治療慢性肝病 (11) 。而現今在慢性肝病方面,目前臨床試驗比較缺乏的部份在於中草藥的標準化、試驗者的隨機化,安慰劑控制組的問題。雖然有些中草藥萃取物具有會造成胃腸道或肝膽上異常病變的有害肝毒素生物鹼 (12) 。然而,其中有一些萃取物的化合物,像是常見的黃酮類已經被證實且有抗氧化、抗纖維化、抗病毒或者抗腫瘤等效益,包括 glycyrrhizin (licorice root) 、phyllanthin (*Phyllanthus amarus*) 、silymarin (milk thistle) 、picroside (*Picrorhiza kurroa*) 和 baicalein (*Scutellaria baicalnsis*) ,這些主要化合物可以提供於未來作為開發預防或治療慢性肝病的藥物 (13-16) 。因此本研究中,我們首先構築會受到 NF-κB 調控的冷光基因轉殖小鼠,以茵陳蒿湯為主要對象,以 NF-κB 基因轉殖鼠配合四氯化碳誘發慢性肝炎,以即時性分子影像及 microarray 為分析工具,配合組織染色切片、專一性纖維化蛋白染色,先驗證茵陳蒿湯治療肝炎的效果,進一步從茵陳蒿湯拆解成單一中藥探討主要的療效藥物,並從該單味藥中找到肝炎的致效成份。未來我們希望,以中醫藥為治療藥物的基礎,在肝炎治療上尋找更有效的中醫藥標靶藥物。

第二章 文獻探討

2.1 肝炎之病因與機轉

肝炎一直是亞洲人罹患以及造成死亡率居高不下的主要疾病。肝炎主要是因為肝臟細胞受到發炎細胞的浸潤，而導致肝細胞損傷的一種疾病。導致肝炎的發生有幾種不同原因，包括病毒、自體免疫、藥物、酒精、毒性物質、寄生蟲及代謝疾病等。其中主要以病毒、藥物及酒精所引起的肝炎最為常見(17-22)。

病毒性肝炎一直是台灣人肝炎最常見的病因，病毒目前已發現的分型包括 A、B、C、D、E 及 G 型，並有各自的傳播途徑及發病機轉。其中又以 B 型肝炎所佔比例最多。B 型肝炎病毒為局部雙股 DNA 病毒，有外套殼、內核殼核心，屬於 hepadnavirus。傳染途徑主要是經由血液或垂直感染。病毒含有四段相互重疊的基因：S、C、P、X，其中 S 基因轉錄轉譯成 HBsAg 為病毒的包膜蛋白，C 基因轉錄轉譯成 HBcAg 和 HBeAg 為病毒的核蛋白，P 基因轉錄成 Polymerase，X 基因轉錄的蛋目與病毒複製有很大的關聯性。B 型肝炎病毒潛伏期約 30 至 180 天，且病毒的複製只會在肝臟組織上進行，但病毒複製後，病毒可隨著血液循環散佈於肝外，在血液中可以偵測到的病毒成份，包含病毒本體、HBcAg 和 HBeAg 內核殼核心抗原及外套殼 HBsAg 抗原。因病毒複製在肝臟造成持續性發炎，最後會導致肝病變肝炎、肝纖維化、肝硬化或是肝癌。

目前工業化社會許多職業傷害的造成，可能導致毒物及藥物性肝炎的發生。許多工業用化學藥劑如四氯化碳、三氯乙烯、黃磷、及有機溶劑苯類等，都可能產生肝臟的傷害。許多藥物如解熱鎮痛的乙醯胺酚 (Acetaminophen)過量使用，也會造成肝損傷，另外某些有毒微生物和黴菌(Aspergillus)所產生的黃麴毒素及蕈類產生的有毒環狀胜

肽，也會造成急性或慢性肝炎。一般而言，化學藥劑對肝臟的毒性主要可以分成兩種，直接毒性和特異體質。直接毒性指的是只要暴露在毒物或藥物下皆會發生肝臟傷害。而特異體質指的是由基因因素使得代謝機能失常、藥物藥物交互作用或是合併肝炎病毒帶原等等，所造成的肝臟傷害，但此種肝炎類型並不常見，也無法預測。

2.2 肝炎臨床治療

西方醫學通常使用以下幾種藥物治療病毒性肝炎：1. 干擾素(interferon α)：為最早被核准用來治療 B 型肝炎的藥物，主要是以基因重組細胞製造出來。其作用機轉是經由抑制 pregenomic HBV RNA 的 packaging。並且調節免疫作用增強肝細胞上核心抗原的呈現。但干擾素具有複雜的副作用，包含全身生理反應、心理、神經系統、血液系統、免疫系統等等，因此干擾素的治療通常須經過適當的評估(23)。2. 抗病毒藥：目前抗病毒藥大多以核酸類似物 (nucleoside analogue) 來抑制 DNA 聚合酶，進而終止肝炎病毒的複製。目前 lamivudine 和 famciclovir 兩種口服藥，對於 B 肝的治療效果強且毒性較低，適用於長期治療肝炎。然而核酸類似物在體內的作用機制比較複雜，雖然在體外試驗是非常有效的 DNA 聚合酶抑制劑，但在動物實驗及臨床研究卻是效果有限(24, 25)。3. 免疫調節劑：針對免疫細胞進行調節，如胸腺素 (thymosin-α1) 、 interleukin 2(IL-2) 或 tumor necrosis factor-alpha (TNF-α) 。胸腺素主要是調節 T 細胞促進淋巴球產生內源性的 IFN-α、IFN-γ、IL-2 以及增加淋巴球 IL-2 receptor 的表現，雖然全都是內源性物質沒有明顯副作用，但在研究及臨床應用上仍持保留的態度。IL-2 或 TNF-α：經由強化 T helper 1 (Th1) 的反應，加強對干擾素的反應，目前臨床還在試用階段，其副作可能導制全身

性水腫和多器官功能失調(26, 27)。4. 雞尾酒療法：藉由各種藥物不同的作用機轉，理論上應該可以得到更好的療效，減少抗藥性的問題。目前臨床上有使用干擾素合併 Ribavirin (雷巴威林) 的雞尾酒療法，適合用在 C 型和 B/C 型肝病毒共感染的患者(28)。5. 基因療法：目前基因療法在治療肝炎病毒尚在研究階段。體外試驗證實有效的療法有 RNA 干擾 （RNA interference, RNAi） ，藉由與某些 mRNA 序列互補的專一性而達到抑制病毒基因表現(29, 30)。

在中醫肝病治療方面，中醫藥治療肝病的臨床用藥已有相當久的經驗，中醫對於肝病常用的中醫方劑進行了多層次多角度的臨床觀察及實驗研究，使肝病臨床用藥的方法更為豐富，而且在科學研究的協助下，賦予許多中藥藥物更多確切作用以及新的註解。目前中醫在肝病用藥已形成辨證用藥為主，並以改善肝功能、抗纖維化、調節免疫及抗病毒等用藥來治療相關肝病。臨床上許多肝病的表現前期通常以肝臟功能血清生化指標異常為辨別。因此改善和恢復患者肝功能的治療策略會以降酶、降絮、降濁、利膽退黃、抗炎護肝促進肝細胞再生、防止肝細胞損傷或增加肝臟代謝功能等。而這些藥物包含清熱解毒藥、清熱利濕藥、涼血活血藥、健脾益氣藥、酸甘化陰藥、疏肝利膽藥等(31-34)。清熱解毒藥、清熱利濕藥，此兩類藥物主要是以減輕肝臟發炎，防止肝細胞壞死及促進肝細胞修復和再生，進而調降 ALT，此類藥物有黃連、板藍根、連翹、黃芩、生甘草、車前草、通草、茯苓、及蒼朮等；涼血活血藥，具有抗凝血及血管擴張的效果，可以增加門靜脈及肝內血液循環，增加肝血流以促進纖維化的溶解加速、活化肝細胞及加速病灶的修復等，常用的藥物如丹參、丹皮、赤芍、紅花、當歸等；疏肝利膽藥，大多具有利膽退黃、減輕肝炎、防止肝細胞壞死及促進肝細胞再生的效果，常用的有柴胡、梔子、大黃、枳實、綿

茵陳等；酸甘化陰藥，主要作用為調節肝細胞生理酸鹼環境，減輕肝細胞內酶的滲出作用，進而減少血清生化指數。常用的有烏梅、木瓜、白芍、五味子、山楂及魚腥草等(33, 34)。肝炎在台灣嚴重的響影到人們的健康，目前西醫藥對許多肝病尚缺乏有效的治療，而中醫在治療肝病具有豐富的經驗及療效，如中醫結合現代科技，必定會有更新的突破。

2.3 茵陳蒿湯在肝病的應用

茵陳蒿湯源自於《傷寒論・陽明病篇》第 180 條：「傷寒七、八日，身黃如橘子色，小便不利，腹微滿者，茵陳蒿湯主之。」，是清熱祛濕的方劑。茵陳蒿湯原出處記載的組成為茵陳六兩、大黃二兩酒浸、梔子十四枚炒，先煮茵陳蒿，再煮梔子、大黃，而現今中醫所使用的比例為茵陳 30 克、梔子 15 克、大黃 10 克。在現代的研究指出該方有明顯增加膽汁分泌，收縮膽囊，促進膽汁排泄，抗病原微生物，降低血清膽固醇及 β 脂蛋白，護肝，消炎，鎮靜，利尿，解熱等作用。因此常用於急性肝炎、黃疸、膽囊炎、膽結石、新生兒溶血性黃疸、食物中毒、口內炎的治療上(35-38)。

茵陳蒿湯是中醫及日本漢方醫學經常用來治療肝炎的方劑，茵陳蒿湯主成單味藥為茵陳蒿、梔子、大黃三種。在中醫常用的組成比例為 6:3:2；日本漢方醫所使用的則是 4:3:1 (TJ-135) (39, 40) 。在此 3 種單味藥中，茵陳蒿可能的致效成分及效果有：capillarisin 具有促膽汁分泌的效果；capillene 及 capillin 可藉由誘發 TGF-β 來抑制肝細胞的凋亡 (41) 。梔子可能的致效成分及效果主要為 genipin，其中含量最高的 geniposide 進入身體腸道後經微生物分解所得的代謝產物，其具有抗發炎的效果 (42) 。大黃可能的致效成分及效果主要為 emodin,

其在許多研究中顯示具有抗發炎抗病毒抗腫瘤等功效 (43, 44) 。以往有許多研究顯示，茵陳蒿湯在大鼠長期口服投予之下, 可以有效地抑制肝纖維化，但是在這些研究中，並未詳細且深入的研究藥物在生物體的作用機轉，因此茵陳蒿湯在治療肝炎的機轉還有待更深入研究 (35, 45-47) 。

2.4 肝炎研究實驗平台

在肝病的研究中，四氯化碳 (CCl_4) 所誘導的肝損傷是目前在肝病藥物的抗肝毒性和保肝作用機制和藥物篩選最佳的動物模式 (48) 。 CCl_4 的代謝機轉主要是由 cytochrome p450 系統轉化成三氯甲基 (trichloromethyl) 以及氯甲基過氧自由基 (trichloromethyl peroxy radicals) 。這些來自於 CCl_4 的代謝物會跟生物體內的大分子形成共價鍵結進而導致脂質過氧化，而此結果會造成肝臟細胞脂肪浸潤和肝臟漸進式的從肝組織傷害到形成纖維化 (49) 。幾十年來，CCl_4 已經在許多研究中被廣泛應用在誘發各種實驗動物肝損傷的平台上 (50, 51) 。而且經由 CCl_4 所誘發的肝硬化的大鼠組織也顯示出與人類的肝硬化相似 (52) 。傳統上，藉由致肝毒性物質所誘發的肝損傷以及肝纖維化可以利用肝組織的變化和血清生化指標中的丙胺酸轉胺酶 (alanine aminotransferase, ALT) 、天門冬胺酸轉胺酶 (aspartate aminotransferase，AST) 、鹼性磷酸酶 (alkaline phosphatase) 及谷胺酸轉化酶 (gamma-glutamyl transferase) 濃度來進行評估 (53-55) 。有許多報告利用上述的方法進行植物藥在肝病療效上的篩選及評估，但在這些研究中需要一個強而有力的對照組藥物。近幾年在臨床使用的 Silymarin 具有很好的保肝效果，可以有效降低肝臟血清生化指標 (56) 。研究指出 Silymarin 具有抗氧化，抗脂質過氧化，抗纖維化，

穩定細胞膜，免疫調節與肝細胞再生的活性 (57-61) 。因此 Silymarin 在各種肝病動物模式中都顯示出有很好的保肝效果，進而目前臨床應用它來治療酒精性肝病，肝硬化，蕈類肝中毒以及藥物所引發的肝病等 (61) 。

基於目前肝病動物模式被限制在終點解剖實驗，以及容易受到干擾的血清生化指標。本研究首先利用基因轉殖鼠搭配分子影像技術進行肝病動物模式的建立，可以即時的在活體狀態下觀察到肝臟發炎程度。我們已經構築會受到 NF-κB 調控的基因轉殖鼠並將其應用在評估牛樟芝、香草酏及生醫材料所造成的免疫反應上 (62-65) 。在本研究中，我們將利用 CCl_4 長期的誘發此基因轉殖鼠形成慢性肝炎，並以 silymarin 為治療藥物，當作此疾病動物模式的先前測試。當測試此平台的可行性之後，更進一步，我們利用此平台探勘茵陳蒿湯及其組成，同時結合 microarray 多靶點的掃描，以期能解開茵陳茵湯主要的致效成份。

2.5 活體即時性肝炎報導平台之建立

傳統上，抗慢性肝炎藥物在活體的研究，大多都是利用動物解剖終點組織病理實驗以及血清生化指標加以評估，但這種方式需要長達數週至數個月的時間，而且需要犧牲相當數量的動物才能達到客觀的標準。除了活體模式 (*in vivo*) 外，以疾病分生為標的之細胞模式也被應用於抗肝炎藥物的篩選。雖然以疾病分生標的之細胞模式進行搜尋，確實可以加快藥物的評估，但是體外試驗 (*in vitro*) 證實有效的藥物，進入活體試驗時的失敗率相當高。此外，有許多方法可以直接以活體試驗偵測肝炎分生標的的活性，例如：免疫組織化學染色法 (immunohistochemistry stain; IHC) 、原位雜交反應 (in situ

hybridization) 等，但這些方法都無法即時性地反應動物體內肝臟發炎的現象。目前，非侵入性 (noninvasive) 、即時性 (real-time) 分子影像技術已經被廣泛地應用在分子、細胞和組織階層的影像化及量化，例如：顯微電腦斷層 (micro-computed tomography; micro-CT) 可應用於當作肝硬化程度的評估工具 (66) ；同步遠紅外線 (Synchrotron Infrared) 及飛行時間型二次離子質譜儀結合光譜儀 (ToF-SIMS Microspectroscopies) 可用來評估脂肪肝切片 (67) ；磁振造影 (magnetic resonance image; MRI) 可使用在臨床預測肝纖維化及藥物治療效果的評估 (68) 。近年來，靈敏度相當高的新興生物冷光影像 (bioluminescence imaging; BLI) 已被運用於偵測及定量小鼠體肝部位生長激素訊息傳遞及肝腫瘤的成像 (69, 70) ，然而在肝纖維化及肝發炎偵測卻尚還未被應用。

2.6 Microarray 分析平台的建立

Microarray 的雛形是由 Augenlicht 等發展的(71)。他們將人類大腸癌細胞 HT-29 的 mRNA 合成約 4000 種 cDNA，再將所有 cDNA 點到狀似小方格的硝化纖維濾紙上。之後抽取自大腸癌早期及晚期病人活體組織樣品的 mRNA，合成放射線標定的 cDNA 探針，與這些濾紙進行雜合，再分析放射線的強度，觀察基因表現的波動。真正出現 microarray 並加入自動化系統技術，是由史丹福大學的 Schena 等（1995）及 Shalon 等（1996）發展的。他們將阿拉伯芥（*Arabidopsis thaliana*）約 50 種 cDNA 利用聚合酶連鎖反應增殖後，點到玻璃玻片上，再將取材自野生型及 HAT4 基因轉殖後阿拉伯芥的 mRNA，分別合成有螢光標定及 lisaamine 標定的 cDNA，進一步將這兩種 cDNA 與玻片進行競爭性的雜合反應。結果發現，在

HAT4 基因的位置，lissamine 的強度較螢光多 50 倍，顯示利用不同標定方式，可以在同一時間在同一個雜合玻片上，分析到不同處理組基因表現的變化 (72)。這套系統被開發後，隨即被應用於監測不同狀態下細胞內所有基因表現的波動，例如酵母菌的細胞週期、果蠅在變態時的發育、細胞不同代謝狀態的基因表現變化(73-76)，另外也應用於分析腫瘤轉移、癌症、其他疾病的基因表現圖譜及疾病病程的預測和疾病的診斷(77-84)。因此，microarray 的技術也常被用來研究中藥及其組成物的作用機轉。此研究中我使用活體分子影像來進行肝炎的即時監控，搭配 microarray 為分析工具所形成的一個新型平台，我們將它命名為「分子影像導引轉錄學平台」(bioluminescent imaging-guided transcriptomic) 。我們利用分子影像進行中藥作用位置的活性偵測，再利用 microarray 進行 gene ontology、pathway 及 clustering 分析，這樣的模式在中醫藥作用機轉的偵測提供非常多的方便性。

第三章 材料與方法

3.1 材料

CCl_4購自昭和化學工業株式會社 (Showa chemical industry co.,ltd) 。橄欖油購自Sigma (St. Louis, MO) 。天狼星紅Sirius red購自Sigma (St. Louis, MO) 。picric acid 購自Panreac (Panreac, Barcelona, Spain) 。水飛薊素 (Silymarin) 購自Sigma (St. Louis, MO) ，並溶於無菌水 (混懸) 最終濃度20 mg/ml 冷凍在-20℃保存。D-Luciferin 購自Xenogen (Hopkinton, MA) ，溶於PBS。茵陳蒿湯、茵陳蒿、大黃、山梔子科學化中藥購自順天堂。Genipin購自Wako (Osaka, Japan) 。Lipopolysaccharide (LPS) 及 3-(4,5-dimethylthiazol-2-yl)-2,5-diphenyltetrazoliumbromide (MTT) 購自Sigma (St. Louis, MO) ，並分別溶於無菌水及磷酸鹽緩衝液 (phosphate-buffered saline; PBS) (137 mM NaCl, 1.4 mM KH_2PO_4, 4.3 mM Na_2HPO_4, 2.7 mM KCl, pH 7.2) 。單株抗體試劑luciferase、IL-1β、TNF-α、TGF-β1和α-SMA購自Santa Cruz (Santa Cruz, CA) 及NF-κB p65 購自Chemicon (Temecula, CA) 。

3.2 NF-κB基因轉殖鼠的構築

實驗室先前探討中藥的抗發炎作用，大多利用 NF-κB/luciferase 之重組細胞株來進行中藥及主要活性物質的測試。為了使報導發炎疾病研究模式更接近真實發炎情況，我們將此細胞平台進一步的推進到 NF-κB/luciferase 基因轉殖鼠之發炎疾病動物模式，以利中醫藥在抗發炎藥物上的探勘，在本研究中主要以研究茵陳蒿湯在抗肝炎上的效果與細部機轉。

我們首先構築 NF-κB 冷光報導的基因轉殖小鼠。構築載體的策略是將 NF-κB response element 接在 TATA-BOX 上游，下游報導基因

採用的是 luciferase gene 如圖 3.1。

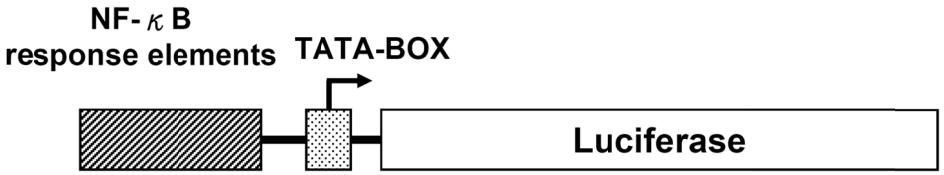

圖 3.1 報導基因架構圖

報導基因架構完成後，利用胚原核顯微技術注射 (pronuclear injection) 的方式，送到老鼠胚胎細胞 (oocytes) 中，再將胚胎植入母鼠體內，構築出帶有 NF-κB/luciferase 的基因轉殖鼠。我們將構築好的基因轉殖鼠與同品系野生株 (wild-type) 小鼠交配，進行子代繁殖。利用聚合酶連鎖反應 (Polymerase chain reaction; PCR) 進行新生小鼠的基因型確認。PCR 所用的引子為 primer-P 5'-AACTGCATAAGGCTATGAAGAGATACGCCC-3' 及 primer-M 5'-TTAAAACCGGGAGGTAGATGAGATGTGACG-3' (62) 。

接著，在獲取 PCR 結果陽性之基因轉殖鼠後，將每公斤體重 150 mg 之冷光素 (luciferin) 以腹腔注射方式打入基因轉殖鼠體內，五分鐘後以異氟烷 (isoflurane) 進行暫時性麻醉，將基因轉殖鼠置於密封不透光裝有 25 mm 鏡頭的 CCD 相機和影像增強器結合構成的影像系統 (IVIS Imaging Systems 200 Series, Xenogen Corporation) 中，進行全身性活體影像分析，利用 Living Images software (Xenogen) 測定冷光值，單位以 photons/sec/cm^2/steradian (photons/sec/cm^2/sr) 表示，結果如圖 3.2。

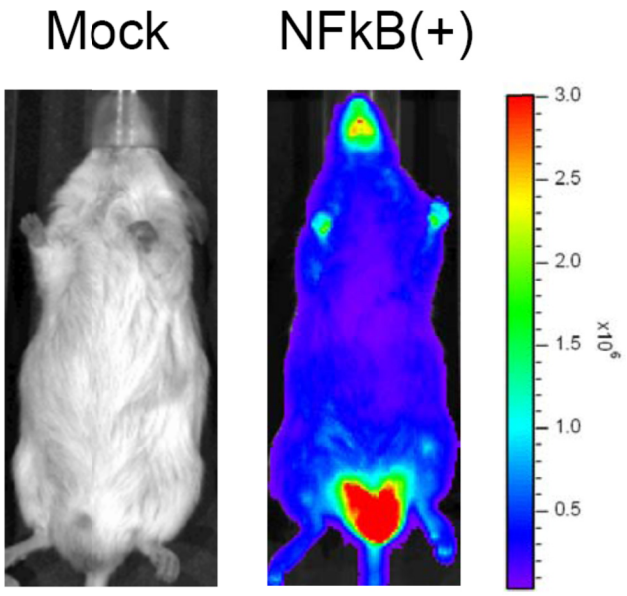

圖 3. 2 NF-κB/luciferase 基因轉殖鼠。冷光表現陰性及陽性鼠在 IVIS200 照影的結果。

3.3 肝纖維化的誘發及藥物投予

中國醫藥大學實驗動物照護及使用委員會的批准下進行。CCl_4 誘發肝纖維化可參考先前文獻 (85) 。我們將 24 頭基因轉殖鼠隨機分成 3 組，每組 8 頭，分別是 (1) mock 組,老鼠以腹腔注射 0.5 ml/kg 橄欖油,每週 2 次,持續 12 週; (2) CCl_4 組,老鼠以腹腔注射 0.5 ml/kg 10% (v/v) 溶在橄欖油的 CCl_4，每週 2 次，持續 12 週； (3) silymarin 組，老鼠以腹腔注射 0.5 ml/kg 10% (v/v) 溶在橄欖油的 CCl_4，每週 2 次，持續 12 週，並在第 5 週開始同時以胃管餵食投予 silymarin 200 mg/kg，每天一次到第 12 週。

茵陳蒿湯治療肝纖維化實驗的藥物投予組別，我們將 30 頭基因轉殖鼠隨機分成 6 組，每組 5 頭，分別是 (1) mock 組,老鼠以腹腔注射 0.5 ml/kg 橄欖油每週 2 次，持續 8 週； (2) CCl_4 組，老鼠以腹腔注射 0.5 ml/kg 10% (v/v) 溶在橄欖油的 CCl_4 每週 2 次，持續 8 週； (3) 茵陳蒿湯組、 (4) 茵陳蒿、 (5) 大黃、 (6) 梔子，分別以

老鼠以腹腔注射 0.5 ml/kg 10% (v/v) 溶在橄欖油的 CCl_4 每週 2 次，持續 8 週，並在第 5 週開始同時以胃管餵食投予依照每天人體劑量的茵陳蒿湯、茵陳蒿、大黃、梔子 150 mg/kg 每天一次到第 8 週。

3.4 體內及器官內冷光酵素活性偵測

將每公斤體重 150 mg 之冷光素 (luciferin) 以腹腔注射方式打入基因轉殖鼠體內，五分鐘後以異氟烷 (isoflurane) 進行麻醉，將基因轉殖鼠置於密封不透光裝有 25 mm 鏡頭的 CCD 相機和影像增強器結合構成的影像系統 (IVIS Imaging Systems 100 Series, Xenogen Corporation) 中，進行全身性活體影像分析，並利用 Living Images software (Xenogen) 測定冷光值，單位以 photons/sec/cm^2/steradian (photons/sec/cm^2/sr) 表示。

進一步進行器官剖檢，冷光素以腹腔注射方式打入基因轉殖鼠體內，五分鐘後將基因轉殖鼠犧牲，並取其全身實質臟器進行冷光值偵測，單位以 photons/sec 表示。

3.5 肝纖維化的定量分析

為了偵測肝臟纖維化，我們將肝臟切片以溶解在飽合苦味酸 (picric acid) 的 0.1% (w/v) 天狼星紅 (Sirius red；Sigma, St Louis, MO) 進行染色。經染色一小時後，切片以 0.5% (v/v) 的醋酸水潤濕，並換過兩次新的醋酸水。接著經過 100%酒精脫水乾燥後，再以阿拉伯膠進行封片後以顯微鏡觀察。我們利用 Image-Pro Plus (Media Cybernetics, Bethesda, MD) 這套軟體進行分析天狼星紅陽性 (紅色絲狀) 的區域。天狼星紅陽性區域代表肝纖維化程度，利用軟體分析結果，將肝纖維化的區域除以觀察總區域所得即為肝纖維化比

例。

3.6 免疫組織化學染色

將肝臟組織從小鼠體內取出後浸泡於10%福馬林(phosphatebuffered formalin solution) 中二天進行固定，然後，以生理食鹽水(saline)沖洗，再將組織塊進行石蠟包埋。石臘包埋的肝臟組織我們將其切成5-μm的切片並且做蘇木紫-伊紅染色法 (hematoxylin and eosin stain; H&E stain)的染色。為了進行免疫組織化學染色(immunohistochemistry stain; IHC) ，切片先以二甲苯 (xylene) 除掉石蠟，然後以一系列濃度梯度之酒精 (99.5%、95%、75% alcohols) 進行覆水作用 (rehydration) 。接著，將切片浸泡在3%雙氧水 (hydrogen peroxide) 中作用十五分鐘以清除組織中的過氧酵素 (endogenous peroxidase)，再以1% 胎牛血清白蛋白 (bovine serum albumin) 作用一小時以阻斷非特異的蛋白質。接著切片再與1:50稀釋的一級抗體於4°C下作用16-24小時。然後，再以接有biotin的二級抗體 (biotinylated secondary antibody) (Zymed Laboratories, South San Francisco, CA) 作用二十分鐘。最後，切片以生物素-過氧化酵素複合物 (avidin-biotin complex; ABC) 的試劑作用二十分鐘，然後再以3,3'-diaminobenzidine (DAB) 染色。染色後的切片於光學顯微鏡下進行判讀。

3.7 RNA 萃取

我們依照 RNeasy Mini kit (Qiagen, Valencia, CA) 的操作步驟萃取組織的 total RNA。隨後再利用 Beckman DU800 分光光度計 (Beckman Coulter, Fullerton, CA) 進行 total RNA 的定量。若樣品的 O.D. 值 A260/A280 比值大於 1.8，則進一步利用 Aglient 2100

bioanalyzer (Agilent Technologies, Santa Clara, CA) 評估其 total RNA 的品質。當樣品的 RNA integrity number (RIN) 高於 8.0 時，樣品才會進入下述的 DNA 微陣列實驗分析。

3.8 DNA 微陣列實驗分析

DNA微陣列 (microarray) 實驗分析方法如Cheng等報告中所述 (86) 。簡述之，將5 μg total RNA利用MessageAmp™ aRNA kit (Ambion, Austin, TX) ，經由試管外轉錄 (*in vitro* transcription) 的步驟增量樣品。增量後的 RNA (amplified RNA，簡稱aRNA) 再和螢光物質Cy5 (Amersham Pharmacia, Piscataway, NJ) 進行標定，當aRNA被Cy5染劑標定上，將使得aRNA成為帶有螢光標定的標的物 (target) 。接著，利用蓋玻片和 Phalanx 公司所提供的雜合反應緩衝劑 (hybridization buffer)，將螢光標定的標的物與 Mouse Whole Genome OneArray™ (Phalanx Biotech Group, Hsinchu, Taiwan) 進行雜合反應 (hybridization) 。於50°C下，經隔夜 (overnight) 的雜合反應之後，藉由後續清洗處理步驟將非專一性結合的標的物從晶片上清除。接著將晶片以離心的方式乾燥，並利用掃描器Axon 4000 Scanner (Molecular Devices, Sunnyvale, CA) 進行螢光強度的掃描。掃描的圖檔利用 Genepix (Molecular Devices Co., PA) 分析軟體 (Genepix 4.1 版) 進行螢光強度進行分析。每一點的訊號經由扣除周圍背景值的方式校正其強度。我們刪除作為內在控制的探針 (probe) 或是訊雜比 (signal-to-noise ratio) 小於零的點。通過這些門檻的點藉由R程式的limma package進行normalization (87) 。經過normalized 資料我們利用 Gene Expression Pattern Analysis Suite v3.1 計算有顯著差異的基因 (88) 。我們選擇大於等於2倍或小於等於2倍變化的基因，利用

WebGestalt (http://bioinfo.vanderbilt.edu/webgestalt/login.php) 網頁分析基因群關聯的訊息路徑。另外，這些表現有差異的基因再藉由TIGR Multiexperiment Viewer (89) (http://www.tm4.org/index.html) 進行階層式叢集分析 (hierarchical clustering analysis) 用以展現它們標的器官的表現形式。接著，將表現有差異的基因表單送到Gene Ontology Tree Machine 網頁 (http://bioinfo.vanderbilt.edu/gotm/) 進行Gene Ontology (GO)分析，以找出這些受調控的基因所影響的細胞行為模組。Gene Ontology Tree Machine是一個在網路上使用，以基因群組 (gene set) 為分析基礎的資料探勘 (data mining) 工具 (90) 。最後，我們利用 BiblioSphere Pathway Edition 軟體 (Genomatix Applications, http://www.genomatix.de/index.html) 建構表現有差異基因之間的交互作用網路 (interaction network) 。BiblioSphere Pathway Edition 軟體以知識庫分析為基礎，整合了文獻探勘 (literature mining) 、基因註解分析和啟動子 (promoter) 序列分析來建構基因交互作用網路 (91) 。本實驗的重複數為三次。

3.9 即時螢光定量聚合酶連鎖反應 (qPCR)

我們利用qPCR的方式定量cytochrome *c* oxidase 基因 (Cox6a2, Cox7a1, and Cox8b) 、interferon inducible GTPase 1 (Iigp1) 及 interferon-inducible gene (Ifi202) 的表現量。RNA 樣品利用 High Capacity cDNA Reverse Transcription Kit (Applied Biosystems, Foster City, CA, USA) 經2小時 37℃反轉錄的反應轉換成cDNA。接著利用1 μl 的 cDNA, 2× SYBR Green PCR Master Mix (Applied Biosystems) ，以及200 nM的正股引子 (forward) 跟反股引子 (reverse) 進行聚合酶反應，反應條件為 95℃ 10分鐘；接著95℃ 15秒，60℃ 1分鐘 40

次循環。這些分析我們利用Applied Biosystems 7300 Real-Time PCR系統且三重複。基因表現的倍率變化我們利用相對CT 值的方法做定量計算。本研究所用引子如下： Cox6a2 forward, 5'-CAGAGAAGGACAGTGCCATTC-3'; Cox6a2 reverse, 5'-GAAGAGCCAGCACAAAGGTC-3'; Cox7a1 forward, 5'-CAATGACCTCCCAGTACACTTG-3'; Cox7a1 reverse, 5'-CCAAGCAGTATAAGCAGTAGGC-3'; Cox8b forward, 5'-TCCCAAAGCCCATGTCTCTG-3'; Cox8b reverse, 5'-CATCCTGCTGGAACCATGAAG-3'; Iigp1 forward, 5'-CTTGACATGGTGACTGAGGATG-3'; Iigp1 reverse, 5'-AGGTGGATAAAGCCCGAATAAC-3'; Ifi202 forward, 5'-AAGGCTGGTTGATGGAGAG-3'; Ifi202 reverse, 5'-GTCAATTCAAAGCAGACAAGTC-3'; glyceraldahyde-3-phosphate dehydrogenase (GAPDH) forward, 5′-TCACCCACACTGTGCCCATCTATGA-3′; GAPDH reverse, 5′-GAGGAAGAGGATGCGGCAGTGG-3′.

3.10 細胞培養及Lipopolysaccharide (LPS) 的處理

重組HepG2/NF-κB細胞株帶有NF-κB-responsive elements可驅使luciferase表現，構築詳細內文參照我們過往發表的文獻 (62) ，以含有10%胎牛血清 (Fetal bovine serum) (HyClone, Logan, Utah) 和400 ng/ml 建那黴素 (Geneticin; G418) 的Dulbecco's modified Eagle medium (DMEM) (Life Technologies, Gaithersburg, MD) 於37°C培養箱中培養。將HepG2/NF-κB培養於96孔盤，24小時後，將培養液置換成DMEM繼續培養24小時，然後再處理不同濃度的LPS作用16小時。

3.11 細胞培養及genipin的處理

重組細胞株HepG2/NF-κB以含有10%胎牛血清 (HyClone, Logan, Utah) 和400 ng/ml建那黴素 (Geneticin; G418) 的Dulbecco′s modified Eagle′s medium (DMEM) (Life Technologies, Gaithersburg, MD) 於37°C培養箱中培養。將HepG2/NF-κB細胞培養於96孔盤，24小時後，再處理100 ng/ml LPS及不同濃度的genipin作用24小時。

3.12 NF-κB活性測試

為了測試發炎誘發物LPS是否會誘發細胞中NF-κB的活性，HepG2/NF-κB處理不同濃度的LPS，16小時之後，以 350 µl Triton lysis buffer (50 mM Tris-HCl, 1% Triton X-100, 1 mM dithiothreitol, pH 7.8) 使細胞溶解，以12,000 xg的轉速，在4°C下離心2分鐘。將20 µl的細胞溶解液與20 µl 冷光試劑 (470 µM luciferin, 33.3 mM dithiothreitol, 270 µM coenzyme A, 530 µM ATP, 20 mM Tricine, 1.07 mM $(MgCO_3)_4$, $Mg(OH)_2$, 2.67 mM $MgSO_4$, 0.1 mM EDTA, pH 7.8) 混合，利用冷光儀 (luminometer, FB15, Zylux Corp., Maryville, TN) 測定冷光值，單位以relative luciferase unit (RLU) 表示。活化倍率的計算方式是以LPS處理細胞的RLU除以未受LPS處理細胞的RLU。

3.13 MTT 分析法

為了測試發炎反應誘發物LPS是否會毒殺細胞，HepG2/NF-κB處理不同濃度的LPS處理24小時，利用MTT比色分析法偵測細胞存活率。細胞存活率(%)的計算公式為：(處理LPS之細胞OD值/未處理LPS之細胞OD值)×100%。

3.14 Genipin動物實驗

所使用的基因轉殖鼠請參照材料與方法3.1及3.2。我們將25頭基

因轉殖鼠 (母鼠6-8週大) 隨機分成5組，每組5頭： (1) mock組，沒有任何的處理； (2) LPS組，腹腔注射4 mg/kg劑量的LPS； (3) LPS加genipin 1 mg/kg組，腹腔注射4 mg/kg劑量的LPS後10分鐘，接著腹腔注射genipin 1 mg/kg；(4) LPS加genipin 10 mg/kg組，腹腔注射4 mg/kg劑量的LPS後10分鐘，接著腹腔注射genipin 10 mg/kg； (5) LPS加genipin 100 mg/kg組，腹腔注射4 mg/kg劑量的LPS經過10分鐘後，接著腹腔注射genipin 100 mg/kg。經過4小時後，基因轉殖鼠以IVIS照影，分析其體內冷光活性，之後解剖摘取實質器官進行冷光照影、組織取樣提供RNA萃取及免疫組織化學染色。

3.15 細胞激素的酵素連結免疫吸附法

我們利用酵素連結免疫吸附法套組 (Enzyme-linked immunosorbent assay, ELISA) OptEIA™ mouse IL-1β 和 TNF-α sets (Pharmingen, San Diego, CA) 進行IL-1β 和 TNF-α的定量。基因轉殖鼠犧牲後，取其血液。於4 °C環境下，以轉速3000 rpm、離心10分鐘，之後，取其血清。血清以每一格200 μl的體積加入作用盤中與盤底材料進行室溫接合反應2小時，接著使用IL-1β或 TNF-α單株抗體進與血清中標的接合2小時，經3次 PBS含0.05% Tween 20洗滌後，以biotin接合的2級抗體進行反應1.5個小時，而後以過氧化氫酶接合avidin的試劑進行催化作用呈色，再以O.D. 450 nm吸收光分析。

3.16 統計分析

實驗所得資料數據我們以平均值±標準差來呈現。大於3個組別的數據，我們利用PASW Statistics (SPSS) 軟體以one way ANOVA及事後檢定LSD 進行分析當p value小於0.05為顯著差異。

第四章 結果

4.1 NF-κB活體即時性肝炎報導平台之建立

4.1.1 Silymarin穩定下降CCl_4誘發的肝臟NF-κB活性

基因轉殖鼠經過投予CCl_4 或 silymarin，在第4 週、第6週、第8週、第12週，經過分子影像照影偵測NF-κB活性，結果呈現如圖4.1。與Mock組對照起來，CCl_4很顯著的誘發小鼠腹腔區域冷光值。經過解剖觀察實質器官後，發現CCl_4的確很專一的誘發肝臟冷光，圖4.2。這個結果顯示， CCl_4誘發小鼠腹腔區域生物冷光訊號是來自於肝臟。以上結果證實CCl_4可以專一的誘發肝臟NF-κB活化，另外silymarin 也顯示可以依投予時間穩定的下降CCl_4在肝臟所誘發的NF-κB活性。

4.1.2 Silymarin 降低肝臟 NF-κB 活性與改善肝纖維化之間的關聯性

為了評估肝病變和肝纖維化的程度，我們利用H&E染色和天狼星紅進行的肝臟切片染色。肝。天狼星紅是一種很強的陰離子染料，已經在膠原蛋白的專一染色與在組織切片纖維化的量化上(92, 93) 。纖維化主要是由於被積累在肝臟組織的膠原蛋白所誘發 (94) 。因此，天狼星紅陽性粉紅絲狀面積可以直接用來標記肝纖維化的程度。如圖4.3所示， H&E染色顯示四氯化碳的攻擊使肝臟組織結構受損，這是由免疫細胞的浸潤、出血、肝細胞形成空泡變性所造成，如圖中箭頭所示。天狼星紅在mock組的肝門靜脈周圍出現陽性區域而非在肝臟實質，天狼星紅染色區域很清晰地出現在肝臟組織上呈網狀結構，經過定量統計肝纖維化面積的比例為3.86±0.54%。圖中CCl_4與silymarin組相較之下，silymarin明顯的改善CCl_4誘導的肝組織病理變化。此外，silymarin組與CCl_4組相較之下，天狼星紅染色區域明顯的減少，經過定量統計經silymarin治療後肝纖維化區域的比例為1.94±0.29%，有顯

著下降的現象。這些結果顯示，silymarin可改善CCl_4誘導的肝纖維化。

我們進一步利用免疫組織化學染色去偵測NF-κB活性與肝纖維化的相關性。我們利用α-SMA抗體進行肝切片的免疫染色，以檢測肌纖維母細胞所產生膠原蛋白是否存在 (95) 。另外，我們利用TGF-β1抗體做免疫組織化學染色，TGF-β1在肝纖維化中扮演著很重要的一種細胞因子 (96) 。如圖4.4所示，在四氯化碳組的肝臟呈現出許多褐色的TGF-β1陽性細胞和α-SMA陽性的肌纖維母細胞。然而，silymarin口服組明顯的降低了肝臟的褐色細胞的數量。這些發現顯示，silymarin明顯改善四氯化碳誘導的肝纖維化，這些結果與上述H&E和天狼星紅組織染色的結果吻合。進一步，我們利用p65 (NF-κB) 抗體進行免疫組織化學染色，結果顯示經過四氯化碳誘導的肝細胞有許多褐色的p65陽性細胞。然而，silymarin明顯下降在肝臟中p65的陽性細胞的數量。這些結果顯示，silymarin可能透過抑制NF-κB、TGF-β1及α-SMA進而改善四氯化碳所誘發的肝纖維化。此外，我們也發現NF-κB的活性與肝纖維化在基因轉殖鼠上所發出的冷光影像關係成正比，因此證實NF-κB活體即時性影像可以當作抗肝纖維化藥物療效評估的可行性。

4.1.3 Silymarin 治療四氯化碳誘發肝纖維化的基因表現圖譜分析

我們進一步利用 microarray 分析了 silymarin 治療組的肝基因反應圖譜，以確定 silymarin 的新穎作用機轉。CCl_4 組基因反應圖譜與 Mock 組相比，在 CCl_4 誘發下有 420 個基因上調 439 個基因下調超過 2 倍以上。而 silymarin 基因反應圖譜在與 CCl_4 組比較下，silymarin 處理之下有 67 個基因變化大於等於 2.0 倍或小於等於-2.0 倍，其中包括 2

個基因上調和 65 個基因下調。進一步，我們將這些基因進行 pathway 的分析。分析結果 (表 4.1) 顯示由 silymarin 顯著改變的 34 個 pathway (p <0.01) ， 在這 34 個 pathway 當中，有一半以上與代謝途徑相關，而另外有一些 pathway 與細胞生存過程的調控和信號轉導有關。而 TGF-β 相關的 pathway，包括 TGF-βsignaling pathway，TGF-β-induced apoptosis 和 TGF-β-mediated pathway 都有明顯的受 silymarin 調控。因為 TGF-β1 與 TGF-β pathway 的調控在肝纖維化的過程中扮演很重要的角色跟作用，而 silymarin 調控這個分子進而調控 pathway 可能有助於改善 CCl_4 所誘發的肝纖維化。在四氯化碳的攻擊之下 silymarin 一共下調了 65 個基因的表現，這些基因倍率變化小於等於 -4.0 倍如表 4.2 顯示。有一半被 silymarin 所下調的基因是與細胞骨架組成和肌肉收縮有關，而其中有 3 個基因，包括 Cox6a2、Cox7a2 和 Cox8b，均與粒腺體電子傳遞鏈有關聯。這些結果顯示，silymarin 可能改善 CCl_4 誘導的肝纖維化，主要是透過調控參與細胞骨架組織和電子傳遞鏈的基因表現。

4.1.4 qPCR 確認受 silymarin 調控的新穎基因表現程度

Microarray結果顯示，與粒腺體呼吸鏈相關的基因，包括Cox6a2, Cox7a1 和 Cox8b基因都受到silymarin的下調。我們進一步利用定量PCR來驗證這些基因的轉錄表現程度。如表4.3所示，Cox6a2、Cox7a1和Cox8b基因在 CCl_4組的表現程度都高於Mock組，倍率分別496.21，21.36和240.38倍。然而，Silymarin組相較於Mock組，Cox6a2，Cox7a1，Cox8b基因的表現倍率分別為9.84，0.72，0.7倍，此結果證明CCl_4所上調的基因表現都被silymarin給抑制了。

(A)

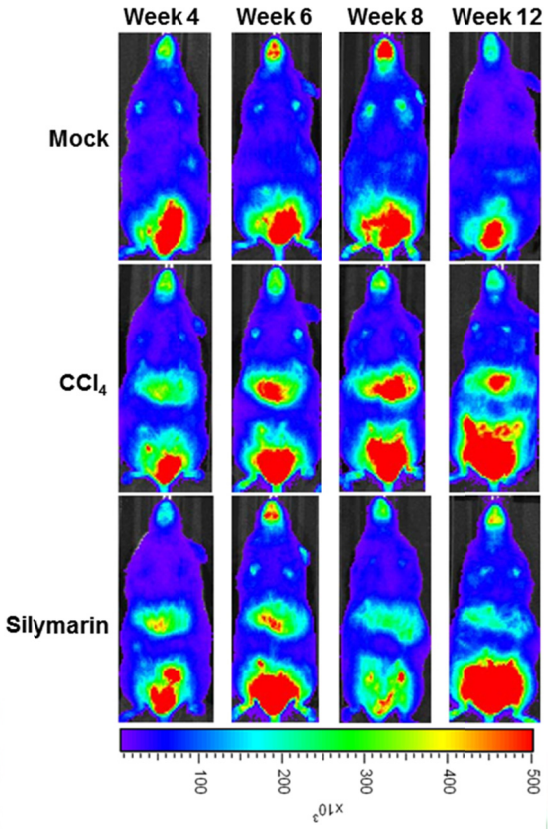

(B)

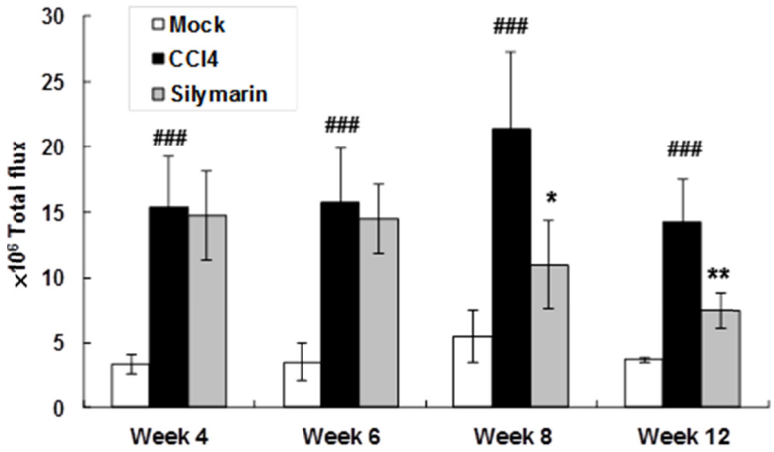

圖 4.1 小鼠肝炎即時性活體 NF-κB/冷光報導。基因轉殖鼠經過投予 CCl_4 或 silymarin，並且在各個指定時間內照影。 (A) 活體影像，小鼠身上的冷色系到暖色系從藍到紅的顏色，分別代表冷光表現強度，單位為 photon/sec，圖中每個組別皆有 8 重複。 (B) 全身影像冷光值的定量統計圖。冷光值以平均值 ± 標準差，組別與 mock 比較， ### 表示 $p<0.001$；與 CCl_4 比較*表示 $p<0.05$，**表示 $p<0.01$。

(A)

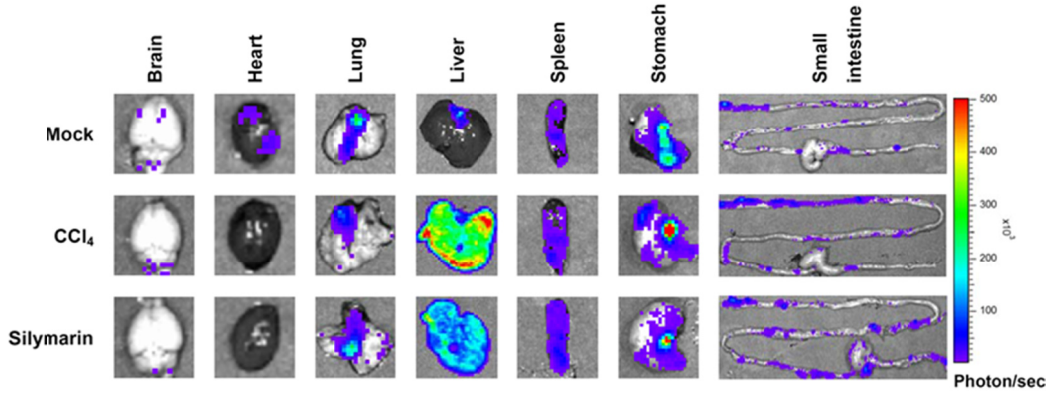

(B)

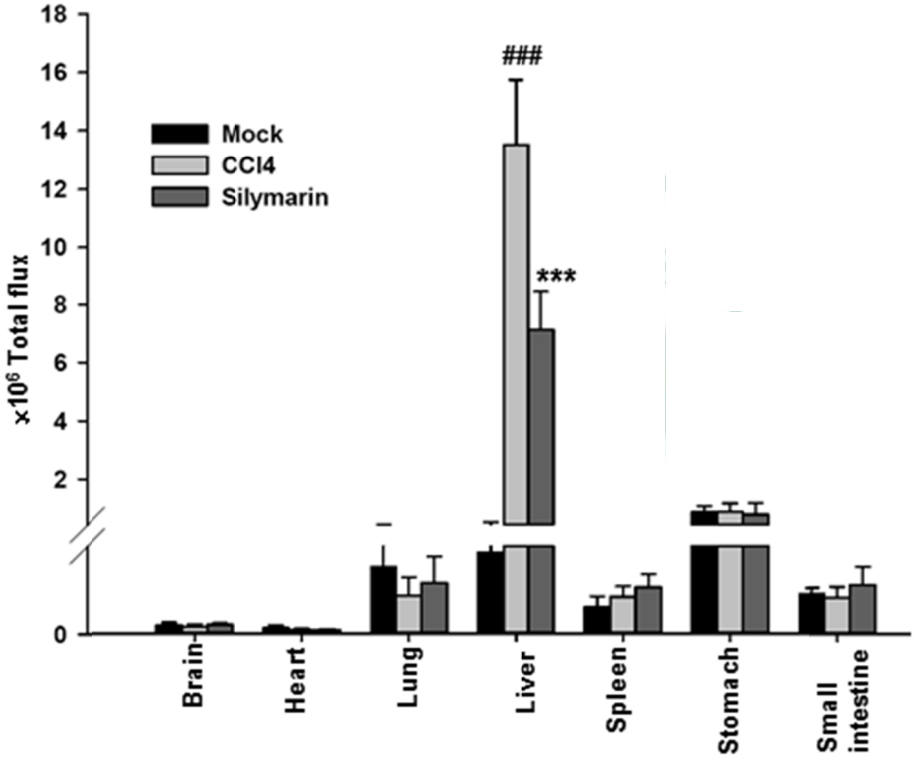

圖 4.2 基因轉殖鼠肝炎及治療後實質臟器的 NF-κB 活性。基因轉殖鼠經過投予 CCl_4 或 silymarin，12 週後小鼠進行解剖及器官的照影。(A) 器官剖檢照影，器官上的冷色系到暖色系從藍到紅的顏色，分別代表冷光表現強度，單位為 photon/sec，圖中每個組別皆有 8 重複。(B) 器官影像冷光值的定量統計圖。冷光值以平均值 ± 標準差，組別與 mock 比較 ##表示 $p<0.01$, ###表示 $p<0.001$；與 CCl_4 比較*表示 $p<0.05$。

(A)

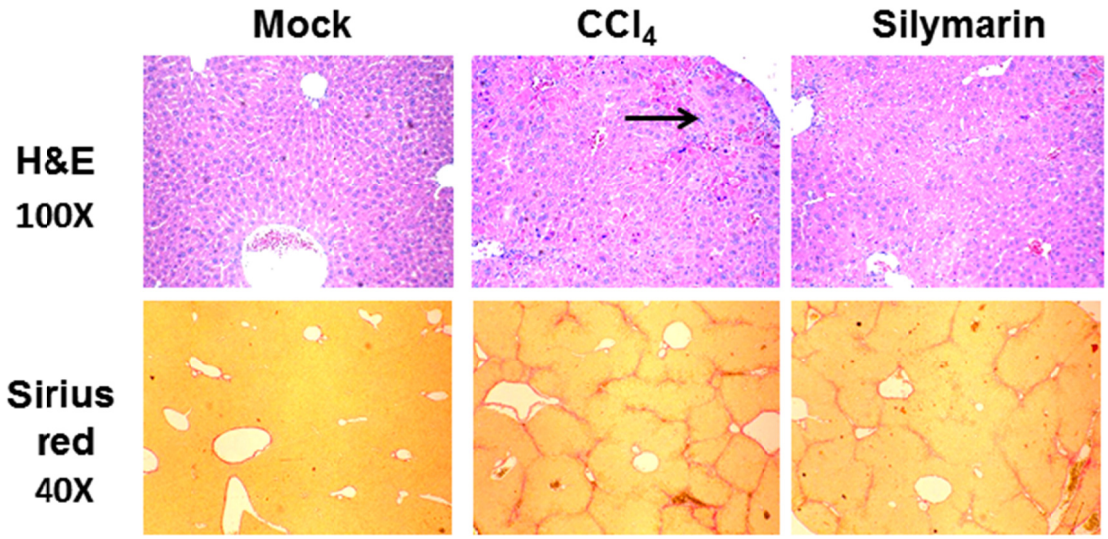

(B)

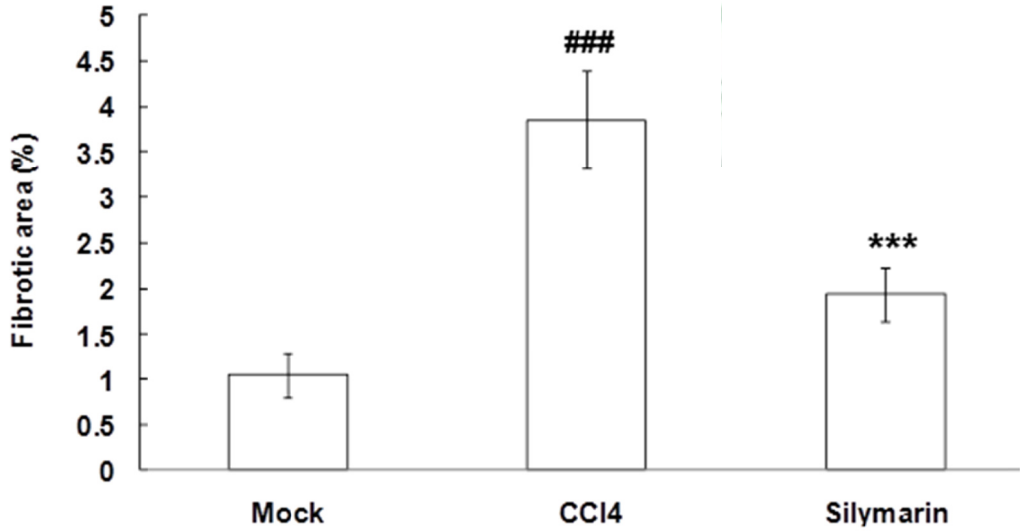

圖4.3 利用H&E及天狼星紅進行肝臟染色。 (A) 組織病理檢查，基因轉殖小鼠投予CCl_4和/或silymarin，經過12週處理後，小鼠進行犧牲解剖摘取肝及肝臟切片，接著進行H&E (100倍) 或天狼星紅染色 (40倍) 鏡檢及拍攝。拍攝圖像皆有8重複。 (B) 藉由天狼星紅對肝臟纖維化進行定量。計算方式以纖維化區域(粉紅絲狀)除以組織全部區域。結果以平均值±標準差表示。組別與mock比較###表示$p<0.001$；與CCl_4比較***表示$p<0.001$。

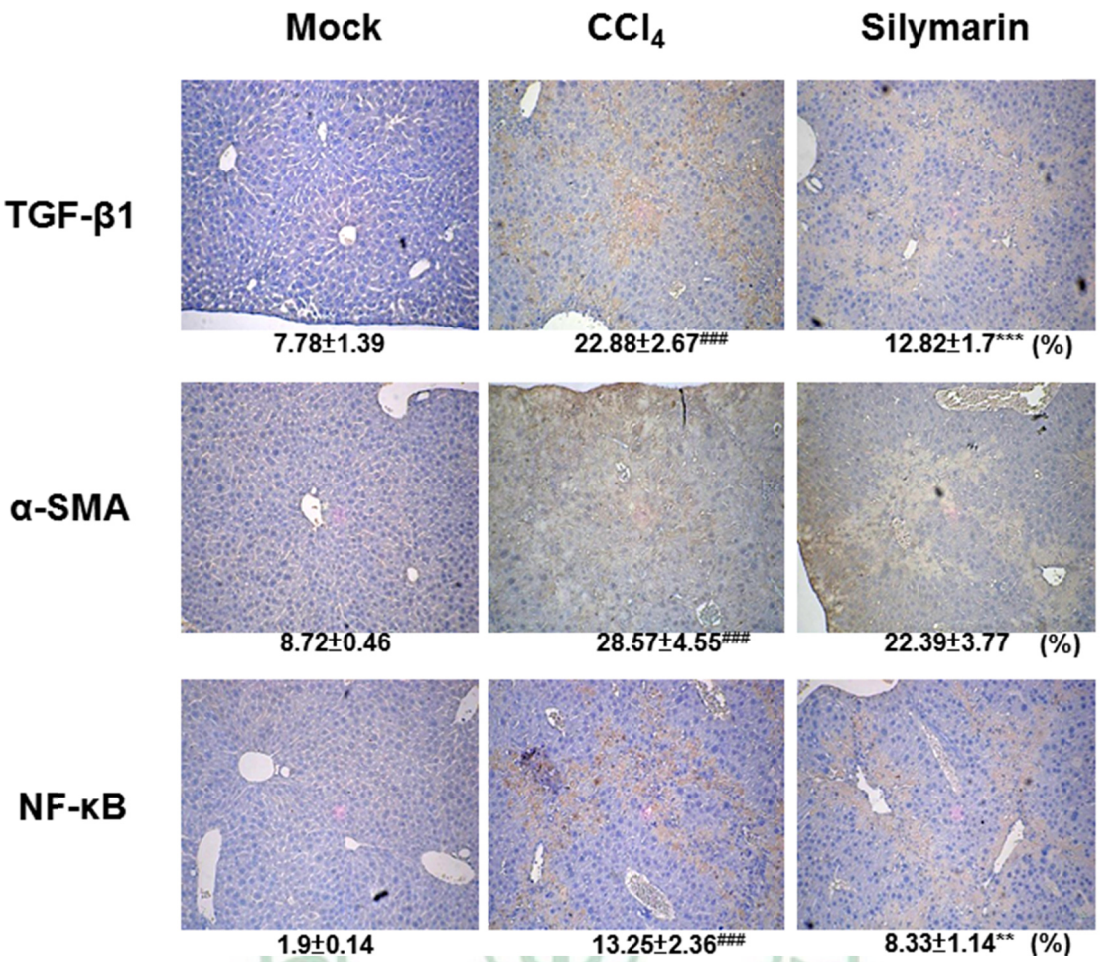

圖 4.4 肝臟免疫組織化學染色。基因轉殖小鼠投予 CCl_4 和/或 silymarin，經過 12 週處理後，小鼠進行犧牲解剖摘取肝及肝臟切片，以 TGF-β1、 α-SMA 及 p65 抗體進行免疫組織化學染色，並進行鏡檢及拍攝 (100 倍) 。拍攝圖像皆有 8 重複。接著，定量 TGF-β1、α-SMA 及 p65 染色結果。結果呈現以抗體陽性呈褐色的區域除以組織全部區域。結果以平均值±標準差表示 (每組 8 重複，每個切片 3 個視野)。組別與 mock 比較###表示 $p<0.001$；與 CCl_4 比較**表示 $p<0.01$，***表示 $p<0.001$。

表 4.1 Silymarin 所調控的 pathway 分析。

Pathway	***p* value**[a]
Regulation of cellular process/ cell cycle and death	
TGF-β signaling pathway	2.75×10^{-7}
p53-mediated pathway	0.00171
Tight junction	0.00014
TGF-β-induced apoptosis	0.00261
Adherens junction	0.00494
TGF-β-mediated pathway	0.00976
Metabolism	
Urea cycle and metabolism of amino groups	2.49×10^{-5}
Citrate cycle	2.45×10^{-6}
Arginine and proline metabolism	0.00016
Galactose metabolism	0.00034
Biosynthesis of steroids	0.00049
Glycine, serine and threonine metabolism	0.00070
Glycolysis / Gluconeogenesis	0.00100
Butanoate metabolism	0.00098
Folate biosynthesis	0.00218
Pyruvate metabolism	0.00223
Fatty acid metabolism	0.00273
Bile acid biosynthesis	0.00273
Alanine and aspartate metabolism	0.00442
Glutathione metabolism	0.00544
Starch and sucrose metabolism	0.00601
Glycosaminoglycan degradation	0.00799
Glutamate metabolism	0.00921
Signal tansduction	
Adipocytokine signaling pathway	8.26×10^{-5}
IL6 signaling pathway	0.00016
PPAR signaling pathway	0.00039
Insulin signaling pathway	0.00047
Vitamin D3 signaling pathway	0.00067
RANKL signaling pathway	0.00548
TNF signaling pathway	0.00629
IGF signaling pathway	0.00655
Chemokine signaling pathway	0.00709
EGF signaling pathway	0.00770
PTH/PTHrP signaling pathway	0.00840

[a] *p* value 的數據是利用 WebGestalt 網頁藉由 hypergeometric test 所計算.

表 4. 2 silymarin 下調 CCl_4 所誘發的肝臟基因表現倍率變化。

Gene symbol	Description	Fold changes[a]
Acta1	Actin, alpha 1, skeletal muscle	-90.21±0.001
Myl1	Myosin, light polypeptide 1	-77.05±0.001
Tnni2	Troponin I, skeletal, fast 2	-49.39±0.001
Atp2a1	ATPase, Ca^{+2} transporting, cardiac muscle, fast twitch 1	-48.46±0.001
Mylpf	Myosin light chain, phosphorylatable, fast skeletal muscle	-41.90±0.001
Mb	Myoglobin	-35.39±0.002
Cox6a2	Cytochrome c oxidase, subunit VI a, polypeptide 2	-28.43±0.003
Cox8b	Cytochrome c oxidase, subunit VIII b	-18.60±0.004
Eno3	Enolase 3, beta muscle	-8.17±0.009
Tnnt1	Troponin T1, skeletal, slow	-7.60±0.011
Tnnc1	Troponin C, cardiac/slow skeletal	-7.56±0.010
Cox7a1	Cytochrome c oxidase, subunit VIIa 1	-6.67±0.015
Eef1a2	Eukaryotic translation elongation factor 1 alpha 2	-4.64±0.022
EG433229	Predicted gene, EG433229, transcript variant 7	-4.06±0.016

[a] 倍率變化表示為平均值±標準差 (n=3) 。

表4.3 qPCR分析Cox6a2、Cox7a1、和 Cox8b 基因表現程度。

Sample	Average C_T of target	Average C_T of GAPDH	ΔC_T[a]	$\Delta\Delta C_T$[b]	Relative to mock
Cox6a2					
Mock	35.82 ± 0.40	19.71 ± 0.03	16.11 ± 0.40	0.00 ± 0.40	1.00
CCl_4	25.80 ± 0.05	18.64 ± 0.05	7.16 ± 0.07	-8.96 ± 0.07	496.21
Silymarin	31.17 ± 0.09	18.36 ± 0.01	12.81 ± 0.09	-3.30 ± 0.09	9.84
Cox7a1					
Mock	29.98 ± 0.10	19.71 ± 0.03	10.27 ± 0.11	0.00 ± 0.11	1.00
CCl_4	24.49 ± 0.04	18.64 ± 0.05	5.85 ± 0.07	-4.42 ± 0.07	21.36
Silymarin	29.10 ±0 .11	18.36 ± 0.01	10.74 ± 0.11	0.47 ± 0.11	0.72
Cox8b					
Mock	32.81 ± 0.11	19.71 ± 0.03	13.09 ± 0.12	0.00 ± 0.12	1.00
CCl_4	23.83 ± 0.05	18.64 ± 0.05	5.18 ± 0.07	-7.91 ± 0.07	240.38
Silymarin	31.97 ± 0.29	18.36 ± 0.01	13.61 ± 0.29	0.52 ± 0.29	0.70

[a] The ΔC_T value is determined by subtracting the average GAPDH C_T value from the average target gene C_T value. The standard deviation of the difference is calculated from the standard deviations of the target gene and GAPDH.

[b] The calculation of $\Delta\Delta C_T$ involves subtraction by the ΔC_T calibrator value. This is a subtraction of an arbitrary constant, so the standard deviation of $\Delta\Delta C_T$ is the same as the standard deviation of ΔC_T value.

4.2 茵陳蒿湯及其組成在肝炎之療效分析

4.2.1 茵陳蒿湯中的大黃與梔子在肝臟明顯抑制CCl_4所誘發的NF-κB活性

基因轉殖鼠經過投予CCl_4 或 silymarin，在第4 週與第8週經過分子影像照影偵測NF-κB活性，結果呈現如圖4.5，經過CCl_4處理後與Mock組對照起來，很顯著的誘發小鼠腹腔區域NF-κB活性。經過解剖後，實質器官經影像照影顯示，CCl_4的確很專一的誘發肝臟冷光 (圖4.6) 。茵陳蒿湯複方及其組成單方包括茵陳蒿、大黃和梔子以口服方式投予，結果發現大黃與梔子在第8週時有顯著的抑制小鼠腹腔CCl_4所誘發的冷光強度。進一步器官剖檢進行冷光影像照影，發現口服大黃及梔子組確實抑制肝臟CCl_4所誘發的冷光。這些結果顯示，大黃與梔子都可以明顯的抑制肝臟CCl_4所誘發的NF-κB活性。

4.2.2 大黃與梔子下降肝臟 NF-κB 活性與改善肝纖維化之間的關係

為了評估肝病理改變和肝纖維化程度，肝臟切片我們利用H&E染色和天狼星紅進行染色，H&E可以用來觀查肝臟組織受到破壞的程度，而天狼星紅陽性粉紅絲狀面積可以直接用來標記肝纖維化的程度。H&E染色很明顯可以看見，CCl_4組的肝臟小葉結構嚴重受損，這是由免疫細胞的浸潤、出血、肝細胞形成空泡變性所造成，反而在大黃或梔子組有明顯的緩解下來。天狼星紅染色區域很清晰地出現在肝臟小葉上呈網狀結構，經過定量統計CCl_4組的肝纖維化面積的比例為3.43±0.1%。與CCl_4組相較之下，肝臟纖維化程度在大黃組為1.58±0.08%與梔子組為0.92±0.05%各有顯著下降。這些結果顯示，大黃與梔子可能是茵陳蒿湯裡主要的肝纖維化療效組成 (圖4.7) 。

4.2.3 梔子主要化合物 genipin 抗肝炎效果

基因轉殖鼠經過投予CCl_4 或 genipin，在第4 週時開始投於genipin, 直到第8週經過分子影像照影偵測NF-κB活性，結果呈現如圖4.8。經過CCl_4處理後與Mock組對照起來，很顯著的誘發小鼠腹腔區域的NF-κB活性。而genipin在三個濃度分別為1、10、100 mg/kg，其中以10 mg/kg的抗肝臟發炎最具效果，另外100 mg/kg，我們推測該濃度過高，可能導致肝毒性。以上結果顯示Genipin 可以在一定的劑量下大約10 mg/kg，在小鼠體內使肝臟下降CCl_4所誘發的NF-κB活性。

(A)

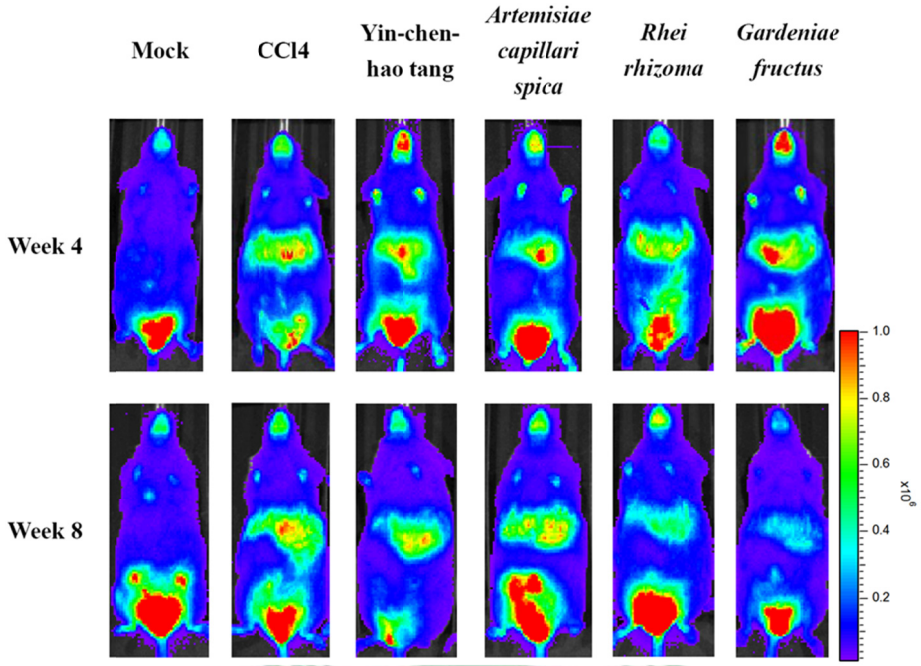

(B)

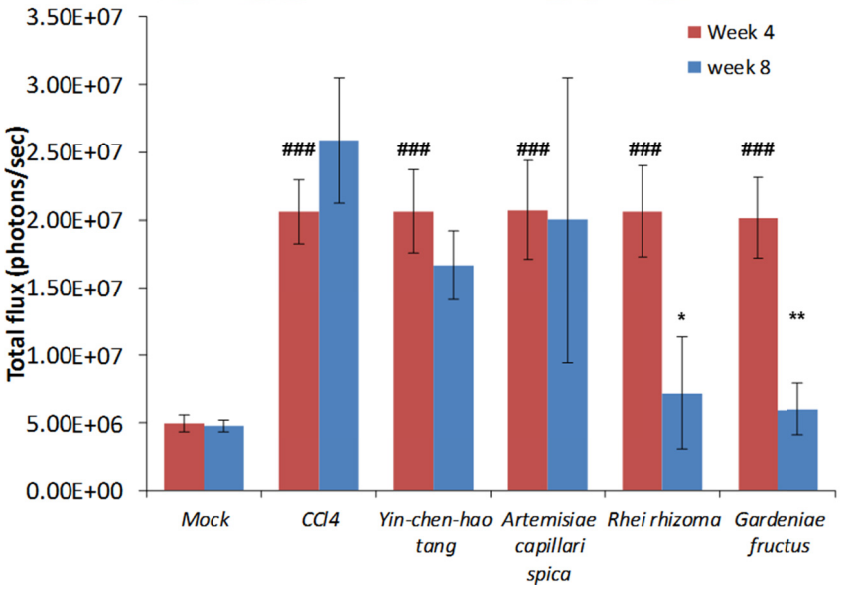

圖 4.5 茵陳蒿湯處理後小鼠活體 NF-κB 冷光的效應。基因轉殖鼠經過投予 CCl_4 或茵陳蒿湯及其組成單方，並且在各個指定時間內照影。(A) 活體影像，小鼠身上的冷色系到暖色系從藍到紅的顏色，分別代表冷光表現強度，單位為 photon/sec，圖中每個組別皆有 5 重複。(B) 全身影像冷光值的定量統計圖。冷光值以平均值 ± 標準差，組別與 mock 比較, ###表示 $p<0.001$；與 CCl_4 比較*表示 $p<0.05$，**表示 $p<0.01$。

(A)

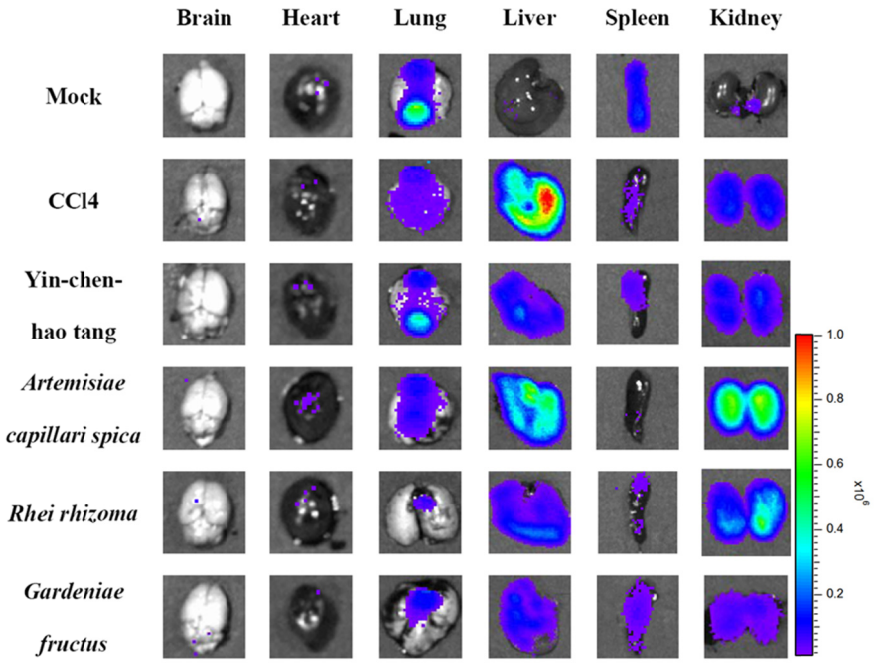

(B)

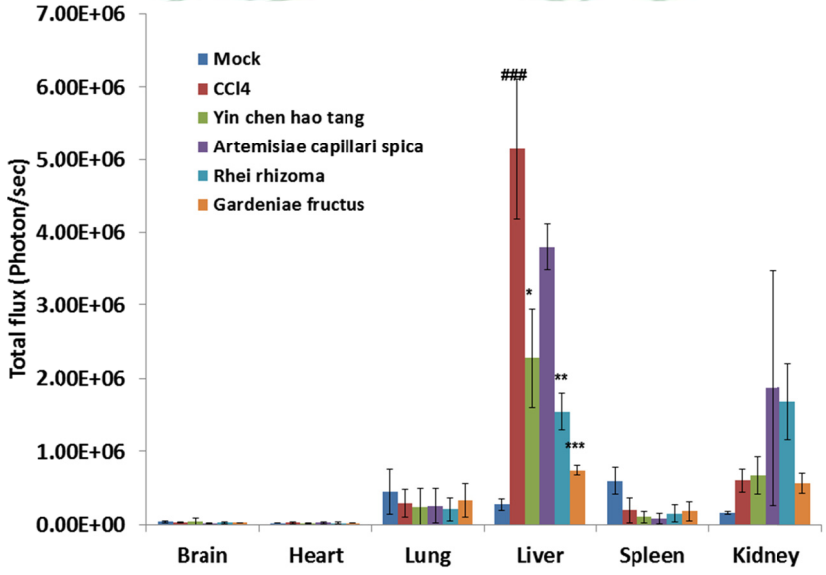

圖 4.6 基因轉殖鼠投予茵陳蒿湯後實質臟器的 NF-κB 活性。基因轉殖鼠經過投予 CCl_4 或或茵陳蒿湯及其組成單方，8 週後小鼠進行解剖及器官的照影。 (A) 器官剖檢照影，器官上的冷色系到暖色系從藍到紅的顏色，分別代表冷光表現強度，單位為 photon/sec，圖中每個組別皆有 5 重複。 (B) 器官影像冷光值的定量統計圖。冷光值以平均值 ± 標準差，組別與 mock 比較， ###表示 $p<0.001$；與 CCl_4 比較，*表示 $p<0.05$，**表示 $p<0.01$，***表示 $p<0.001$。

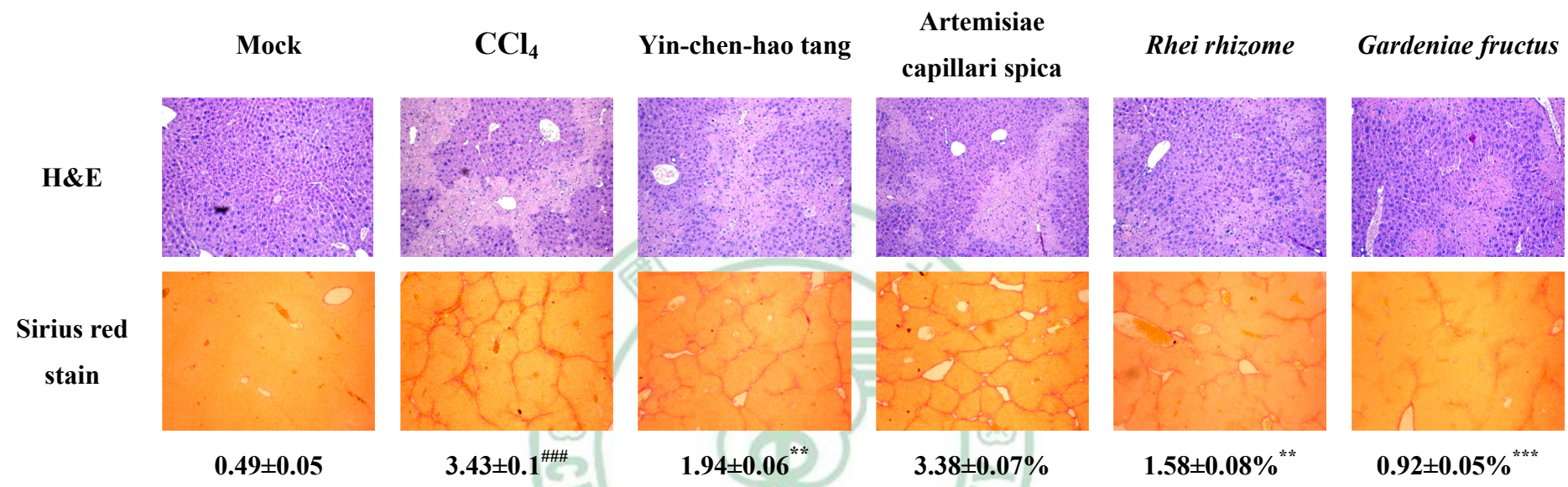

圖 4.7 肝臟利用 H&E 及天狼星紅進行組織染色。在組織病理檢查，基因轉殖小鼠投予 CCl_4 或茵陳蒿湯及其組成單方，經過 8 週處理後，小鼠進行犧牲解剖摘取肝及肝臟切片，接著進行 H&E (100 倍) 或天狼星紅染色 (40 倍) 鏡檢及拍攝。拍攝圖像皆有 5 重複。藉由天狼星紅對肝臟纖維化進行定量結果表示在其圖下，計算方式以纖維化區域(粉紅絲狀) 除以組織全部區域。結果以平均值±標準差表示。組別與 mock 比較 ###表示 $p<0.001$；與 CCl_4 比較**表示 $p<0.01$，***表示 $p<0.001$。

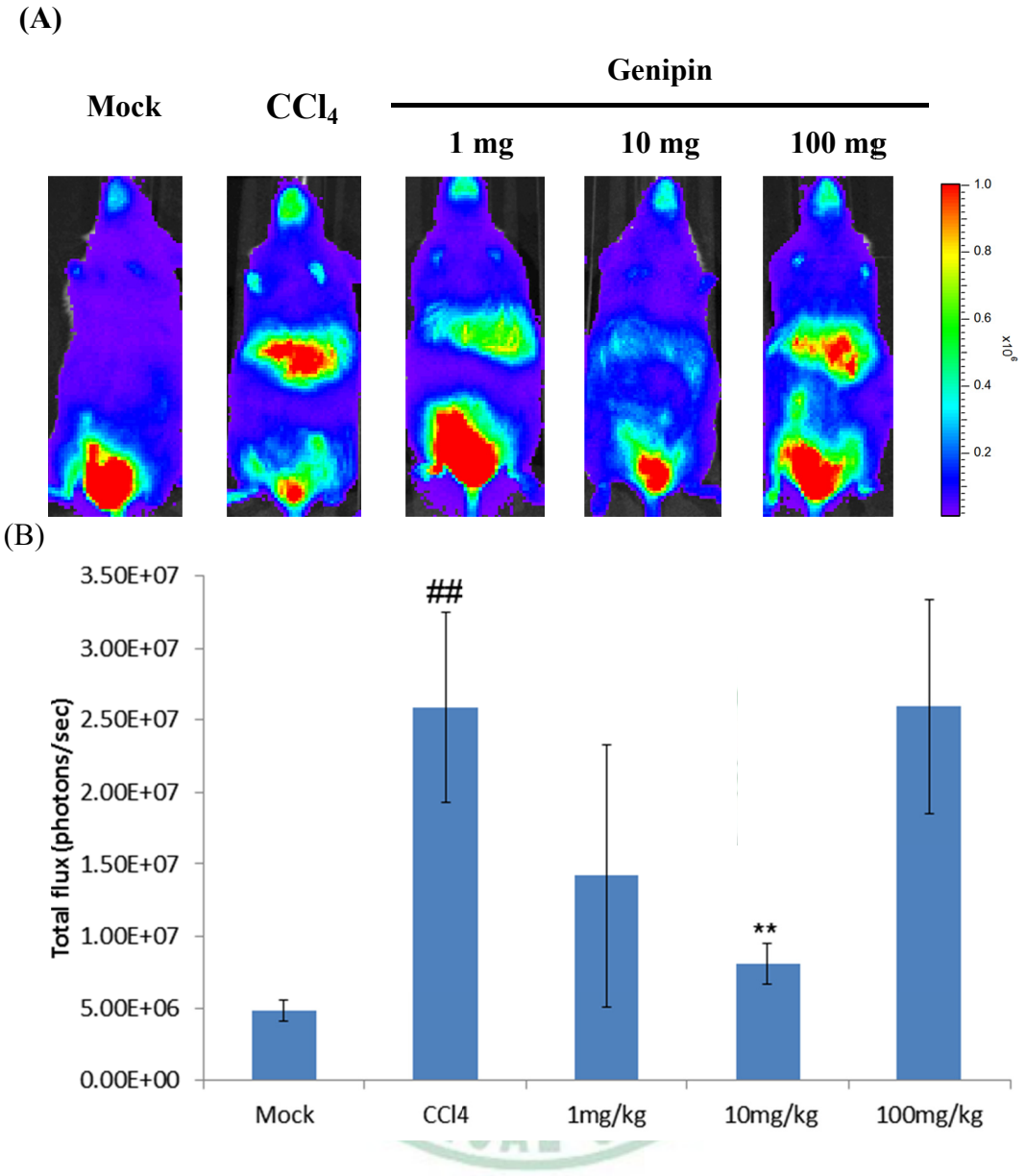

圖 4.8 Genipin 在小鼠肝炎模式中活體 NF-κB 冷光的效應。基因轉殖鼠經過投予 CCl_4 和/或 1、10、100 mg/kg 的 geinpin，並且在第 8 週照影。(A) 活體影像，小鼠身上的冷色系到暖色系從藍到紅的顏色，分別代表冷光表現強度，單位為 photon/sec，圖中每個組別皆有 5 重複。(B) 全身影像冷光值的定量統計圖。冷光值以平均值 ± 標準差，組別與 mock 比較， ##表示 $p<0.001$；與 CCl_4 比較**表示 $p<0.01$。

4.3 Genipin抗發炎分析

4.3.1 Genipin在體外(*in vitro*) 和體內 (*in vivo*) 影響的NF-κB活性

為了要評估genipin對LPS所誘發的NF-κB活性的影響，我們首先將LPS和不同濃度的genipin處理到HepG2/NF-κB的重組細胞，LPS很明顯誘發NF-κB的活性有1.8倍，而genipin顯著抑制NF-κB的活性呈現劑量反應(圖4.9)。而且在genipin處理過程中並無觀察到細胞毒性，這些結果顯示，genipin在體外實驗確實可以抑制NF-κB的活性。

接著，我們利用LPS及不同濃度的genipin處理到基因殖鼠，並且在4小時後進行偵測經NF-κB活性，如圖4.10所示。比較未處理LPS組，LPS組在腹部區域發出的冷光強度增加約14.7倍。然而，genipin在體內可顯著抑制LPS所誘發的冷光，且抑制效果呈也現出劑量反應 (1、10和100 mg/kg) 。這些結果暗示，genipin在體內抑制了NF-κB活性，因此我們選擇了100 mg/kg這個濃度進行更進一步的實驗。由於我們先前研究已經證明NF-κB所驅使的冷光與發炎反應有密切關係，這些結果也顯示，genipin在體內抑制了急性全身性發炎反應。

4.3.2 Genipin 在基因轉殖鼠各個實質臟器的 NF-κB 活性

我們進一步進行器官剖檢的影像照影，用以評估genipin的主要作用標的器官，如圖4.11所示。結果發現處理LPS的基因轉殖鼠其各個器官的冷光強度比對照組高，尤其是肝臟、脾臟、胃及小腸等器官冷光強度明顯的增加。而經過投予genipin後，在腦、心臟、肝臟及腎臟的LPS所誘發冷光都有明顯的下降。我們發現genipin在腦、心臟、肝臟及腎臟有各個不同程度顯著差異。因此，我們接著利用cytokine ELISA、免疫組織化學染色進行分析，進一步我們萃取這些器官的的RNA利用DNA microarray分析genipin的作用基因。

4.3.3. Genipin 抑制IL-1β 和 TNF-α表現

IL-1β和TNF-α是急性發炎反應的細胞因子，大量的產生表示開始急性的發炎並導致後端的發炎反應 (97) 。我們進一步利用ELISA和免疫組織化學染色分析IL-1β和TNF-α，以驗證genipin是否抑制全身性發炎反應。如圖4.12所示，ELISA分析結果，LPS組的小鼠血清中IL-1β和TNF-α的濃度分別為969 ± 47 pg/ml和339 ± 25 pg/ml。然而，genipin的投予組降低了IL-1β和TNF-α的表現量。利用IL-1β和TNF-α抗體進行免疫組織化學染色結果顯示，與mock組相比，在LPS組的器官有大量褐色的IL-1β或TNF-α活性細胞，而且在LPS組棕色區域的比例均有顯著增加 (圖4.13) 。然而，genipin這些器官IL-1β和TNF-α活性區的比例顯著下降。所以Genipin組的IL-1β和TNF-α在血清和器官表現量都有明顯下降，這結果顯示，genipin會透過抑制cytokine的產生進而抑制發現反應。

4.3.4 Microarray分析genipin調控的基因表現圖譜

Microarray 結果先利用 Gene Expression Pattern Analysis Suite v3.1 進行分析腦、心臟、肝臟和腎臟受到LPS和/或genipin處理後具有差異的基因表現變化。在microarray上的全部30968個基因中，在LPS組及LPS/Genipin組有79個基因呈現有差異的倍率變化。我們更進一步利用WebGestalt工具將這些基因進行定義，並且經過分析獲得genipin在這些器官中的細胞生理狀態變化的總覽。Gene ontology類別 (GO categories) 只要是它們包含至少兩個基因且其p值小於0.01就會被認定為該GO類別成立。如圖4.14所示，大部份的顯著表現差異的基因被歸類到免疫相關 (immunity-related) 的GO類別裡，例如抗原生成及抗原呈現 (antigen processing and presentation) 、B細胞分化的調

控、發炎反應以及急性期發炎反應等類別。只有少數基因被歸納到代謝類別裡。

這些基因反應圖譜，我們進一步利用TIGR Multiexperiment Viewer 進行hierarchical clustering分析。如圖4.15所示，有趣的是，從結果中發現到在這些器官中受LPS所響影到的基因，全被genipin給反向調控。大多數的基因表現都被LPS給活化，而genipin則下調了LPS所誘發的基因表現。只有5個基因，包括Endothelial-specific receptor tyrosine kinase、Notch-regulated ankyrin repeat protein (Nrarp) 、SH3-binding kinase 1、Sucrose nonfermenting protein (SNF) -related kinase 以及 Lysosomal-associated protein transmembrane 5 (LAPTM5) 基因，分別是由LPS所下調，而geinpin活化了這些受LPS抑制基因表現。此外，在這些顯著差異的基因中，大約有三分之一的基因是屬於chemokine ligand、chemokine receptor和IFN-induced protein基因。這些結果顯示，genipint可以抑制並且下調LPS所誘發的chemokine ligand、chemokine receptor和IFN-induced protein。

在這些表現具有顯著差異的基因，我們也Genomatix Applications軟體及資料庫分析了基因與基因間的相互關聯度。基因間的關聯度是根據Genomatix Knowledge Base，以及DNA的啟動子 (promoter) 序列分析。有趣的是，大多數基因都直接連接NF-κB並且以NF-κB為一個核心的網路結構 (network) (圖4.16) 。這些結果顯示，NF-κB可能扮演著genipin調控基因network裡的主要角色。

4.3.5 利用 qPCR 驗證 genipin 新穎調控基因的表現

Microarray分析結果顯示，有三分之一有差異變化的基因屬於chemokine ligand、 chemokine receptor及 IFN-induced protein族群的基

因，因此我們接著利用qPCR 的分析加以驗證microarray 的結果。我們利用qPCR將IFN-induced protein 這族群的基因進行定量分析，包含Iigp1 和 Ifi202 基因。因為這些基因的表現在我們的Network分析裡顯示會直接的受到NF-κB調控。如表4.4所示，與mock組相比較下，LPS組的 Iigp1 和 Ifi202 基因表現程度分別為6.62倍及55.4倍。然而，LPS上調的Iigp1 和 Ifi202 基因在LPS/genipin組是被下調的。與mock組相比較下，LPS/genipin組的Iigp1 和 Ifi202 基因分別為5.17倍及28.33倍。qPCR與microarray分析的數據一致，這結果顯示genipin 會下調LPS所誘發的 Iigp1 和 Ifi202基因表現。

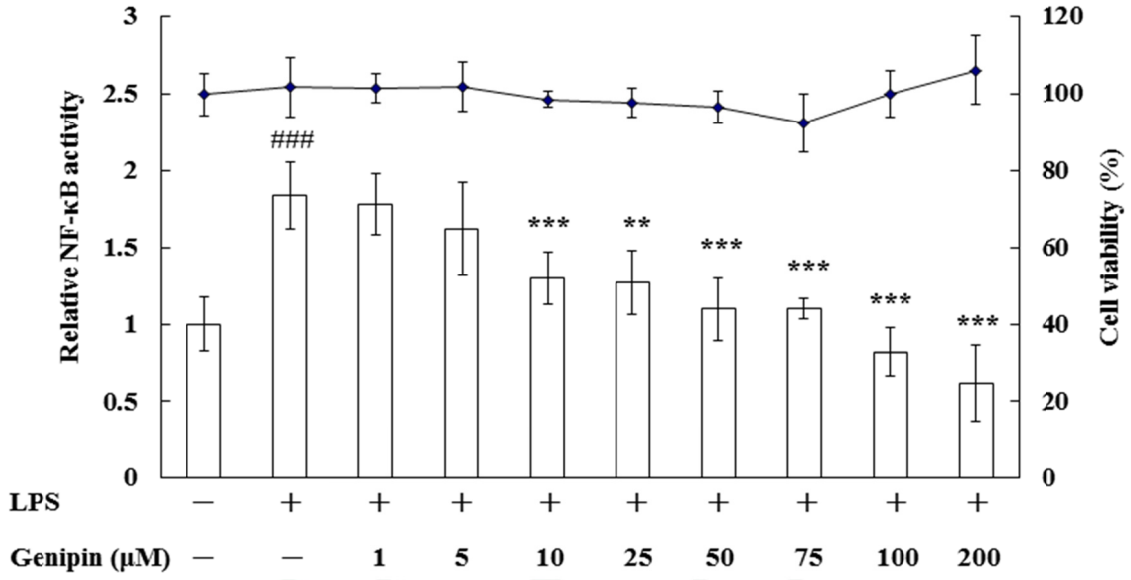

圖 4.9 Genipin 抑制 HepG2 細胞 NF-κB 的活性。帶有 NF-κB/luc 的 HepG2 重組細胞以 100 ng/ml LPS 及不同濃度的 genipin 處理，並於 37℃培養 24 小時後，分別利用冷光儀測定冷光活性及 MTT 試劑測試細胞存活率。長條圖顯示出 NF-κB 活性的關係。上方的折線圖表示細胞存活率，單位以%表示並且與 solvent 控制組比較計算存活率。所得結果皆有三重複以平均值±標準差表示。與 mock 組比較，###表示 $p<0.001$；與 LPS 組比較，**表示 $p<0.01$，***表示 $p<0.001$。

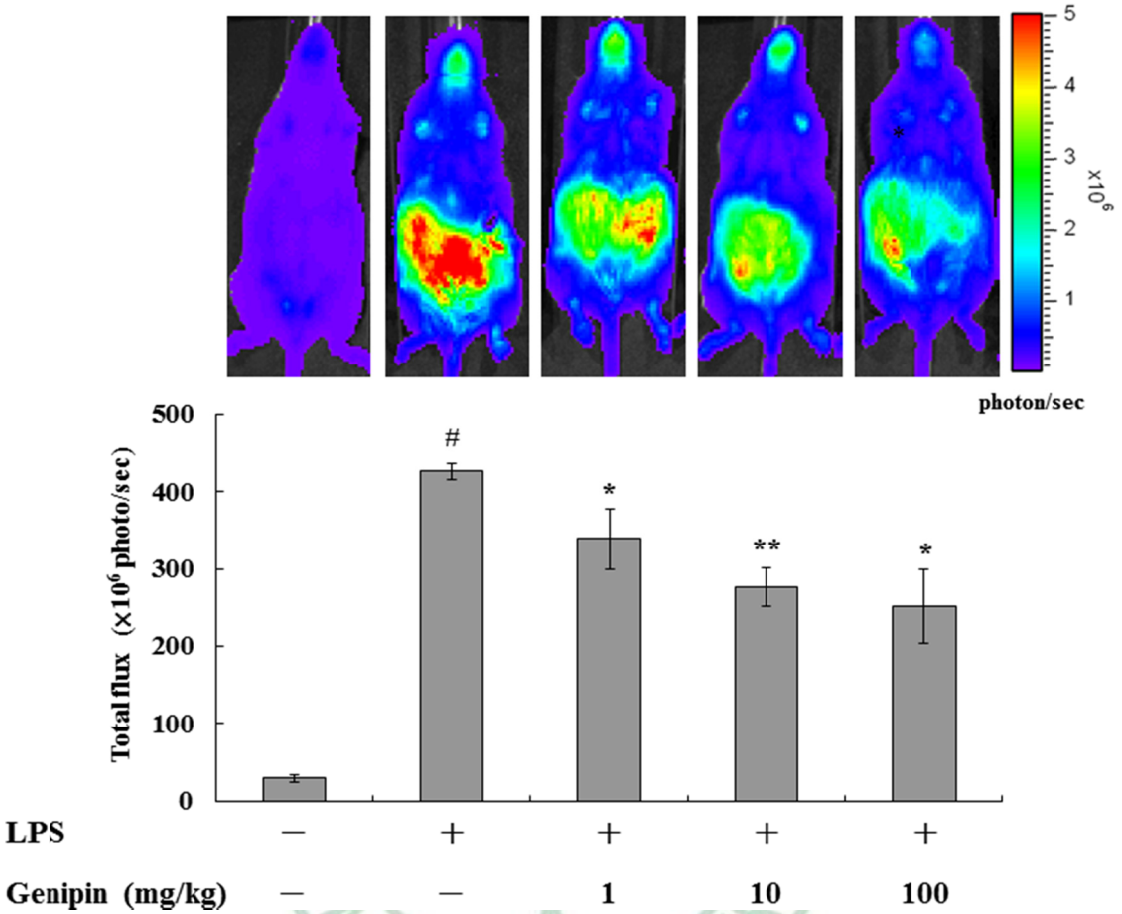

圖4.10 Genipin抑制基因轉殖鼠NF-κB的活性。將LPS (4 mg/kg) 及genipin 以1、10、100 mg/kg的劑量腹腔注射方式給予，小鼠經過4小時之後，腹腔注射方式給予D-luciferin，5分鐘之後進行影像分析。上方圖示為活體影像結果，小鼠身上的冷色系到暖色系從藍到紅的顏色，分別代表冷光表現強度，單位為photon/sec，圖中每個組別皆有5重複。全身影像冷光值的定量統計圖。冷光值以平均值 ± 標準差，與mock組比較， #表示$p<0.05$；與LPS比較 *表示$p<0.05$, **表示$p<0.01$。

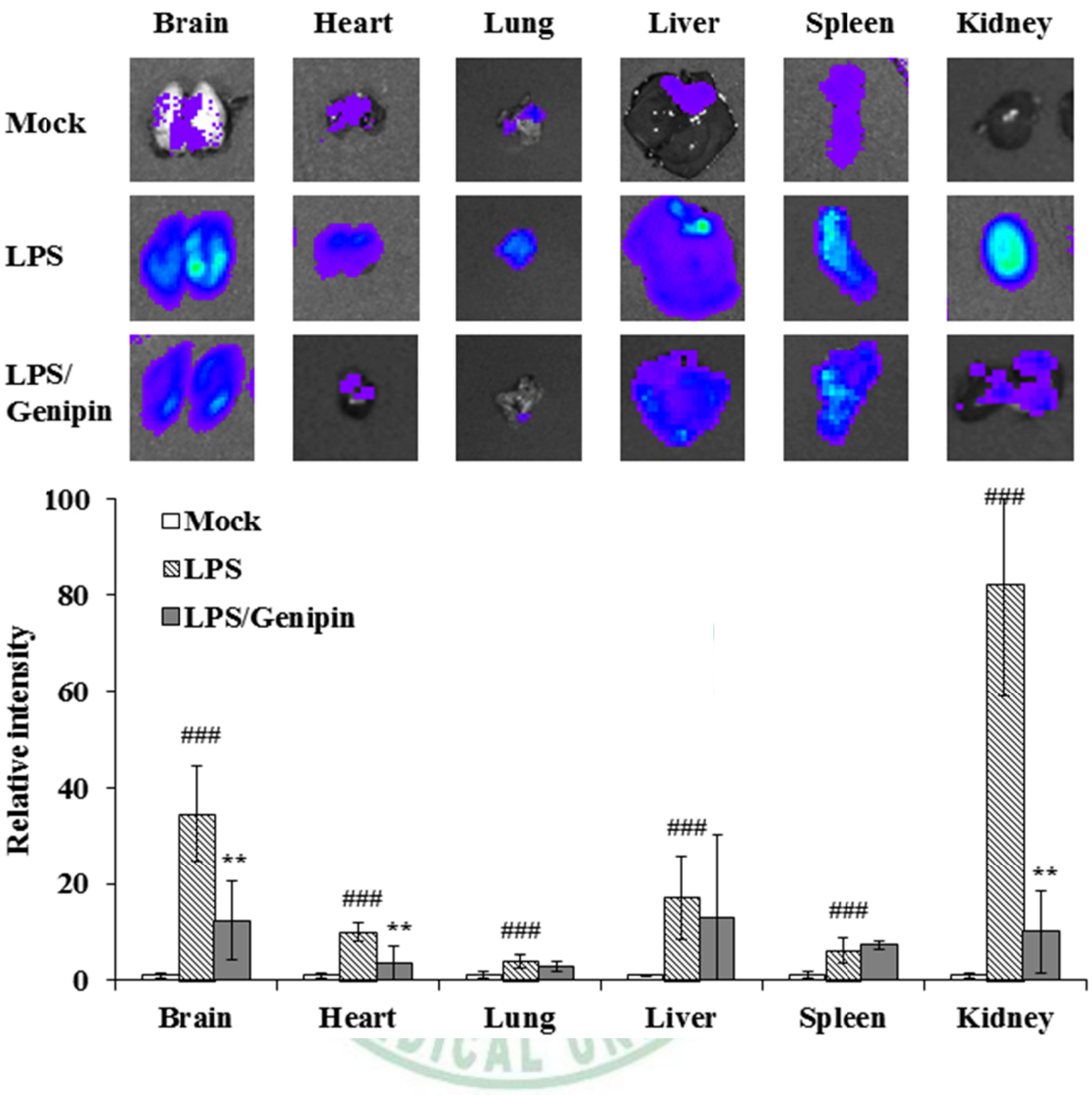

圖4.11 NF-κB活性在各個不同器官上的表現。將LPS (4 mg/kg)和/或 Genipin 以100 mg/kg的劑量腹腔注射方式給予，小鼠經過4小時之後，腹腔注射方式給予D-luciferin，5分鐘之後小鼠快速的經過解剖摘取器官並進行影像分析。每個組別皆有5重複的影像。器官冷光質的定量分析結果顯示在下方。結果以相對冷光強度表示，並且全都以mock組冷光值為基準。冷光值以平均值 ± 標準差，與mock組比較， ### 表示$p<0.001$；與LPS比較**表示$p<0.01$。

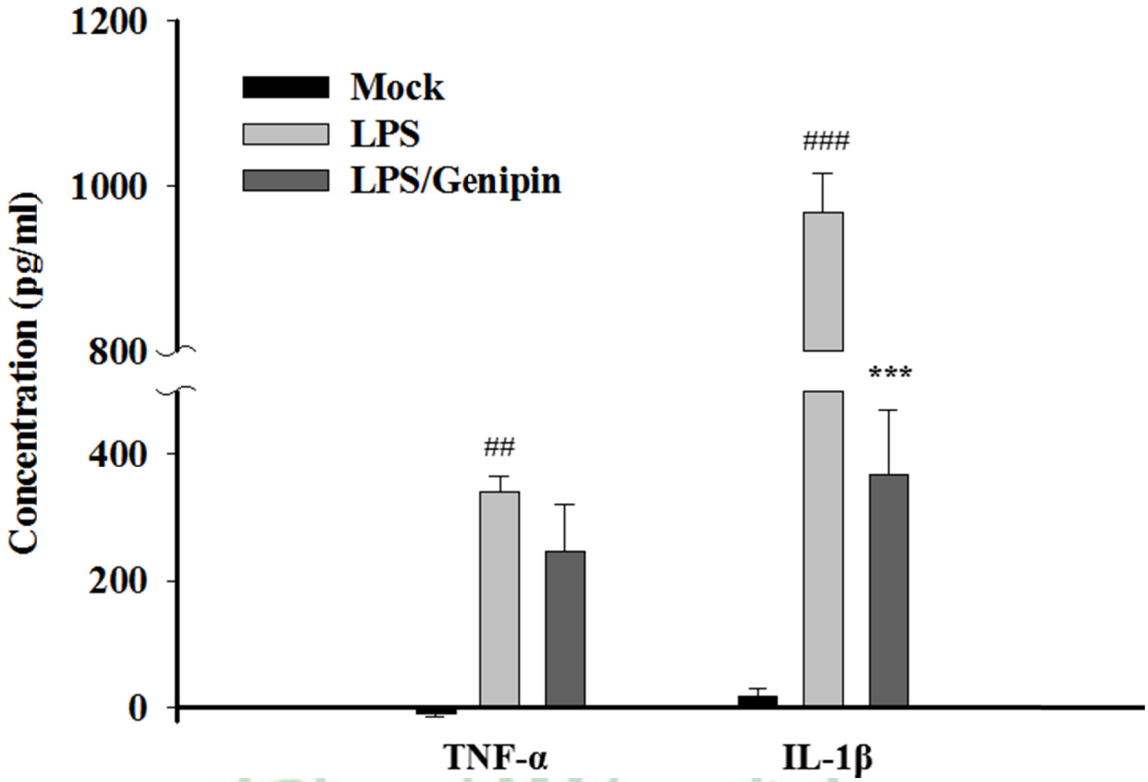

圖4.12 Genipin抑制LPS誘導IL-1β和TNF-α產生的效果。將LPS (4 mg/kg) 和/或Genipin 以100 mg/kg的劑量腹腔注射方式給予。之後，我們利用ELISA偵測IL-1β和TNF-α在血清裡的濃度。濃度值以平均值 ± 標準差，與mock組比較，##表示$p<0.01$，###表示$p<0.001$；與LPS比較***表示$p<0.001$。

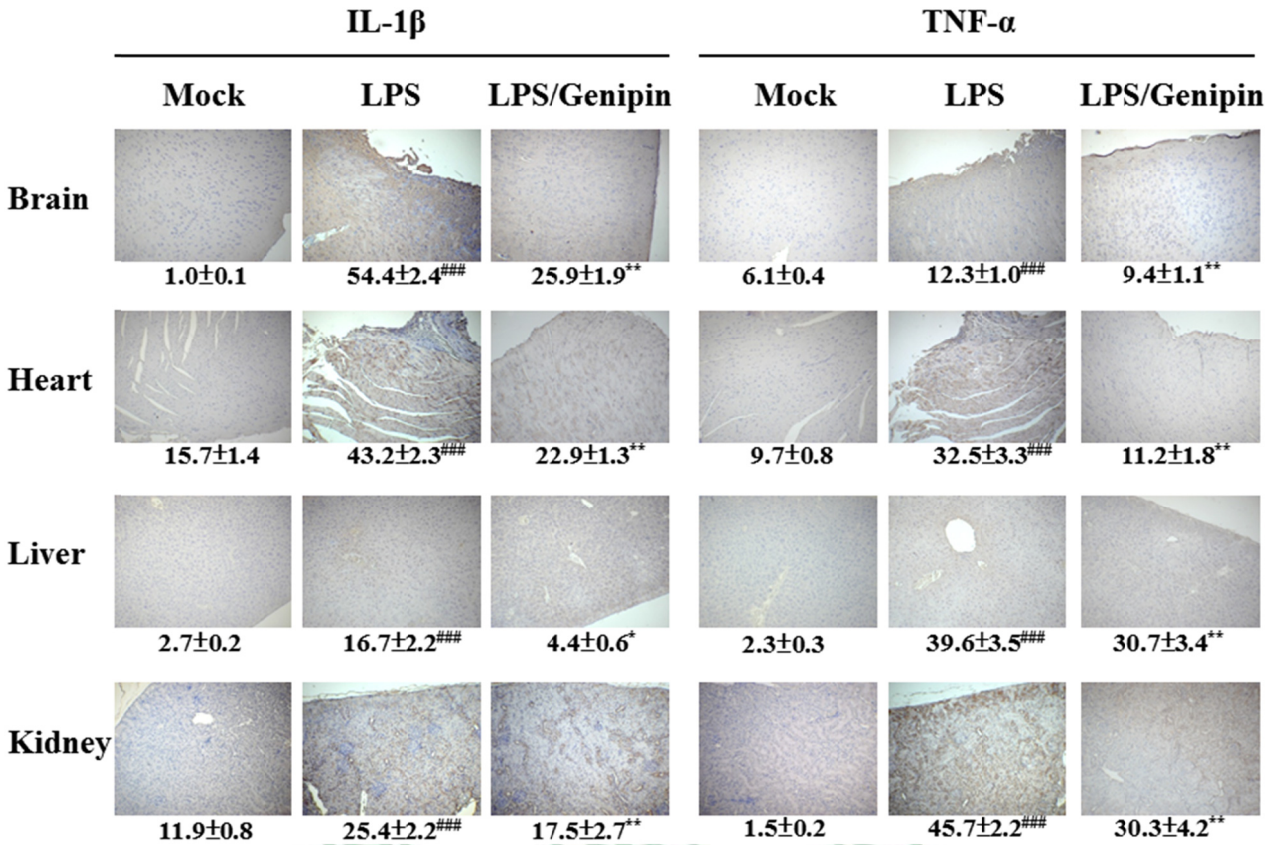

圖 4.13 腦、心臟、肝臟和腎的免疫組織化學染色。將LPS (4 mg/kg)和/或Genipin 以100 mg/kg的劑量腹腔注射方式給予。取得器官切片後，使用IL-1β和TNF-α抗體進行免疫組織化學染色，再以顯微鏡100倍觀察。IL-1β和TNF-α陽性區域 (%) 的定量數值顯示在圖下方。定量值以平均值±標準差，與mock組比較，###表示$p<0.001$；與LPS比較*表示$p<0.05$，**表示$p<0.01$，圖中每個組別皆有5重複。

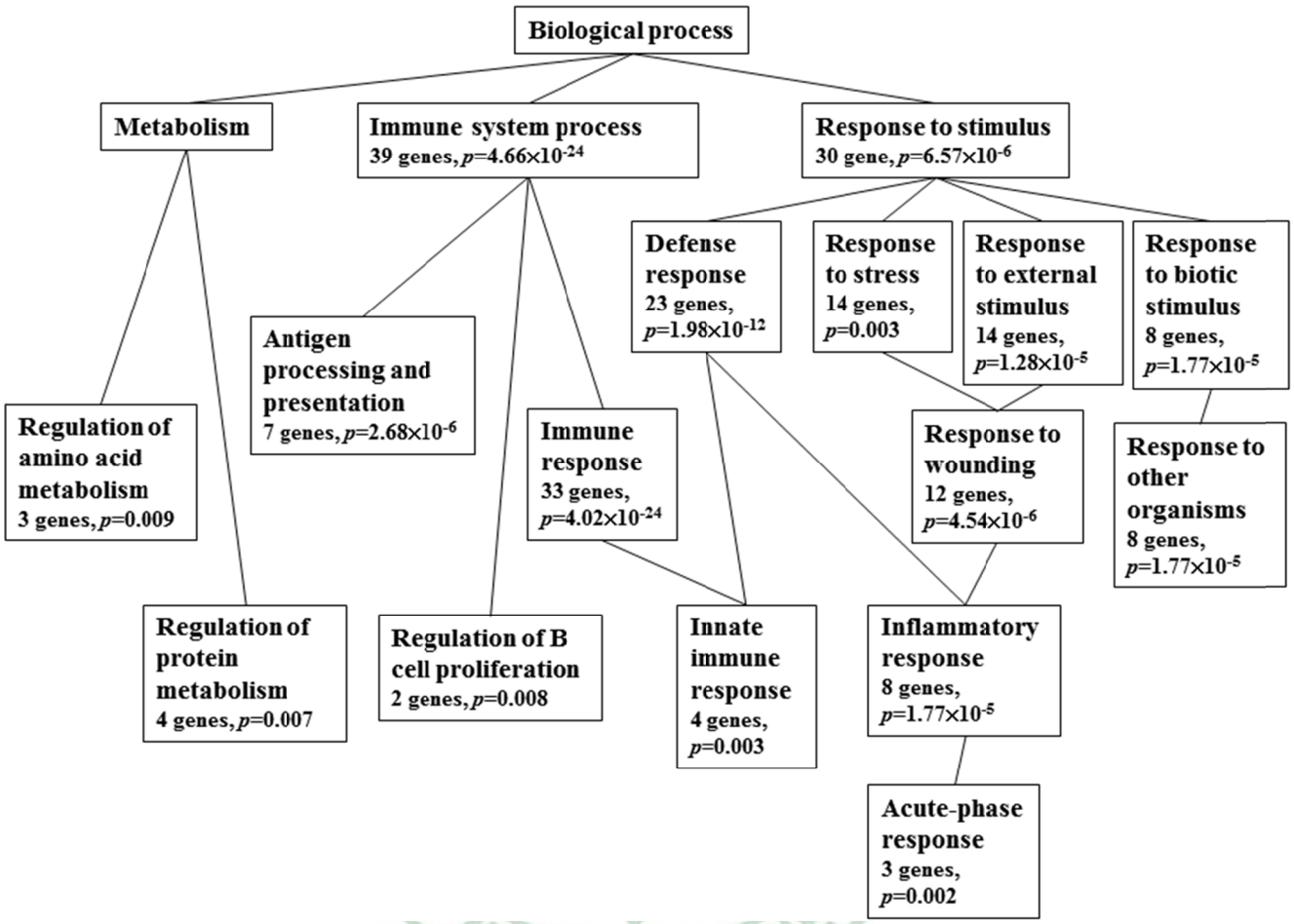

圖 4.14 以 GO 分析在 LPS 和 LPS/genipin 兩個組別中腦、心臟、肝臟和腎臟具有差異性的基因。利用 Gene Ontology Tree Machine 會將有表現差異的基因進行組織及分到該類別，圖中所示為 $p<0.01$ 且最少有兩個基因的 GO 類別就會被顯示出來.

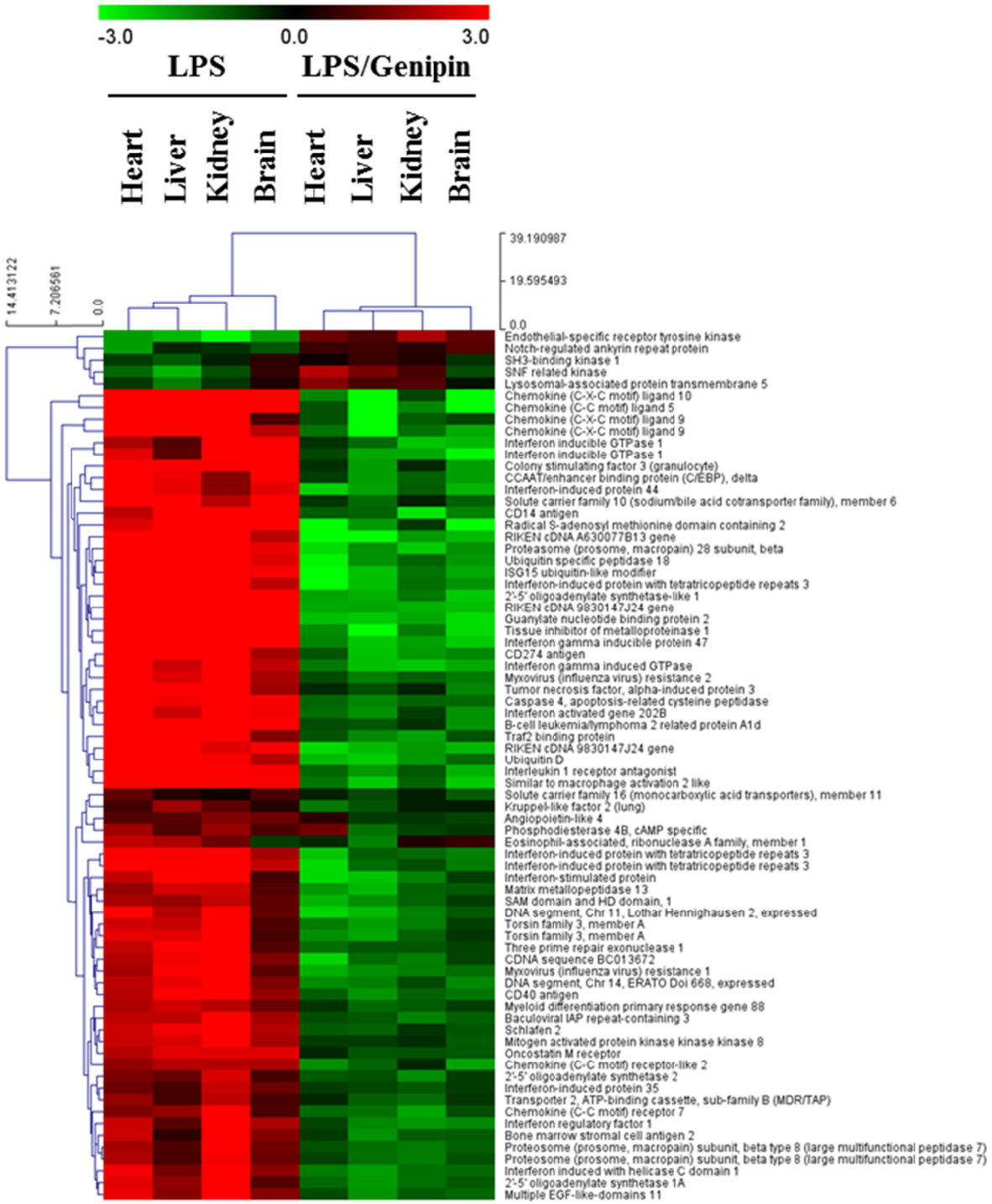

圖 4.15 以 Hierarchical clustering 分析在 LPS 和 LPS/genipin 兩個組別中，腦、心臟、肝臟和腎臟具有差異性的基因。經過標準化 (Normalize) 後的數據 log2 值在圖中的以顏色漸層的方式呈現 (數值轉換色差顯示在最上方)。基因的轉錄表現上升以紅色表示，表現下降以綠色表示。

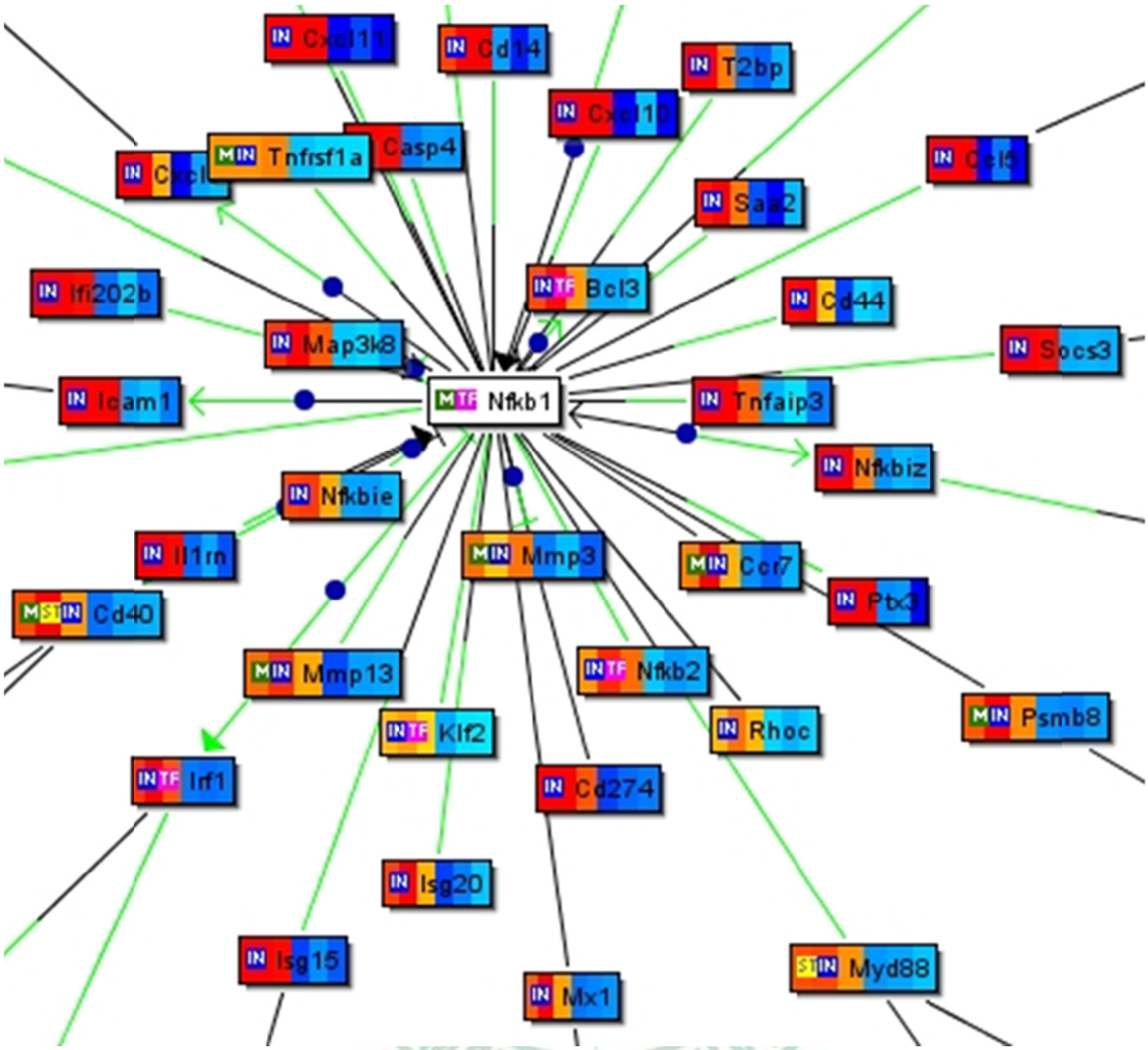

圖 4.16 以 Network 分析在 LPS 和 LPS/genipin 兩個組別中，腦、心臟、肝臟和腎臟具有差異性的基因。輸入的基因在圖中的格子裡會被標上 IN 藍底，轉錄因子 (transcription factor) 的基因在圖中的格子裡會被標上 TF 粉紅底，基因的產物會被標上 ST 黃底，這些標記皆有互相關聯，都是屬於 Genomatix 訊息傳遞路徑的一部份。在程式中，如果一個基因彩色方格有標記是一個轉錄因子且可以接合到一個已知且有這個轉錄因子結合位的 promoter 時，這個連結線將會以一半的綠色線靠近具有這個轉錄因子結合位的基因這邊。

表 4.4 qPCR 定量 Iigp1 和 Ifi202 表現程度。

Sample	Average C_T of target	Average C_T of GAPDH	ΔC_T[a]	$\Delta\Delta C_T$[b]	Relative to mock
Iigp1					
Mock	26.10±0.04	17.13±0.05	8.96±0.06	0.00±0.06	1.00
LPS	23.31±0.05	17.07±0.02	6.24±0.06	-2.72±0.06	6.62
LPS/Genipin	23.84±0.07	17.25±0.01	6.59±0.08	-2.37±0.08	5.17
Ifi202					
Mock	32.11±0.11	17.13±0.05	14.97±0.12	0.00±0.12	1.00
LPS	26.25±0.04	17.07±0.02	9.18±0.05	-5.79±0.05	55.40
LPS/Genipin	27.40±0.02	17.25±0.01	10.15±0.02	-4.82±0.02	28.33

[a] The ΔC_T value is determined by subtracting the average C_T value of GAPDH gene from the average C_T value of target gene. The standard deviation of the difference is calculated from the standard deviations of the target gene and GAPDH gene.

[b] The calculation of $\Delta\Delta C_T$ involves subtraction by the ΔC_T calibrator value. This is a subtraction of an arbitrary constant, so the standard deviation of$\Delta\Delta C_T$ is the same as the standard deviation of ΔC_T value.

第五章 討論

5.1 NF-κB活體即時性肝炎報導平台之建立

本研究，我們利用 NF-κB 活體即時性肝炎報導平台，並以 silymarin 進行測試。利用這個平台我們發現 silymarin 可以依投予時間穩定的下降肝臟 CCl_4 所誘發的 NF-κB 活性。此外，NF-κB 活性與肝纖維化在基因轉殖鼠上所發出的冷光影像關係成正比，因此 NF-κB 活體即時性影像可以當作肝臟發炎及肝纖維化的即時偵測的平台。新興的生物冷光影像具有相當高靈敏度和即時性非侵入性的技術，可以即時的在活體的報導疾病的進程與評估治療的效果。這個技術目前已被應廣泛的應用在微生物感染的監控、腫瘤細胞的轉移、腫瘤標記及生物體-生物材料的交互作用 (62, 98-100) 。進一步，生物冷光影像照影也被用來預測小鼠肝腫瘤的大小 (101) 。我們先前的研究，已經構築帶有 NF-κB/luciferase 基因的基因轉殖鼠並且也直接的證實了 NF-κB 驅使的冷光可以用來評估生物體-生物材料間的交互作用、評估放射線對生物體的反應、評估香草醛 (vanillin) 在體內發炎性腸病的效果以及分析牛樟芝抗發炎的效果 (62, 64, 65, 102) 。本研究中，我們成功的利用生物冷光影像照影評估 CCl_4 所誘發的肝損傷程度。利用 CCl_4 進行誘發肝損傷是目前導致肝毒性的最佳的方法，並且也是最常使用來篩選抗肝毒性或保肝藥物的模式 (48) 。CCl_4 的代謝機轉主要是由 cytochrome p450 系統轉化成三氯甲基以及氯甲基過氧自由基。這些來自於 CCl_4 的代謝物會跟生物體內的大分子形成共價鍵結進而導致脂質過氧化，而此結果會造成肝臟細胞脂肪浸潤和肝臟漸進式的從肝組織傷害到形成纖維化 (49) 。幾十年來，CCl_4 已經在許多研究中被廣泛應用在誘發各種實驗動物肝損傷的平台上 (50, 51) 。而且經由 CCl_4 所誘發的肝硬化的大鼠組織也顯示出與人類的肝硬化

相似 (52) 。傳統上，藉由致肝毒性物質所誘發的肝損傷以及肝纖維化可以利用肝組織的變化和血清生化指標中的丙胺酸轉胺酶、天門冬胺酸轉胺酶、鹼性磷酸酶及谷胺酸轉化酶濃度來進行評估 (53-55) 。由於由各種病因引起的持續性肝臟發炎進而導致肝纖維化又 NF-κB 在調節發炎反應發揮了關鍵作用 (1) 因此我們嚐試應用應用 NF-κB 基因轉殖鼠來報導 CCl_4 所誘發的肝纖維化。藉由天狼星紅染色和免疫組織化學染色的分析，可以顯示 CCl_4 所誘導的專一性肝臟 NF-κB 活化和冷光強度與肝纖維化成正相關。這個結果顯示，我們利用 NF-κB 生物冷光影像應用在 CCl_4 誘發肝纖維化的動物模式上是可行的。

Silymarin 是一個為人所熟知用來治療肝病的保肝劑 (56) 。它目前已有許多研究顯示可能具有抗氧化、抗脂質過氧化、抗纖維化、細胞膜的穩定、免疫調節以及肝臟再生的活性 (57-61) 。 Silymarin 在許多實驗性的肝病研究平台上提供了很有效的保護作用。因此目前也被應用在臨床治療酒精性肝病、肝硬化、蕈類肝中毒以及藥物所引發的肝病等 (61) 。在本研究中，生物冷光影像照影顯示口服 silymain 可以專一的下降 CC_4 在肝臟所誘發的 NF-κB 的活性。而且藉著 silymarin 的投予治療，我們也觀察到降低 NF-κB 的活性跟降低肝纖維化的確有相當大的關聯，顯示 NF-κB 活體冷光影像照影可以用來評估在活體內 silymarin 的治療效果的可行性。更進一步，我們也發現，silymarin 在下降 CCl_4 所誘發的肝臟 NF-κB 活性具有很好的專一性。

接著，我們利用NF-κB活體冷光影像導引轉錄學平台分析進行探勘新穎標的與silymarin的保肝機轉。先前的研究指出，silymarin抗纖維化和抗發炎的效果主要是關係到TGF-β1 pathway (103) 。Silymarin

可透過下調大鼠在膽道纖維化的TGF-β1 mRNA進而抑制profibrotic procollage-αa和TIMP-1基因的表現 (57) 。進一步，肝臟在受到鄰苯三酚曝露下，silymarin 可以調節有關氧化壓力 (oxidative stress) 、細胞週期 (cell cycle) 、細胞骨架 (cytoskeletal network) 、細胞-細胞附著 (cell-cell adhesion) ，胞外基質、發炎 及細胞凋亡的基因 (104) 。本研究中，microarray的數據顯示在CCl_4誘發肝纖維化之下，silymarin調控TGF-β1-associated、TGF-β-induced apoptosis 及 TGF-β-mediated pathway，此結果與先前的文獻一致。此外，我利用microarray分析silymarin治療組的肝基因反應圖譜，發現silymarin除了可透過調控TGF-β-mediated pathway 降低CCl_4所誘發的NF-κB。更一步我們在這microarray的數據中也發現了一些新穎的標的基因，在NF-κB活體即時性影像導引轉錄體學的分析，某些Cox基因被silymarin 下調。我們新發現silymarin可下調細胞骨架基因和粒線體電子傳遞鏈基因的表現。目前已知CCl_4可以誘發細胞骨架的再組織，並且進一步造成誘發肝星狀細胞 (hepatic stellate cells) 分化成類肌纖維母細胞 (myofibroblast-like cells) (105) 。Silymarin 下調一群組成細胞骨架的基因，我們推測silymarin 可能透過抑制細胞骨架的再組織而抑制肝星狀細胞的轉型，進而達到改善肝纖維化的效果。CCl_4誘發肝纖維化的過程牽涉到自由基產物，而自由基會顯著的導致整個粒腺體呼吸鏈狀態的改變 (106-108) 。電子傳遞因子被歸納為4種複合體如：NADH reductase、uccinate reductase、cytochrome *c* reductase及 Cox (109) 。

Cox扮演氧化機轉很重要的角色，並且是粒腺體電子傳遞鏈中電子從cytochrome *c*傳送到氧分子*的*終點反應因子 (109) 。從先前的研究與文獻中發現，在大鼠經CCl_4誘發的肝纖維化中， NADH reductase的活性會下降，且Cox 的活性會增加 (106, 108, 110) 。在我們的結

果也顯示，Cox的一些基因表現被CCl_4給提高了。而NADH reductase的下降與活性損失會導致電子連結到O_2^-氧以及超氧化陰離子(superoxide anion) 的產生，進而導致病態粒腺體的呼吸鏈氧吸收量上升。隨後， CCl_4促進了電子轉移到氧分子上並且驅使粒線體生產ATP進而提高Cox的活性 (108) 。另一方面，以前的研究顯示，從大鼠研究中發現silymarin會抑制粒線體氧氣的消耗量和增加NADH的還原酶還原鐵的活性大於基本值的量 (111, 112) 。此外，我們的結果顯示，比較於Mock組，silymarin可以降低CCl4所誘導大於基礎表現量的Cox基因的表現。這些結果也暗示，silymarin可能會抵消CCl_4造成的粒線體電子傳遞鏈變化，因此可能關係到silymarin是如何改善CCl_4所誘導肝纖維化的其中一個因素。

5.2 茵陳蒿湯及其組成在肝炎之療效分析

過往在中藥抗慢性肝炎在活體的研究，大多都是利用組織病理實驗以及血清生化指標加以評估，但這種方式需要長達數週至數個月的時間，而且需要犧牲相當數量的動物才能達到客觀的標準。除了活體模式外，以疾病分生為標的之細胞模式也被應用於中藥抗肝炎的搜尋。雖然以疾病分生標的之細胞模式進行搜尋，確實可以加快藥物的評估，但是體外試驗證實有效的藥物，進入活體試驗時的失敗率相當高。此外，有許多方法可以直接以活體試驗偵測肝炎分生標的的活性，例如：免疫組織化學染色法 (immunohistochemistry stain; IHC) 、原位雜交反應 (in situ hybridization) 等，但這些方法都無法即時性地反應動物體內肝臟發炎的現象。以茵陳蒿湯為主要對象，以 NF-κB 基因轉殖鼠配合四氯化碳誘發慢性肝炎，以即時性分子影像及 microarray 為分析工具，配合組織染色切片、專一性纖維化蛋白染色，首先驗證茵陳

蒿湯在治療肝炎的效果，進一步從茵陳蒿湯拆解成單一中藥探討主要的療效藥物，並從該單味藥中找到肝炎的致效成份並從該單味藥中找到肝炎的致效成份。在前述的模式以 silymarin 測試的研究中，我們已經驗證該平台是非常可行的，而中藥的抗肝炎研究模式中，欠缺的部份如即時的評估療效，以及中藥投予週期、劑量等也可以利用此平台來加以分析。

以往有許多研究顯示，茵陳蒿湯在大鼠長期口服投予之下具有相當好的抑制肝纖維化 (35, 45-47) 。茵陳蒿湯透過抑制interferon (IFN)-γ和IL-12產生而改善小鼠被concanavalin A (con A)所誘發肝炎 (113) 。茵陳蒿湯在膽汁淤積性肝纖維化的大鼠模式中也有緩解肝纖維化的效果 (114) 。我們的結果也顯示，在利用活體冷光影像照影技術，CCl4所誘發的肝炎經過4週的茵陳蒿湯治療的確有一定程度的緩解。茵陳蒿湯在許多不同的肝纖維化動物模式中，都有相當好的效果，進一步，在這些研究中，也有被提出可能的致效成份是哪些。有文獻指出，茵陳蒿湯裡面的致效成份可能是大黃裡的Emodin (46) ，有的則指出可能是由Genipin所扮演致效成份 (47) 。在此研究中，我們將茵陳蒿湯拆方分為茵陳蒿、大黃及梔子三組各別進行測試。從結果當中發現，以大黃及梔子在降低CCl4所誘發的NF-κB效果非常的好，其中又以梔子的效果最為明顯。

梔子在歷史上廣泛的被應用在臨床治療急性及慢性的肝病。梔子被研究最透徹的主要化物是genipin。因為現今研究大多以geniposide最終代謝物genipin來探討治療的效果及其機轉。先前的研究指出，從梔子萃取出來的geniposide可調節大鼠肝臟的cytochrome P-450-dependent monooxygenases、glutathione 及 glutathione S-transferase (115) 。Genipin可以抑制被IFN-gamma誘導過的巨噬細胞中IL-1beta、IL-6以及

IL-12p70 的生合成 (113) 。Genipin抑制傷口誘發的細胞轉移和增殖，同時也會下降collagen type I TGF-beta1 及 α-SMA 的mRNA 和 蛋白質表現，另外也 會抑制Smad2的訊息傳遞 (116) 。從我們的研究中也顯示，梔子無論在肝臟發炎指標NF-κB或是組織切片染色H&E的細胞完整度上來看都有很明顯的效果，另外利用天狼星紅染色觀察肝纖維化程度，在梔子組與CCl_4組比較也有很明顯的勝出。因此，我們推測梔子中所含的genipin可能為茵陳蒿湯的致效成份之一。

5.3 Genipin抗發炎機轉分析

梔子的果實是一個在傳統中醫藥用草本植物,已用於治療發炎，黃膽及肝病病上 (117) 。Genipin 是從geniposide代謝後的產物，而geniposide一開始被發現於梔子 (118) 。Genipin已被用來作為在食品工業中的藍色著色劑 (119) 。它還被用來當作生物組織定固的交聯劑 (120) 。Genipin 目前被研究出來有許多的藥理活性，例如抗微生物、保肝活性及神經再生的效果 (121, 122) 。Genipin在抗局部發炎的潛力也有被研究發表 (42, 123) ; 然而，Genipin在體內對抗全身發炎的反應機制及療效還有待理清。有幾個研究顯示，在一些細胞模式中genipin呈現出很好的抗發炎效果，例如在LPS處理過的腦膠質細胞 (brain microglial cells) 、被LPS誘發的小鼠巨噬細胞、人類白血病細胞以及大鼠腎上腺嗜鉻細胞瘤細胞 (adrenal pheochromocytoma cells) (124, 125) 。此外，以往的研究顯示，genipin具有抑制角叉菜膠 (carrageenan) 誘發的大鼠足蹠腫脹、巴豆油誘發的小鼠耳腫脹、concanavalin A誘導小鼠肝炎、鹽酸/乙醇誘導大鼠胃炎的重要外用消炎作用，和LPS誘發的大鼠腦發炎 (42, 113, 123, 126) 。在這項研究中，我們發現，genipin的腹腔給藥可以抑制NF-κB活性，並在許多器

官產生cytokine。這些結果顯示，genipin不僅可以外用，而且在全身體內抗發炎具有一定的潛力。

在這項研究中，我們利用即時性活體冷光影像監測genipin在體內抗急性全身性發炎模型的潛力。LPS是革蘭氏陰性菌外膜的主要組成結構成分。從革蘭氏陰性菌釋放LPS會活化一些細胞產生發炎性cytokine，例如巨噬細胞和中性粒細胞。隨後生產的cytokine會導致的粘附分子表現及發炎性細胞聚集 (127) 。有研究指出，LPS結合Toll-like receptor 4/CD14的複合體會活化NF-κB，然後上調發炎性cytokine的基因表現，例如TNF-α、IL-1β和IL-6 (127) 。此外，以往的研究顯示，LPS在一些關鍵器官如肝，腎，脾，肺和心臟所誘發的發炎反應差異很大 (128) 。在本研究中，證明了LPS確實可以誘發在急性全身性發炎反應期的血清和器官的cytokine表現量增加。而LPS誘發體內NF-κB活性與先前LPS引起NF-κB活化的全身性發炎反應結果相當吻合。此外，LPS會誘發NF-κB活性，所以結果顯示主要由LPS處理後受到影響的主要器官大部份座落在心，肝，脾，腎。因此，這些研究結果顯示，抑制冷光強度可以用來反映在體內即時的發炎情況。另外，除了先前已知的器官，LPS也對大腦產生了影響。

NF-κB生物冷光影像顯示LPS誘發大腦，心臟，肝臟，腎臟的NF-κB活性會受到geinpin的抑制。我們進一步的分析這些器官的基因表現譜，以闡明genipin的抗發炎機制。GO分類結果顯示，有差異的表現基因大部份是屬於免疫相關的GO類別。此外，很有趣的發現，genipin可以逆轉受到LPS影響的基因表現程度。值得注意的是，LPS活化了大部份的基因，但卻下調了endothelial-specific receptor tyrosine kinase，Nrarp，SH3-binding kinase，SNF-related kinase，和LAPTM5基因的表現像。 LAPTM5是一種溶酶體蛋白，特別是表現在骨髓和

淋巴系統。LAPTM5會反向調控B細胞的細胞表面受體 (BCR) 的表現量以及B細胞的活化促使的小鼠細胞溶酶體的BCR降解 (129) 。nrarp是一種小分子蛋白，轉錄由Notch signaling pathway調控。先前的研究已經證明，Nrarp會專一抑制T細胞的發育和造血系統 (130) 。Endothelial-specific receptor tyrosine kinase是一種受體，最主要參與胚胎血管的形成。也有研究指出，Endothelial-specific receptor tyrosine kinase的補充和活化NF-κB2的A20結合抑制物，進而抑制NF-κB活化 (131) 。LPS下調endothelial-specific receptor tyrosine kinase、Nrarp和LAPTM5基因的表現，暗示LPS可能促進B細胞活化、T細胞的發展和NF-κB活化。然而，genipin可能會抑制掉透過對這些基因的上調，進而抑制B細胞活化，T細胞的發育和NF-κB的活化。

在79具有表現差異的基因中，74個基因被LPS上調和genipn下調，這些基因有三分之一是屬於chemokine ligand、chemokine receptor、和IFN-induced protein 基因。會吸引Helper T細胞T_H1細胞趨化的基因，chemokine (C-X-C motif) ligand 9 (CXCL9) 、CXCL10和chemokine (C-C motif) ligand (CCL5) ，分別在本研究中被LPS上調和genipin下調。體外研究指出，CXCL9 (又稱為IFN-γ誘導的monokine) 和CXCL10 (又稱IFN-γ誘導蛋白10) 會刺激活化CXCR3陽性的T細胞和自然殺手細胞。而他們也是在傳染病和慢性發炎疾病時T細胞遷移的關鍵因子 (132) 。CCL5的 (也稱為RANTES；cytokine) 一般免疫反應後產生的，並有助於增強和適應性往後的免疫反應 (133) 。除了這些chemokine，有一些IFN-induced proteins也會受到LPS的影響。例如，IFN-inducible GTPase和IFN-γ-inducible protein 47 都屬於免疫相關的GTP酶，在調解先天免疫力去對抗細胞內的病原體扮演很關鍵角色 (134) 。IFN-activated gene 202B (Ifi202) 是屬於IFN-inducible 200-protein家族，

在利用BWF1小鼠為實驗模式中發現，ifi202是一個重要的樹突狀細胞的NF-κB活化因子，並參與IL-12的表現 (135) 。另外，helicase C domain 1誘發的IFN可以作為一種病毒感染的細胞質傳感器和活化抗病毒的免疫反應 (136) 。

第六章 結論

我們是第一個利用NF-κB活體影像搭配microarray的分析，很成功的應用在對CCl_4誘發的肝纖維化治療效果和silymarin新穎作用機制的評估和測定上。此疾病動物模式在對於肝臟發炎的研究上變得相當的便利，可在第一時間即時的觀察到發炎誘發情況，以及藥物治療狀況。我們認為此方法極適合用來探堪目前有效的中醫藥並更深入的探堪複雜的中醫藥裡的致效成份。以此動物模式為基礎，利用現今中醫在臨床上常用在肝炎緩解的方劑-茵陳蒿湯來進行研究，進一步從茵陳蒿湯拆解成單一中藥探討主要的療效藥物，發現梔子對於抗肝纖維化有很好的效果，並從中進行文獻的分析找到genipin可能是肝炎的致效成份。進一步，我們利用此平台對genipin進行抗發炎的機轉分析。我們發現，急性全身性發炎模式中genipin呈現出系統性的抗發炎作用。進一步，genipin透過新穎的機制抑制發炎，包括下調chemokine ligand，chemokine receptor，IFN-induced protein productions的表現量。這些結果表明，genipin可能是一個治療肝炎及全身炎症反應的候選藥物。

參考文獻

1. Luedde, T., and Schwabe, R. F. (2011) NF-kappaB in the liver--linking injury, fibrosis and hepatocellular carcinoma. *Nat Rev Gastroenterol Hepatol* **8**, 108-118
2. Saravanan, S., Velu, V., Nandakumar, S., Madhavan, V., Shanmugasundaram, U., Murugavel, K. G., Balakrishnan, P., Kumarasamy, N., Solomon, S., and Thyagarajan, S. P. (2009) Hepatitis B virus and hepatitis C virus dual infection among patients with chronic liver disease. *J Microbiol Immunol Infect* **42**, 122-128
3. Lohse, A. W., and Mieli-Vergani, G. (2010) Autoimmune hepatitis. *J Hepatol*
4. Pascale, A., Pais, R., and Ratziu, V. (2010) An overview of nonalcoholic steatohepatitis: past, present and future directions. *J Gastrointestin Liver Dis* **19**, 415-423
5. Jaeschke, H. (2005) Role of inflammation in the mechanism of acetaminophen-induced hepatotoxicity. *Expert Opin Drug Metab Toxicol* **1**, 389-397
6. Hayden, M. S., and Ghosh, S. (2011) NF-kappaB in immunobiology. *Cell Res* **21**, 223-244
7. Siebenlist, U., Franzoso, G., and Brown, K. (1994) Structure, regulation and function of NF-kappa B. *Annu Rev Cell Biol* **10**, 405-455
8. Sun, S. C. (2011) Non-canonical NF-kappaB signaling pathway. *Cell Res* **21**, 71-85
9. Mukhopadhyay, A., Manna, S. K., and Aggarwal, B. B. (2000) Pervanadate-induced nuclear factor-kappaB activation requires tyrosine phosphorylation and degradation of IkappaBalpha. Comparison with tumor necrosis factor-alpha. *J Biol Chem* **275**, 8549-8555
10. Baeuerle, P. A., and Baichwal, V. R. (1997) NF-kappa B as a frequent target for immunosuppressive and anti-inflammatory molecules. *Adv Immunol* **65**, 111-137
11. Zhang, L., Wang, G., Hou, W., Li, P., Dulin, A., and Bonkovsky, H. L. (2010) Contemporary clinical research of traditional Chinese medicines for chronic hepatitis B in China: an analytical review. *Hepatology* **51**, 690-698
12. Schuppan, D., Jia, J. D., Brinkhaus, B., and Hahn, E. G. (1999) Herbal products for liver diseases: a therapeutic challenge for the new millennium. *Hepatology* **30**, 1099-1104
13. Schrofelbauer, B., Raffetseder, J., Hauner, M., Wolkerstorfer, A., Ernst, W., and Szolar, O. H. (2009) Glycyrrhizin, the main active compound in liquorice,

attenuates pro-inflammatory responses by interfering with membrane-dependent receptor signalling. *Biochem J* **421**, 473-482

14. Krithika, R., Mohankumar, R., Verma, R. J., Shrivastav, P. S., Mohamad, I. L., Gunasekaran, P., and Narasimhan, S. (2009) Isolation, characterization and antioxidative effect of phyllanthin against CCl4-induced toxicity in HepG2 cell line. *Chem Biol Interact* **181**, 351-358
15. Polyak, S. J., Morishima, C., Lohmann, V., Pal, S., Lee, D. Y., Liu, Y., Graf, T. N., and Oberlies, N. H. (2010) Identification of hepatoprotective flavonolignans from silymarin. *Proc Natl Acad Sci U S A* **107**, 5995-5999
16. Li-Weber, M. (2009) New therapeutic aspects of flavones: the anticancer properties of Scutellaria and its main active constituents Wogonin, Baicalein and Baicalin. *Cancer Treat Rev* **35**, 57-68
17. El-Serag, H. B. (2012) Epidemiology of viral hepatitis and hepatocellular carcinoma. *Gastroenterology* **142**, 1264-1273 e1261
18. Schaefer, E. A., and Pratt, D. S. (2012) Autoimmune hepatitis: current challenges in diagnosis and management in a chronic progressive liver disease. *Curr Opin Rheumatol* **24**, 84-89
19. Grant, L. M., and Rockey, D. C. (2012) Drug-induced liver injury. *Curr Opin Gastroenterol* **28**, 198-202
20. Mathurin, P., and Lucey, M. R. (2012) Management of alcoholic hepatitis. *J Hepatol* **56 Suppl 1**, S39-45
21. Gu, X., and Manautou, J. E. (2012) Molecular mechanisms underlying chemical liver injury. *Expert Rev Mol Med* **14**, e4
22. Xu, H., Qian, H., Zhu, W., Zhang, X., Yan, Y., Mao, F., Wang, M., and Xu, W. (2012) Mesenchymal stem cells relieve fibrosis of Schistosoma japonicum-induced mouse liver injury. *Exp Biol Med (Maywood)* **237**, 585-592
23. Morales, J. M., Kamar, N., and Rostaing, L. (2012) Hepatitis C and renal disease: epidemiology, diagnosis, pathogenesis and therapy. *Contrib Nephrol* **176**, 10-23
24. Wiens, A., Venson, R., Correr, C. J., and Pontarolo, R. (2011) Cost-effectiveness of telbivudine versus lamivudine for chronic hepatitis B. *Braz J Infect Dis* **15**, 225-230
25. Mubareka, S., Leung, V., Aoki, F. Y., and Vinh, D. C. (2010) Famciclovir: a focus on efficacy and safety. *Expert Opin Drug Saf* **9**, 643-658
26. Ciancio, A., and Rizzetto, M. (2010) Thymalfasin in the treatment of hepatitis B and C. *Ann N Y Acad Sci* **1194**, 141-146
27. Stevceva, L. (2002) Cytokines and their antagonists as therapeutic agents.

Curr Med Chem **9**, 2201-2207

28. Chuang, W. L., Dai, C. Y., Chang, W. Y., Lee, L. P., Lin, Z. Y., Chen, S. C., Hsieh, M. Y., Wang, L. Y., and Yu, M. L. (2005) Viral interaction and responses in chronic hepatitis C and B coinfected patients with interferon-alpha plus ribavirin combination therapy. *Antivir Ther* **10**, 125-133
29. Ashfaq, U. A., Yousaf, M. Z., Aslam, M., Ejaz, R., Jahan, S., and Ullah, O. (2011) siRNAs: potential therapeutic agents against hepatitis C virus. *Virol J* **8**, 276
30. Ivacik, D., Ely, A., and Arbuthnot, P. (2011) Countering hepatitis B virus infection using RNAi: how far are we from the clinic? *Rev Med Virol* **21**, 383-396
31. Hu, Y., Chen, L., Shu, J., Yao, Y., and Yan, H. M. (2012) Clinical study on treatment of infantile cytomegalovirus hepatitis with integrated Chinese and Western medicine. *Chin J Integr Med* **18**, 100-105
32. 楊運高 (2006) *有效養肝降酶抗病毒藥物手冊*, 人民軍醫出版社, 中華人民共合國, ISBN:7509100461
33. 黃進明 (1994) *B 型肝炎・中醫療法*, 昭人出版社 ISBN:9579937311
34. 馬光亞 (1998) *中醫如何診治肝病*, 九思出版社 ISBN:9579936099
35. Arab, J. P., Ramirez, C., Munoz, P., Pizarro, M., Solis, N., Riquelme, A., and Arrese, M. (2009) Effects of Japanese herbal medicine Inchin-ko-to on endotoxin-induced cholestasis in the rat. *Ann Hepatol* **8**, 228-233
36. Kobayashi, H., Horikoshi, K., Yamataka, A., Lane, G. J., Yamamoto, M., and Miyano, T. (2001) Beneficial effect of a traditional herbal medicine (inchin-ko-to) in postoperative biliary atresia patients. *Pediatr Surg Int* **17**, 386-389
37. Kaiho, T., Tsuchiya, S., Yanagisawa, S., Takeuchi, O., Togawa, A., Okamoto, R., Saigusa, N., and Miyazaki, M. (2008) Effect of the herbal medicine Inchin-Ko-To for serum bilirubin in hepatectomized patients. *Hepatogastroenterology* **55**, 150-154
38. Weber-Mzell, D., Zaupa, P., Petnehazy, T., Kobayashi, H., Schimpl, G., Feierl, G., Kotanko, P., and Hollwarth, M. (2006) The role of nuclear factor-kappa B in bacterial translocation in cholestatic rats. *Pediatr Surg Int* **22**, 43-49
39. Ohwada, S., Kobayashi, I., Harasawa, N., Tsuda, K., and Inui, Y. (2009) Severe acute cholestatic hepatitis of unknown etiology successfully treated with the Chinese herbal medicine Inchinko-to (TJ-135). *World J Gastroenterol* **15**, 2927-2929
40. Sakaida, I., Tsuchiya, M., Kawaguchi, K., Kimura, T., Terai, S., and Okita, K. (2003) Herbal medicine Inchin-ko-to (TJ-135) prevents liver fibrosis and

enzyme-altered lesions in rat liver cirrhosis induced by a choline-deficient L-amino acid-defined diet. *J Hepatol* **38**, 762-769

41. Yamamoto, M., Ogawa, K., Morita, M., Fukuda, K., and Komatsu, Y. (1996) The herbal medicine Inchin-ko-to inhibits liver cell apoptosis induced by transforming growth factor beta 1. *Hepatology* **23**, 552-559
42. Koo, H. J., Lim, K. H., Jung, H. J., and Park, E. H. (2006) Anti-inflammatory evaluation of gardenia extract, geniposide and genipin. *J Ethnopharmacol* **103**, 496-500
43. Shuangsuo, D., Zhengguo, Z., Yunru, C., Xin, Z., Baofeng, W., Lichao, Y., and Yan'an, C. (2006) Inhibition of the replication of hepatitis B virus in vitro by emodin. *Med Sci Monit* **12**, BR302-306
44. Kumar, A., Dhawan, S., and Aggarwal, B. B. (1998) Emodin (3-methyl-1,6,8-trihydroxyanthraquinone) inhibits TNF-induced NF-kappaB activation, IkappaB degradation, and expression of cell surface adhesion proteins in human vascular endothelial cells. *Oncogene* **17**, 913-918
45. Ikeda, H., Nagashima, K., Yanase, M., Tomiya, T., Arai, M., Inoue, Y., Tejima, K., Nishikawa, T., Watanabe, N., Kitamura, K., Isono, T., Yahagi, N., Noiri, E., Inao, M., Mochida, S., Kume, Y., Yatomi, Y., Nakahara, K., Omata, M., and Fujiwara, K. (2006) The herbal medicine inchin-ko-to (TJ-135) induces apoptosis in cultured rat hepatic stellate cells. *Life Sci* **78**, 2226-2233
46. Imanishi, Y., Maeda, N., Otogawa, K., Seki, S., Matsui, H., Kawada, N., and Arakawa, T. (2004) Herb medicine Inchin-ko-to (TJ-135) regulates PDGF-BB-dependent signaling pathways of hepatic stellate cells in primary culture and attenuates development of liver fibrosis induced by thioacetamide administration in rats. *J Hepatol* **41**, 242-250
47. Inao, M., Mochida, S., Matsui, A., Eguchi, Y., Yulutuz, Y., Wang, Y., Naiki, K., Kakinuma, T., Fujimori, K., Nagoshi, S., and Fujiwara, K. (2004) Japanese herbal medicine Inchin-ko-to as a therapeutic drug for liver fibrosis. *J Hepatol* **41**, 584-591
48. Hayashi, H., and Sakai, T. (2011) Animal models for the study of liver fibrosis: new insights from knockout mouse models. *Am J Physiol Gastrointest Liver Physiol* **300**, G729-738
49. Comporti, M., Arezzini, B., Signorini, C., Vecchio, D., and Gardi, C. (2009) Oxidative stress, isoprostanes and hepatic fibrosis. *Histol Histopathol* **24**, 893-900
50. Weber, L. W., Boll, M., and Stampfl, A. (2003) Hepatotoxicity and mechanism of action of haloalkanes: carbon tetrachloride as a toxicological model. *Crit Rev Toxicol* **33**, 105-136

51. Choi, J. H., Kim, D. W., Yun, N., Choi, J. S., Islam, M. N., Kim, Y. S., and Lee, S. M. (2011) Protective Effects of Hyperoside against Carbon Tetrachloride-Induced Liver Damage in Mice. *J Nat Prod* **74**, 1055-1060
52. Weiler-Normann, C., Herkel, J., and Lohse, A. W. (2007) Mouse models of liver fibrosis. *Z Gastroenterol* **45**, 43-50
53. Nanji, A. A., Jokelainen, K., Tipoe, G. L., Rahemtulla, A., and Dannenberg, A. J. (2001) Dietary saturated fatty acids reverse inflammatory and fibrotic changes in rat liver despite continued ethanol administration. *J Pharmacol Exp Ther* **299**, 638-644
54. Sun, H., Che, Q. M., Zhao, X., and Pu, X. P. (2010) Antifibrotic effects of chronic baicalein administration in a CCl4 liver fibrosis model in rats. *Eur J Pharmacol* **631**, 53-60
55. Tacke, F., Wustefeld, T., Horn, R., Luedde, T., Srinivas Rao, A., Manns, M. P., Trautwein, C., and Brabant, G. (2005) High adiponectin in chronic liver disease and cholestasis suggests biliary route of adiponectin excretion in vivo. *J Hepatol* **42**, 666-673
56. Down, W. H., Chasseaud, L. F., and Grundy, R. K. (1974) Effect of silybin on the hepatic microsomal drug-metabolising enzyme system in the rat. *Arzneimittelforschung* **24**, 1986-1988
57. Jia, J. D., Bauer, M., Cho, J. J., Ruehl, M., Milani, S., Boigk, G., Riecken, E. O., and Schuppan, D. (2001) Antifibrotic effect of silymarin in rat secondary biliary fibrosis is mediated by downregulation of procollagen alpha1(I) and TIMP-1. *J Hepatol* **35**, 392-398
58. Carlos Pascual, R. G. J. A. P. M. (1993) Effect of silymarin and silybinin on oxygen radicals. *DRUG DEVELOPMENT RESEARCH* **29**, 73-77
59. Muriel, P., and Mourelle, M. (1990) The role of membrane composition in ATPase activities of cirrhotic rat liver: effect of silymarin. *J Appl Toxicol* **10**, 281-284
60. Muriel, P., and Mourelle, M. (1990) Prevention by silymarin of membrane alterations in acute CCl4 liver damage. *J Appl Toxicol* **10**, 275-279
61. Pradhan, S. C., and Girish, C. (2006) Hepatoprotective herbal drug, silymarin from experimental pharmacology to clinical medicine. *Indian J Med Res* **124**, 491-504
62. Ho, T. Y., Chen, Y. S., and Hsiang, C. Y. (2007) Noninvasive nuclear factor-kappaB bioluminescence imaging for the assessment of host-biomaterial interaction in transgenic mice. *Biomaterials* **28**, 4370-4377
63. Hsiang, C. Y., Chen, Y. S., and Ho, T. Y. (2009) Nuclear factor-kappaB bioluminescence imaging-guided transcriptomic analysis for the assessment of

host-biomaterial interaction in vivo. *Biomaterials* **30**, 3042-3049

64. Hseu, Y. C., Huang, H. C., and Hsiang, C. Y. (2010) Antrodia camphorata suppresses lipopolysaccharide-induced nuclear factor-kappaB activation in transgenic mice evaluated by bioluminescence imaging. *Food Chem Toxicol* **48**, 2319-2325
65. Wu, S. L., Chen, J. C., Li, C. C., Lo, H. Y., Ho, T. Y., and Hsiang, C. Y. (2009) Vanillin improves and prevents trinitrobenzene sulfonic acid-induced colitis in mice. *J Pharmacol Exp Ther* **330**, 370-376
66. Domenicali, M., Caraceni, P., Giannone, F., Baldassarre, M., Lucchetti, G., Quarta, C., Patti, C., Catani, L., Nanni, C., Lemoli, R. M., and Bernardi, M. (2009) A novel model of CCl4-induced cirrhosis with ascites in the mouse. *J Hepatol* **51**, 991-999
67. Le Naour, F., Bralet, M. P., Debois, D., Sandt, C., Guettier, C., Dumas, P., Brunelle, A., and Laprevote, O. (2009) Chemical imaging on liver steatosis using synchrotron infrared and ToF-SIMS microspectroscopies. *PLoS One* **4**, e7408
68. Talwalkar, J. A., Yin, M., Fidler, J. L., Sanderson, S. O., Kamath, P. S., and Ehman, R. L. (2008) Magnetic resonance imaging of hepatic fibrosis: emerging clinical applications. *Hepatology* **47**, 332-342
69. Frank, S. J., Wang, X., He, K., Yang, N., Fang, P., Rosenfeld, R. G., Hwa, V., Chaudhuri, T. R., Deng, L., and Zinn, K. R. (2006) In vivo imaging of hepatic growth hormone signaling. *Mol Endocrinol* **20**, 2819-2830
70. Brader, P., Riedl, C. C., Woo, Y., Ponomarev, V., Zanzonico, P., Wen, B., Cai, S., Hricak, H., Fong, Y., Blasberg, R., and Serganova, I. (2007) Imaging of hypoxia-driven gene expression in an orthotopic liver tumor model. *Mol Cancer Ther* **6**, 2900-2908
71. Augenlicht, L. H., Wahrman, M. Z., Halsey, H., Anderson, L., Taylor, J., and Lipkin, M. (1987) Expression of cloned sequences in biopsies of human colonic tissue and in colonic carcinoma cells induced to differentiate in vitro. *Cancer Res* **47**, 6017-6021
72. Schena, M., Shalon, D., Davis, R. W., and Brown, P. O. (1995) Quantitative monitoring of gene expression patterns with a complementary DNA microarray. *Science* **270**, 467-470
73. DeRisi, J. L., Iyer, V. R., and Brown, P. O. (1997) Exploring the metabolic and genetic control of gene expression on a genomic scale. *Science* **278**, 680-686
74. Lashkari, D. A., DeRisi, J. L., McCusker, J. H., Namath, A. F., Gentile, C., Hwang, S. Y., Brown, P. O., and Davis, R. W. (1997) Yeast microarrays for genome wide parallel genetic and gene expression analysis. *Proc Natl Acad*

Sci U S A **94**, 13057-13062

75. Schena, M., Shalon, D., Heller, R., Chai, A., Brown, P. O., and Davis, R. W. (1996) Parallel human genome analysis: microarray-based expression monitoring of 1000 genes. *Proc Natl Acad Sci U S A* **93**, 10614-10619
76. Stathopoulos, A., and Levine, M. (2002) Whole-genome expression profiles identify gene batteries in Drosophila. *Dev Cell* **3**, 464-465
77. Alizadeh, A. A., Eisen, M. B., Davis, R. E., Ma, C., Lossos, I. S., Rosenwald, A., Boldrick, J. C., Sabet, H., Tran, T., Yu, X., Powell, J. I., Yang, L., Marti, G. E., Moore, T., Hudson, J., Jr., Lu, L., Lewis, D. B., Tibshirani, R., Sherlock, G., Chan, W. C., Greiner, T. C., Weisenburger, D. D., Armitage, J. O., Warnke, R., Levy, R., Wilson, W., Grever, M. R., Byrd, J. C., Botstein, D., Brown, P. O., and Staudt, L. M. (2000) Distinct types of diffuse large B-cell lymphoma identified by gene expression profiling. *Nature* **403**, 503-511
78. Calvano, S. E., Xiao, W., Richards, D. R., Felciano, R. M., Baker, H. V., Cho, R. J., Chen, R. O., Brownstein, B. H., Cobb, J. P., Tschoeke, S. K., Miller-Graziano, C., Moldawer, L. L., Mindrinos, M. N., Davis, R. W., Tompkins, R. G., and Lowry, S. F. (2005) A network-based analysis of systemic inflammation in humans. *Nature* **437**, 1032-1037
79. DeRisi, J., Penland, L., Brown, P. O., Bittner, M. L., Meltzer, P. S., Ray, M., Chen, Y., Su, Y. A., and Trent, J. M. (1996) Use of a cDNA microarray to analyse gene expression patterns in human cancer. *Nat Genet* **14**, 457-460
80. Heller, R. A., Schena, M., Chai, A., Shalon, D., Bedilion, T., Gilmore, J., Woolley, D. E., and Davis, R. W. (1997) Discovery and analysis of inflammatory disease-related genes using cDNA microarrays. *Proc Natl Acad Sci U S A* **94**, 2150-2155
81. Huang, E., Cheng, S. H., Dressman, H., Pittman, J., Tsou, M. H., Horng, C. F., Bild, A., Iversen, E. S., Liao, M., Chen, C. M., West, M., Nevins, J. R., and Huang, A. T. (2003) Gene expression predictors of breast cancer outcomes. *Lancet* **361**, 1590-1596
82. Pittman, J., Huang, E., Dressman, H., Horng, C. F., Cheng, S. H., Tsou, M. H., Chen, C. M., Bild, A., Iversen, E. S., Huang, A. T., Nevins, J. R., and West, M. (2004) Integrated modeling of clinical and gene expression information for personalized prediction of disease outcomes. *Proc Natl Acad Sci U S A* **101**, 8431-8436
83. Pomeroy, S. L., Tamayo, P., Gaasenbeek, M., Sturla, L. M., Angelo, M., McLaughlin, M. E., Kim, J. Y., Goumnerova, L. C., Black, P. M., Lau, C., Allen, J. C., Zagzag, D., Olson, J. M., Curran, T., Wetmore, C., Biegel, J. A., Poggio, T., Mukherjee, S., Rifkin, R., Califano, A., Stolovitzky, G., Louis, D.

N., Mesirov, J. P., Lander, E. S., and Golub, T. R. (2002) Prediction of central nervous system embryonal tumour outcome based on gene expression. *Nature* **415**, 436-442

84. Ross, D. T., Scherf, U., Eisen, M. B., Perou, C. M., Rees, C., Spellman, P., Iyer, V., Jeffrey, S. S., Van de Rijn, M., Waltham, M., Pergamenschikov, A., Lee, J. C., Lashkari, D., Shalon, D., Myers, T. G., Weinstein, J. N., Botstein, D., and Brown, P. O. (2000) Systematic variation in gene expression patterns in human cancer cell lines. *Nat Genet* **24**, 227-235
85. Sakaida, I., Terai, S., Yamamoto, N., Aoyama, K., Ishikawa, T., Nishina, H., and Okita, K. (2004) Transplantation of bone marrow cells reduces CCl4-induced liver fibrosis in mice. *Hepatology* **40**, 1304-1311
86. Cheng, H. M., Li, C. C., Chen, C. Y., Lo, H. Y., Cheng, W. Y., Lee, C. H., Yang, S. Z., Wu, S. L., Hsiang, C. Y., and Ho, T. Y. (2010) Application of bioactivity database of Chinese herbal medicine on the therapeutic prediction, drug development, and safety evaluation. *J Ethnopharmacol* **132**, 429-437
87. Smyth, G. K., and Speed, T. (2003) Normalization of cDNA microarray data. *Methods* **31**, 265-273
88. Montaner, D., Tarraga, J., Huerta-Cepas, J., Burguet, J., Vaquerizas, J. M., Conde, L., Minguez, P., Vera, J., Mukherjee, S., Valls, J., Pujana, M. A., Alloza, E., Herrero, J., Al-Shahrour, F., and Dopazo, J. (2006) Next station in microarray data analysis: GEPAS. *Nucleic Acids Res* **34**, W486-491
89. Saeed, A. I., Sharov, V., White, J., Li, J., Liang, W., Bhagabati, N., Braisted, J., Klapa, M., Currier, T., Thiagarajan, M., Sturn, A., Snuffin, M., Rezantsev, A., Popov, D., Ryltsov, A., Kostukovich, E., Borisovsky, I., Liu, Z., Vinsavich, A., Trush, V., and Quackenbush, J. (2003) TM4: a free, open-source system for microarray data management and analysis. *Biotechniques* **34**, 374-378
90. Zhang, B., Schmoyer, D., Kirov, S., and Snoddy, J. (2004) GOTree Machine (GOTM): a web-based platform for interpreting sets of interesting genes using Gene Ontology hierarchies. *BMC Bioinformatics* **5**, 16
91. Seifert, M., Scherf, M., Epple, A., and Werner, T. (2005) Multievidence microarray mining. *Trends Genet* **21**, 553-558
92. Lopez-De Leon, A., and Rojkind, M. (1985) A simple micromethod for collagen and total protein determination in formalin-fixed paraffin-embedded sections. *J Histochem Cytochem* **33**, 737-743
93. Jimenez, W., Pares, A., Caballeria, J., Heredia, D., Bruguera, M., Torres, M., Rojkind, M., and Rodes, J. (1985) Measurement of fibrosis in needle liver biopsies: evaluation of a colorimetric method. *Hepatology* **5**, 815-818
94. Bataller, R., and Brenner, D. A. (2005) Liver fibrosis. *J Clin Invest* **115**,

209-218

95. Wells, R. G. (2005) The role of matrix stiffness in hepatic stellate cell activation and liver fibrosis. *J Clin Gastroenterol* **39**, S158-161
96. Lotersztajn, S., Julien, B., Teixeira-Clerc, F., Grenard, P., and Mallat, A. (2005) Hepatic fibrosis: molecular mechanisms and drug targets. *Annu Rev Pharmacol Toxicol* **45**, 605-628
97. Hortner, M., Nielsch, U., Mayr, L. M., Heinrich, P. C., and Haan, S. (2002) A new high affinity binding site for suppressor of cytokine signaling-3 on the erythropoietin receptor. *Eur J Biochem* **269**, 2516-2526
98. Xiong, Y. Q., Willard, J., Kadurugamuwa, J. L., Yu, J., Francis, K. P., and Bayer, A. S. (2005) Real-time in vivo bioluminescent imaging for evaluating the efficacy of antibiotics in a rat Staphylococcus aureus endocarditis model. *Antimicrob Agents Chemother* **49**, 380-387
99. Contag, C. H., and Bachmann, M. H. (2002) Advances in in vivo bioluminescence imaging of gene expression. *Annu Rev Biomed Eng* **4**, 235-260
100. Ottobrini, L., Lucignani, G., Clerici, M., and Rescigno, M. (2005) Assessing cell trafficking by noninvasive imaging techniques: applications in experimental tumor immunology. *Q J Nucl Med Mol Imaging* **49**, 361-366
101. Sarraf-Yazdi, S., Mi, J., Dewhirst, M. W., and Clary, B. M. (2004) Use of in vivo bioluminescence imaging to predict hepatic tumor burden in mice. *J Surg Res* **120**, 249-255
102. Chang, C. T., Lin, H., Ho, T. Y., Li, C. C., Lo, H. Y., Wu, S. L., Huang, Y. F., Liang, J. A., and Hsiang, C. Y. (2011) Comprehensive assessment of host responses to ionizing radiation by nuclear factor-κB bioluminescence imaging-guided transcriptomic analysis. *PLoS One*, in press
103. Ai, W., Zhang, Y., Tang, Q. Z., Yan, L., Bian, Z. Y., Liu, C., Huang, H., Bai, X., Yin, L., and Li, H. (2010) Silibinin attenuates cardiac hypertrophy and fibrosis through blocking EGFR-dependent signaling. *J Cell Biochem* **110**, 1111-1122
104. Upadhyay, G., Tiwari, M. N., Prakash, O., Jyoti, A., Shanker, R., and Singh, M. P. (2010) Involvement of multiple molecular events in pyrogallol-induced hepatotoxicity and silymarin-mediated protection: evidence from gene expression profiles. *Food Chem Toxicol* **48**, 1660-1670
105. De Minicis, S., Seki, E., Uchinami, H., Kluwe, J., Zhang, Y., Brenner, D. A., and Schwabe, R. F. (2007) Gene expression profiles during hepatic stellate cell activation in culture and in vivo. *Gastroenterology* **132**, 1937-1946
106. Krahenbuhl, S., and Reichen, J. (1992) Adaptation of mitochondrial metabolism in liver cirrhosis. Different strategies to maintain a vital function.

Scand J Gastroenterol Suppl **193**, 90-96

107. Britton, R. S., and Bacon, B. R. (1994) Role of free radicals in liver diseases and hepatic fibrosis. *Hepatogastroenterology* **41**, 343-348
108. Shiryaeva, A., Baidyuk, E., Arkadieva, A., Okovityy, S., Morozov, V., and Sakuta, G. (2008) Hepatocyte mitochondrion electron-transport chain alterations in CCl(4) and alcohol induced hepatitis in rats and their correction with simvastatin. *J Bioenerg Biomembr* **40**, 27-34
109. Boyer, P. D. (1997) The ATP synthase--a splendid molecular machine. *Annu Rev Biochem* **66**, 717-749
110. Tanaka, A., Morimoto, T., Wakashiro, S., Ikai, I., Ozawa, K., and Orii, Y. (1987) Kinetic alterations of cytochrome c oxidase in carbon tetrachloride induced cirrhotic rat liver. *Life Sci* **41**, 741-748
111. Chavez, E., and Bravo, C. (1988) Silymarin-induced mitochondrial Ca2+ release. *Life Sci* **43**, 975-981
112. Pietrangelo, A., Montosi, G., Garuti, C., Contri, M., Giovannini, F., Ceccarelli, D., and Masini, A. (2002) Iron-induced oxidant stress in nonparenchymal liver cells: mitochondrial derangement and fibrosis in acutely iron-dosed gerbils and its prevention by silybin. *J Bioenerg Biomembr* **34**, 67-79
113. Mase, A., Makino, B., Tsuchiya, N., Yamamoto, M., Kase, Y., Takeda, S., and Hasegawa, T. (2010) Active ingredients of traditional Japanese (kampo) medicine, inchinkoto, in murine concanavalin A-induced hepatitis. *J Ethnopharmacol* **127**, 742-749
114. Asakawa, T., Yagi, M., Tanaka, Y., Asagiri, K., Kobayashi, H., Egami, H., Tanikawa, K., and Kage, M. (2012) The herbal medicine Inchinko-to reduces hepatic fibrosis in cholestatic rats. *Pediatr Surg Int* **28**, 379-384
115. Kang, J. J., Wang, H. W., Liu, T. Y., Chen, Y. C., and Ueng, T. H. (1997) Modulation of cytochrome P-450-dependent monooxygenases, glutathione and glutathione S-transferase in rat liver by geniposide from Gardenia jasminoides. *Food Chem Toxicol* **35**, 957-965
116. Kitano, A., Saika, S., Yamanaka, O., Ikeda, K., Reinach, P. S., Nakajima, Y., Okada, Y., Shirai, K., and Ohnishi, Y. (2006) Genipin suppresses subconjunctival fibroblast migration, proliferation and myofibroblast transdifferentiation. *Ophthalmic Res* **38**, 355-360
117. Tseng, T. H., Chu, C. Y., Huang, J. M., Shiow, S. J., and Wang, C. J. (1995) Crocetin protects against oxidative damage in rat primary hepatocytes. *Cancer Lett* **97**, 61-67
118. He, M. L., Cheng, X. W., Chen, J. K., and Zhou, T. S. (2006) Simultaneous determination of five major biologically active ingredients in different parts of

Gardenia jasminoides fruits by HPLC with diode-array detection. *Chromatographia* **64**, 713-717

119. Fujikawa, S., Fukui, Y., Koga, K., and Kumada, J. (1987) Brilliant skyblue pigment formation from gardenia fruits. *Journal of fermentation technology* **65**, 419-424
120. Sung, H. W., Huang, R. N., Huang, L. L., Tsai, C. C., and Chiu, C. T. (1998) Feasibility study of a natural crosslinking reagent for biological tissue fixation. *J Biomed Mater Res* **42**, 560-567
121. Yamamoto, M., Miura, N., Ohtake, N., Amagaya, S., Ishige, A., Sasaki, H., Komatsu, Y., Fukuda, K., Ito, T., and Terasawa, K. (2000) Genipin, a metabolite derived from the herbal medicine Inchin-ko-to, and suppression of Fas-induced lethal liver apoptosis in mice. *Gastroenterology* **118**, 380-389
122. Yamazaki, M., and Chiba, K. (2008) Genipin exhibits neurotrophic effects through a common signaling pathway in nitric oxide synthase-expressing cells. *Eur J Pharmacol* **581**, 255-261
123. Koo, H. J., Song, Y. S., Kim, H. J., Lee, Y. H., Hong, S. M., Kim, S. J., Kim, B. C., Jin, C., Lim, C. J., and Park, E. H. (2004) Antiinflammatory effects of genipin, an active principle of gardenia. *Eur J Pharmacol* **495**, 201-208
124. Nam, K. N., Choi, Y. S., Jung, H. J., Park, G. H., Park, J. M., Moon, S. K., Cho, K. H., Kang, C., Kang, I., Oh, M. S., and Lee, E. H. (2010) Genipin inhibits the inflammatory response of rat brain microglial cells. *Int Immunopharmacol* **10**, 493-499
125. Park, K. S., Kim, B. H., and Chang, I. M. (2010) Inhibitory Potencies of Several Iridoids on Cyclooxygenase-1, Cyclooxygnase-2 Enzymes Activities, Tumor Necrosis factor-alpha and Nitric Oxide Production In Vitro. *Evid Based Complement Alternat Med* **7**, 41-45
126. Lee, J. H., Lee, D. U., and Jeong, C. S. (2009) Gardenia jasminoides Ellis ethanol extract and its constituents reduce the risks of gastritis and reverse gastric lesions in rats. *Food Chem Toxicol* **47**, 1127-1131
127. Andonegui, G., Bonder, C. S., Green, F., Mullaly, S. C., Zbytnuik, L., Raharjo, E., and Kubes, P. (2003) Endothelium-derived Toll-like receptor-4 is the key molecule in LPS-induced neutrophil sequestration into lungs. *J Clin Invest* **111**, 1011-1020
128. Mathison, J. C., and Ulevitch, R. J. (1979) The clearance, tissue distribution, and cellular localization of intravenously injected lipopolysaccharide in rabbits. *J Immunol* **123**, 2133-2143
129. Ouchida, R., Kurosaki, T., and Wang, J. Y. (2010) A role for lysosomal-associated protein transmembrane 5 in the negative regulation of

surface B cell receptor levels and B cell activation. *J Immunol* **185**, 294-301

130. Yun, T. J., and Bevan, M. J. (2003) Notch-regulated ankyrin-repeat protein inhibits Notch1 signaling: multiple Notch1 signaling pathways involved in T cell development. *J Immunol* **170**, 5834-5841
131. Hughes, D. P., Marron, M. B., and Brindle, N. P. (2003) The antiinflammatory endothelial tyrosine kinase Tie2 interacts with a novel nuclear factor-kappaB inhibitor ABIN-2. *Circ Res* **92**, 630-636
132. Ellis, S. L., Gysbers, V., Manders, P. M., Li, W., Hofer, M. J., Muller, M., and Campbell, I. L. (2010) The cell-specific induction of CXC chemokine ligand 9 mediated by IFN-gamma in microglia of the central nervous system is determined by the myeloid transcription factor PU.1. *J Immunol* **185**, 1864-1877
133. O'Sullivan, J. B., Ryan, K. M., Harkin, A., and Connor, T. J. (2010) Noradrenaline reuptake inhibitors inhibit expression of chemokines IP-10 and RANTES and cell adhesion molecules VCAM-1 and ICAM-1 in the CNS following a systemic inflammatory challenge. *J Neuroimmunol* **220**, 34-42
134. MacMicking, J. D. (2004) IFN-inducible GTPases and immunity to intracellular pathogens. *Trends Immunol* **25**, 601-609
135. Yamauchi, M., Hashimoto, M., Ichiyama, K., Yoshida, R., Hanada, T., Muta, T., Komune, S., Kobayashi, T., and Yoshimura, A. (2007) Ifi202, an IFN-inducible candidate gene for lupus susceptibility in NZB/W F1 mice, is a positive regulator for NF-kappaB activation in dendritic cells. *Int Immunol* **19**, 935-942
136. Balan, V., Nelson, D. R., Sulkowski, M. S., Everson, G. T., Lambiase, L. R., Wiesner, R. H., Dickson, R. C., Garcia, A., Moore, P. A., Yu, R., and Subramanian, G. M. (2006) Modulation of interferon-specific gene expression by albumin-interferon-alpha in interferon-alpha-experienced patients with chronic hepatitis C. *Antivir Ther* **11**, 901-908

New functional genomics platform for analyzing the effects of Yin-Chen-Hao-Tang and its novel effective components in liver disease

Graduate Institute of Chinese Medicine, China Medical University

Advisor: Professor Tin-Yun Ho

Student: Chia-Cheng Li

Chronic liver disease is a global health problem that affects hundreds of millions of people. Liver damage followed by the persistent inflammation leads to hepatic fibrosis and cirrhosis. The inflammation is regulated by the transcription factor, nuclear factor-κB (NF-κB). Therefore, we applied bioluminescent imaging-guided transcriptomic analysis to evaluate the feasibility of NF-κB-dependent bioluminescent image on the assessment of liver disease progression and therapeutic efficacies of herbs. Transgenic mice, carrying the luciferase genes driven by NF-κB, were given with carbon tetrachloride (CCl_4) and/or silymarin. *In vivo* NF-κB activity was evaluated by bioluminescent imaging, liver fibrosis was judged by Sirius red staining and immunohistochemistry, and gene expression profiles of silymarin-treated livers were analyzed by DNA microarray. CCl_4 enhanced the NF-κB-dependent hepatic luminescence and induced hepatic fibrosis, while silymarin reduced the CCl_4-induced hepatic luminescence and improved CCl_4-induced liver fibrosis. Microarray analysis showed that silymarin altered the transforming growth factor-β-mediated pathways, which play pivotal roles in the progression of liver fibrosis. Moreover, we newly identified that silymarin downregulated the expression levels of cytoskeleton

organization genes and mitochondrion electron-transfer chain genes, such as cytochrome *c* oxidase Cox6a2, Cox7a1, and Cox8b genes. We further applied this platform to evaluate the therapeutic potentials of Yin-Chen-Hao-Tang and its novel effective components. We found that Fructus Gardeniae, the component of Yin-Chen-Hao-Tang, was effective for the treatment of liver fibrosis. Furthermore, genipin from Fructus Gardeniae exhibited anti-fibrogenic and anti-inflammatory effects via downregulation of chemokine ligand, chemokine receptor, and interferone-induced protein productions. In conclusion, our data showed the feasibility of NF-κB-dependent bioluminescent image on the assessment of disease progression and therapeutic efficacies. Moreover, the therapeutic potentials and mechainsms of Yin-Chen-Hao-Tang and its constituents silynmarin and genipin were further identified by bioluminescent imaging-guided transcriptomic analysis.

誌謝

感謝我的父母親的栽培，以及兄弟姊妹支持與鼓勵，讓我求學的過程一路順利。感謝我的指導教授侯庭鏞老師在研究上的協助與指點，也感謝共同指導老師項千芸老師與吳世祿老師在研究技術與想法的無私分享。感謝從大學、碩班及博班這 11 年來曾經一起在這實驗室努力過的學長姊弟妹們互相幫忙與照顧，我永遠記得一個學長曾經對我說「把實驗室當成你家廚房」，這句話我到現在才真正了解它的含意。感謝那些曾經一起打拚與切磋的同學們。最後感謝所有曾經在我身邊出現過的任何人，因為有你們的存在，我才能完成博士學程。

Food and Chemical Toxicology 50 (2012) 1568–1575

Contents lists available at SciVerse ScienceDirect

Food and Chemical Toxicology

journal homepage: www.elsevier.com/locate/foodchemtox

Identification of novel mechanisms of silymarin on the carbon tetrachloride-induced liver fibrosis in mice by nuclear factor-κB bioluminescent imaging-guided transcriptomic analysis

Chia-Cheng Li [a], Chien-Yun Hsiang [b], Shih-Lu Wu [c], Tin-Yun Ho [a,d,*]

[a] Graduate Institute of Chinese Medicine, China Medical University, Taichung 40402, Taiwan
[b] Department of Microbiology, China Medical University, Taichung 40402, Taiwan
[c] Department of Biochemistry, China Medical University, Taichung 40402, Taiwan
[d] Department of Nuclear Medicine, China Medical University Hospital, Taichung 40447, Taiwan

ARTICLE INFO

Article history:
Received 13 September 2011
Accepted 14 February 2012
Available online 22 February 2012

Keywords:
Liver fibrosis
Silymarin
Nuclear factor-κB
Bioluminescent imaging
DNA microarray
Cytochrome *c* oxidase

ABSTRACT

In this study, we applied bioluminescent imaging-guided transcriptomic analysis to evaluate and identify the therapeutic potentials and novel mechanisms of silymarin on carbon tetrachloride (CCl_4)-induced liver fibrosis. Transgenic mice, carrying the luciferase genes driven by nuclear factor-κB (NF-κB), were given with CCl_4 and/or silymarin. *In vivo* NF-κB activity was evaluated by bioluminescent imaging, liver fibrosis was judged by Sirius red staining and immunohistochemistry, and gene expression profiles of silymarin-treated livers were analyzed by DNA microarray. CCl_4 enhanced the NF-κB-dependent hepatic luminescence and induced hepatic fibrosis, while silymarin reduced the CCl_4-induced hepatic luminescence and improved CCl_4-induced liver fibrosis. Microarray analysis showed that silymarin altered the transforming growth factor-β-mediated pathways, which play pivotal roles in the progression of liver fibrosis. Moreover, we newly identified that silymarin downregulated the expression levels of cytoskeleton organization genes and mitochondrion electron-transfer chain genes, such as cytochrome *c* oxidase Cox6a2, Cox7a1, and Cox8b genes. In conclusion, the correlation of NF-κB-dependent luminescence and liver fibrosis suggested the feasibility of NF-κB bioluminescent imaging for the evaluation of liver fibrosis progression and therapeutic potentials. Moreover, our findings suggested that silymarin might exhibit anti-fibrotic effects *in vivo* via altering the expression of genes involved in cytoskeleton organization and mitochondrion electron-transfer chain.

1. Introduction

Liver fibrosis is a pathological sequel of chronic inflammatory liver injury caused by various etiologies, such as hepatitis virus infection, autoimmune injury, alcohol, and toxins/drugs. Following hepatic inflammation and damage, hepatic stellate cells change to myofibroblast-like cells and produce a large amount of extracellular matrix like type I collagen. The accumulation of collagen in the hepatic parenchyma further leads to the fibrosis of liver (Bataller and Brenner, 2005; Lotersztajn et al., 2005). Production of proinflammatory cytokines, such as interleukin-1β, tumor necrosis factor-α and interferon-γ, contribute to the progression of hepatic inflammation and sequential fibrosis (Luedde and Schwabe, 2011). The production of cytokines is further controlled by the transcription factor, nuclear factor-κB (NF-κB) (Baldwin, 1996). NF-κB is an inducible nuclear transcription factor that consists of heterodimers of RelA (p65), c-Rel, RelB, p50/NF-κB1, and p52/NF-κB2. NF-κB activity is activated by a large variety of stimuli, such as microbes, inflammatory cytokines, and physical and chemical stresses. When stimulated, NF-κB binds to the NF-κB-responsive element present in the promoters of inflammatory genes, resulting in the induction of gene expression and the inflammatory process. Accordingly, NF-κB is a critical molecule involved in the regulation of inflammatory cytokine production and inflammation (Bonizzi and Karin, 2004; Karin and Ben-Neriah, 2000; Siebenlist et al., 1994). Moreover, controlling NF-κB activation has become a pharmacological target, particularly in the chronic inflammatory disorders (Baeuerle and Baichwal, 1997).

Abbreviations: CCl_4, carbon tetrachloride; Cox, cytochrome *c* oxidase; GAPDH, glyceraldahyde-3-phosphate dehydrogenase; H&E, hematoxylin and eosin; NF-κB, nuclear factor-κB; α-SMA, α-smooth muscle actin; TGF-β, transforming growth factor-β.

* Corresponding author. Address: Graduate Institute of Chinese Medicine, China Medical University, 91 Hsueh-Shih Road, Taichung 40402, Taiwan. Tel.: +886 4 22053366 3302; fax: +886 4 22053764.
E-mail address: cyhsiang@mail.cmu.edu.tw (T.-Y. Ho).

0278-6915/$ - see front matter © 2012 Elsevier Ltd. All rights reserved.
doi:10.1016/j.fct.2012.02.025

Silymarin, a flavonoligan mixture of milk thistle (*Silybum marianum*), is an important herbal hepatoprotective drug (Abenavoli et al., 2010). Silymarin possesses a variety of pharmacological activities, such as anti-inflammatory, immunomodulatory, antioxidant, and anti-viral activities (Polyak et al., 2007; Saller et al., 2001; Shaker et al., 2010). Silymarin exhibits hepatoprotective effects by altering cytoplasmic membrane architecture and, in turn, preventing the penetration of hepatotoxic substances, such as carbon tetrachloride (CCl_4), thioacetamide and D-galactosamine, into cells (Abenavoli et al., 2010; Basiglio et al., 2009). It also possesses the anti-fibrotic activity by retarding the activation of hepatic stellate cells (Chandan et al., 2008). Although the pharmacological mechanisms of silymarin have been reported, silymarin-altered hepatic gene expression profiles remained to be elucidated for the identification of novel targets and mechanisms for silymarin-mediated protection in the liver.

Bioluminescence imaging is a sensitive and noninvasive technique for real-time reporting and quantification of therapy efficacy in living animals (Hseu et al., 2011; Wu et al., 2009). This technique has been used for the assessment of host responses to biomaterials (Ho et al., 2007; Xiong et al., 2005). It has also been applied for imaging disease progression and diagnosis (Dothager et al., 2009; Ottobrini et al., 2005). Microarray is a popular research and screening tool for differentially expressed genes. Microarray-based gene expression patterns have been used to predict the candidate biomarkers, predict the therapeutic efficacies of drugs, and recognize the toxic potential of drug candidate (Baur et al., 2006; Lamb et al., 2006; Suter et al., 2004). We have previously applied NF-κB bioluminescent imaging-guided transcriptomic analysis to assess the host responses to biomaterials and ionizing radiation *in vivo* (Ho et al., 2007; Hsiang et al., 2009). In this study, we applied NF-κB bioluminescent image to evaluate both the progression of CCl_4-induced liver injury and the therapeutic effects of silymarin. Microarray analysis was further applied to globally elucidate the gene expression profiles of silymarin and to find novel mechanisms of silymarin on CCl_4-induced liver injury. Our data showed the feasibility of NF-κB-dependent bioluminescent image on the assessment of disease progression and therapeutic efficacies. Moreover, we newly identified that silymarin exhibited anti-fibrotic effects *in vivo* via regulating transforming growth factor-β (TGF-β)-mediated pathways and altering the expression of genes involved in cytoskeleton organization and mitochondrion electron-transfer chain.

2. Materials and methods

2.1. Induction of liver fibrosis and silymarin treatment

Mouse experiments were conducted under ethics approval from the China Medical University Animal Care and Use Committee. Transgenic mice, carrying the NF-κB-driven luciferase genes, were constructed previously (Ho et al., 2007). CCl_4-induced liver fibrosis was performed as described previously (Sakaida et al., 2004). Silymarin was purchased from Sigma (St. Louis, MO) and suspended in distilled water to a final concentration 20 mg/ml. A total of 24 transgenic mice was randomly divided into three groups of eight mice: (1) mock, mice were intraperitoneally administered with 0.5 ml/kg olive oil twice a week for 12 weeks, (2) CCl_4, mice were intraperitoneally administered with 0.5 ml/kg 10% CCl_4 in olive oil twice a week for 12 weeks, and (3) silymarin, mice were intraperitoneally administered with 0.5 ml/kg 10% CCl_4 in olive oil twice a week for 12 weeks, and silymarin was given orally at a dose of 200 mg/kg once a day from week 5 to 12 after CCl_4 administration.

2.2. In vivo and ex vivo imaging of luciferase activity

For *in vivo* imaging, mice were anesthetized with isoflurane and injected intraperitoneally with 150 mg luciferin/kg body weight. Five minutes later, mice were placed face up in the chamber and imaged for 1 min with the camera set at the highest sensitivity by IVIS Imaging System® 200 Series (Xenogen, Hopkinton, MA). For *ex vivo* imaging, mice were anesthetized and injected with luciferin intraperitoneally. Five minutes later, mice were sacrificed, and tissues were rapidly removed, placed in the IVIS system, and imaged with the same setting used for *in vivo* studies. Photons emitted from tissues were quantified using Living Image® software (Xenogen, Hopkinton, MA). Signal intensity was quantified as the sum of all detected photon counts from selected tissues and presented as photon/s.

2.3. Quantitative analysis of liver fibrosis

For detecting hepatic fibrosis, liver sections were stained with 0.1% Sirius red (Sigma, St. Louis, MO) in a saturated aqueous solution of picric acid (Panreac, Barcelona, Spain). One hour later, slides were rinsed in two changes of acidified water (0.5% glacial acetic acid in water), dehydrated in three changes of 100% ethanol, cleared in xylene, mounted in a resinous medium, and then observed under a light microscope. Sirius red-positive areas were measured using Image-Pro Plus (Media Cybernetics, Bethesda, MD). The proportions of hepatic fibrotic area (%) were calculated as areas occupied with red color/area of whole tissue.

2.4. Histological and immunohistochemical examination

Parafilm-embedded liver tissues were cut into 5-μm sections and stained with hematoxylin and eosin (H&E). For immunohistochemistry, sections were deparaffinized in xylene and rehydrated in graded alcohol. Endogenous peroxidase was quenched with 3% hydrogen peroxide in methanol for 15 min and the nonspecific binding was blocked with 1% bovine serum albumin at room temperature for 1 h. Sections were incubated with antibodies against p65 (Chemicon, Temecula, CA), TGF-β1 (Santa Cruz, Santa Cruz, CA), or α-smooth muscle actin (α-SMA) (Santa Cruz, Santa Cruz, CA) at 1:50 dilution overnight at 4 °C and then incubated with biotinylated secondary antibody (Zymed Laboratories, Carlsbad, CA) at room temperature for 20 min. Finally, slides were incubated with avidin–biotin complex reagent and stained with 3,3′-diaminobenzidine according to manufacturer's protocol (Histostain®-Plus kit, Zymed Laboratories, Carlsbad, CA). TGF-β1, α-SMA, and NF-κB-positive areas were measured using Image-Pro Plus (Media Cybernetics, Bethesda, MD) to quantify the expression levels of TGF-β1, α-SMA, and NF-κB. The proportions of TGF-β1, α-SMA, and NF-κB-positive areas were calculated as areas occupied with brown color/area of whole tissue.

2.5. Total RNA isolation

Total RNA was extracted from livers using the RNeasy Mini kit (Qiagen, Valencia, CA) and further treated with RNase-free DNase I (Qiagen, Valencia, CA) to remove contaminating DNA. Total RNA was quantified using the spectrophotometer (Beckman Coulter, Fullerton, CA), and samples with A260/A280 ratios greater than 1.8 were further evaluated using Agilent 2100 bioanalyzer (Agilent Technologies, Santa Clara, CA). The RNA sample with a RNA integrity number greater than 8.0 was accepted for microarray analysis.

2.6. Microarray analysis

Microarray analysis was performed as described previously (Cheng et al., 2010). Briefly, fluorescent RNA targets were prepared from 5 μg of total RNA using MessageAmp™ aRNA kit (Ambion, Austin, TX) and Cy5 dye (Amersham Pharmacia, Piscataway, NJ). Fluorescent targets were hybridized to the Mouse WG-6 Expression Bead Chip (Immunina, San Diego, CA) and scanned by an Axon 4000 scanner (Molecular Devices, Sunnyvale, CA). Number of replicates was three. The Cy5 fluorescent intensity of each spot was analyzed by genepix 4.1 software (Molecular Devices, Sunnyvale, CA). The signal intensity of each spot was corrected by subtracting background signals in the surrounding. We filtered out spots that signal-to-noise ratio was less than 0 or control probes. Spots that passed these criteria were normalized by the limma package of the R program using quantile normalization. Normalized data were tested for differential expression using Gene Expression Pattern Analysis Suite v3.1 (Montaner et al., 2006). Genes with fold changes $\geqslant 2.0$ or $\leqslant -2.0$ were further selected and tested enriched pathways on WebGestalt web site (http://bioinfo.vanderbilt.edu/webgestalt/login.php) by hypergeometric test.

2.7. Quantitative real-time polymerase chain reaction (qPCR)

The expression levels of cytochrome *c* oxidase genes (Cox6a2, Cox7a1, and Cox8b) were validated by qPCR. RNA samples were reverse-transcribed for 2 h at 37 °C with High Capacity cDNA Reverse Transcription kit (Applied Biosystems, Foster City, CA). qPCR was performed by using 1 μl of cDNA, 2× SYBR Green PCR Master Mix (Applied Biosystems, Foster City, CA), and 200 nM of forward and reverse primers. The reaction condition was followed: 10 min at 95 °C, and 40 cycles of 15 s at 95 °C, 1 min at 60 °C. Each assay was run on an Applied Biosystems 7300 Real-Time PCR system in triplicates. The efficiency of PCR was measured by the serial dilution test. A 4-log dilution range was generated using 10-fold serial dilutions of the DNA with four concentration points at 10^8, 10^7, 10^6, and 10^5 copies/μl. Fold changes were calculated using the comparative CT method. Primer sets used in this study were designed using Primer3 program (http://frodo.wi.mit.edu/primer3/). The specificities of primer sets were analyzed by nucleotide BLAST (http://blast.ncbi.nlm.nih.gov/Blast.cgi). Each primer set was able to amplify a

target DNA fragment from the respective gene with specificity. The primer set for each gene is followed: Cox6a2 forward, 5′-CAGAGAAGGACAGTGCCATTC-3′; Cox6a2 reverse, 5′-GAAGAGCCAGCACAAAGGTC-3′; Cox7a1 forward, 5′-CAATGACCTCCCA GTACACTTG-3′; Cox7a1 reverse, 5′-CCAAGCAGTATAAGCAGTAGGC-3′; Cox8b forward, 5′-TCCCAAAGCCCATGTCTCTG-3′; Cox8b reverse, 5′-CATCCTGCTGGAACCAT GAAG-3′; glyceraldahyde-3-phosphate dehydrogenase (GAPDH) forward, 5′-TCACC CACACTGTGCCCATCTATGA-3′; GAPDH reverse, 5′-GAGGAAGAGGATGCGGCAGTGG-3′. Previous study has shown that the levels of GAPDH mRNA and protein in livers are consistent in mice given with CCl_4 (Hellerbrand et al., 1999). Therefore, we used GAPDH gene as the reference gene in this study.

2.8. Statistic analysis

Data were presented as mean ± standard error. Data were analyzed by one-way ANOVA and post hoc LSD test using PASW Statistics (SPSS) version 12. A p value less than 0.05 was considered as statistically significant.

3. Results

3.1. Silymarin exhibited a steady decrease of CCl_4-induced NF-κB activity in the liver

Transgenic mice were given with CCl_4 and/or silymarin and imaged for the NF-κB-driven luminescence on week 4, 6, 8, and 12. As shown in Fig. 1, administration of CCl_4 significantly induced the NF-κB-dependent bioluminescent signal in the abdominal region as compared with mock group. *Ex vivo* imaging displayed that CCl_4 specifically induced the luminescence in the liver (Fig. 2). Oral administration of silymarin significantly suppressed the CCl_4-induced luminescent intensity in the abdominal region and the suppression displayed a time-dependent manner. *Ex vivo* imaging also displayed that silymarin specifically reduced CCl_4-induced NF-κB-driven bioluminescence in the liver. These findings suggested that CCl_4 induced NF-κB activation in the liver with specificity, while silymarin displayed a steady decrease of CCl_4-induced NF-κB activity in the liver.

3.2. The decrease of NF-κB activity by silymarin in the liver was correlated with the improvement of liver fibrosis

To evaluate the histological changes of liver and the degree of liver fibrosis, we stained the hepatic sections with H&E and Sirius red. Hepatic fibrosis is induced by the accumulation of collagen in the hepatic parenchyma (Bataller and Brenner, 2005). Sirius red is a strong anionic dye that has been used for the quantification of collagen in tissue sections for many years (Jimenez et al., 1985; Lopez-De Leon and Rojkind, 1985). Therefore, Sirius red-positive area can be a direct marker for the degree of liver fibrosis. As shown in Fig. 3, no apparent pathological alternations were found in mock group. Sirius red-positive region in the mock group was appeared around the central vein but not in the hepatic parenchyma. CCl_4 damaged the lobular structure of liver, which was characterized by the infiltration of immune cells, hemorrhage, vacuolar degeneration, and necrosis of hepatocytes. Sirius red-stained areas were clearly appeared in the boundaries of liver lobules and the proportion of the hepatic fibrotic area was 3.86 ± 0.54%. In contrast, silymarin improved the histological changes induced by CCl_4. The CCl_4-induced hemorrhage and necrosis in livers were ameliorated by silymarin. Moreover, Sirius red-stained areas in the silymarin group were reduced as compared with CCl_4 group, and

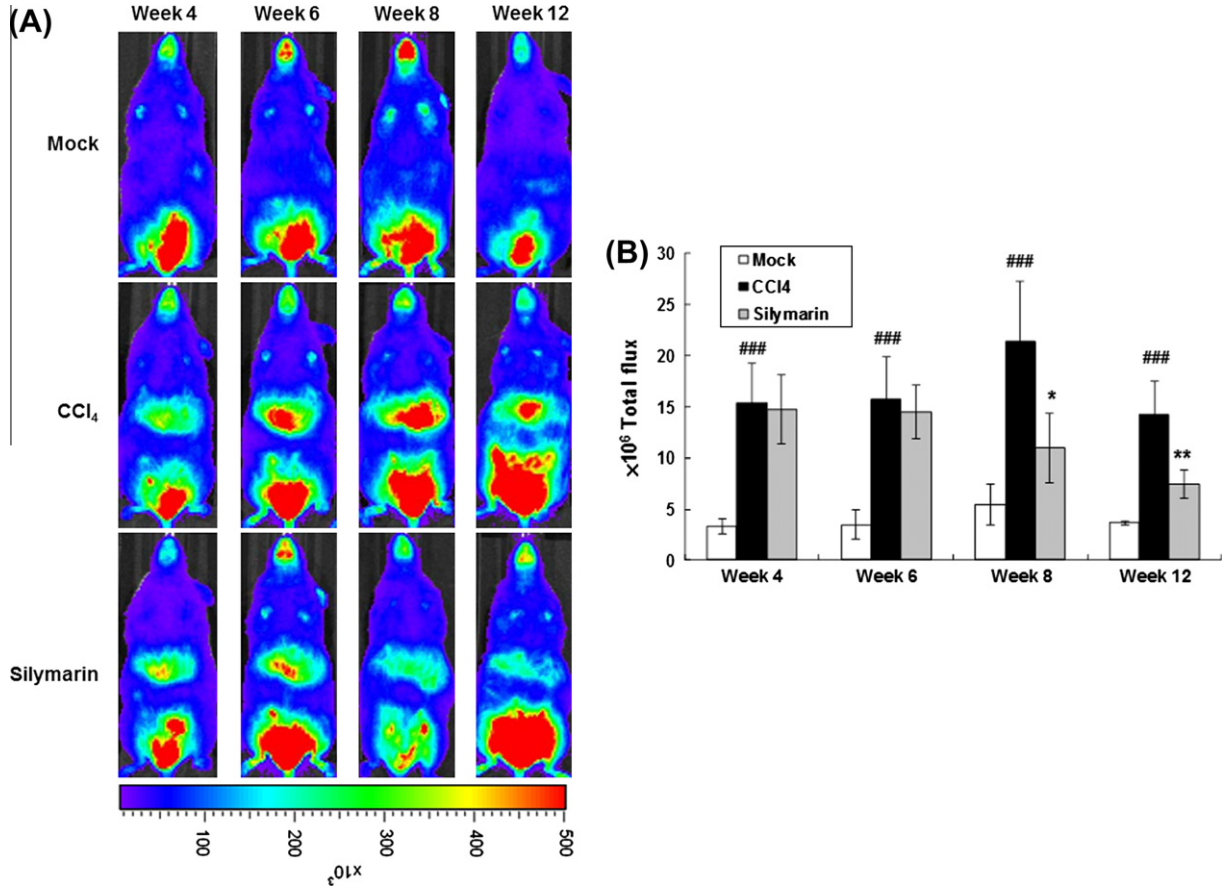

Fig. 1. NF-κB-dependent bioluminescence in living mice. Transgenic mice were administered with CCl_4 and/or silymarin, and imaged at indicated periods. (A) *In vivo* imaging. The color overlay on the image represents the photon/s emitted from the animal, as indicated by the color scales. Photos are representative images (n = 8). (B) Quantification of photon emission from whole animal. Values are mean ± standard error (n = 8). ###p < 0.001, compared with mock. $^{*}p$ < 0.05, $^{**}p$ < 0.01, compared with CCl_4.

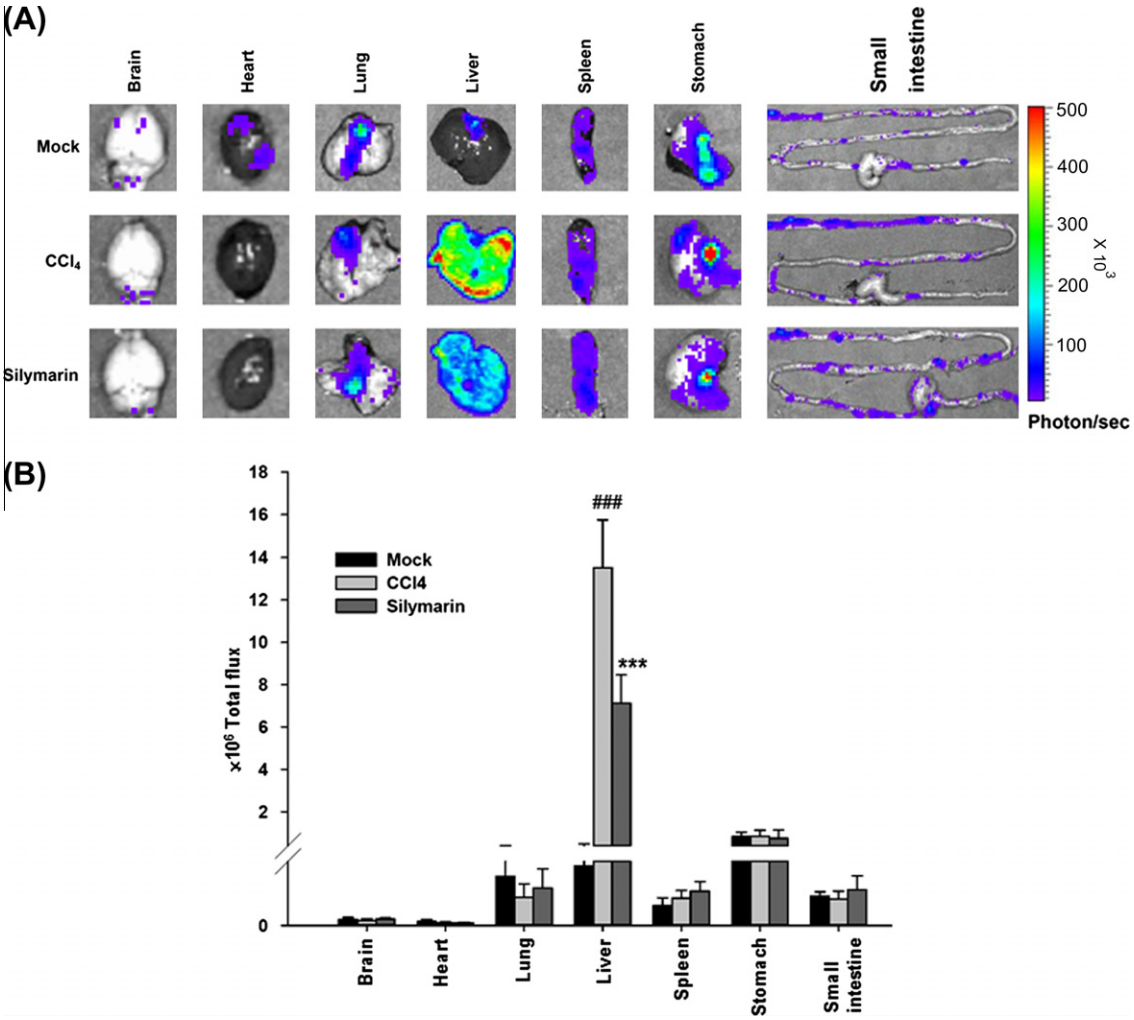

Fig. 2. NF-κB-dependent bioluminescence in individual organs. Transgenic mice were administered with CCl_4 and/or silymarin. Twelve weeks later, mice were sacrificed and organs were subjected to image. (A) *Ex vivo* imaging. The color overlay on the image represents the photon/s emitted from the organ, as indicated by the color scales. Photos are representative images ($n = 8$). (B) Quantification of photon emission from organs. Values are mean ± standard error ($n = 8$). ###$p < 0.001$, compared with mock. ***$p < 0.001$, compared with CCl_4.

the proportion of fibrotic areas (1.94 ± 0.29%) was significantly decreased by silymarin. These data suggested that silymarin improved the CCl_4-induced liver fibrosis.

We further performed immunohistochemical staining to correlate the liver fibrosis with NF-κB activity. Liver sections were immunostained with α-SMA antibody to detect the presence of myofibroblasts that produce collagen (Wells, 2005). Sections were also immunostained with antibody against TGF-β1, a cytokine playing a pivotal role in the liver fibrosis (Lotersztajn et al., 2005). As shown in Fig. 4, there were many brown TGF-β1-positive cells and α-SMA-positive myofibroblasts in the CCl_4-treated liver. However, oral administration of silymarin decreased the number of brown cells in the liver. The proportions of TGF-β1, α-SMA, and NF-κB-positive areas were increased in CCl_4 group and decreased in silymarin group, suggesting that CCl_4 induced the expression of TGF-β1, α-SMA, and NF-κB, while silymarin inhibited the CCl_4-induced TGF-β1, α-SMA, and NF-κB expression. Moreover, these findings suggested that silymarin ameliorated CCl_4-induced liver fibrosis, which was coincident with aforementioned histological data. Immunostaining with antibody against p65 revealed that there were many brown p65-positive cells in the CCl_4-treated liver. However, silymarin decreased the number of p65-positive cells in the liver. These data suggested that silymarin might improve CCl_4-induced liver fibrosis via inhibition of NF-κB, TGF-β1, and α-SMA. Moreover, the correlation between NF-κB activity, liver fibrosis, and bioluminescent imaging suggested the feasibility of NF-κB-dependent bioluminescent imaging for the evaluation of therapeutic efficacy of drugs for hepatic fibrosis.

3.3. Analysis of gene expression profile of silymarin in the CCl_4-treated liver

We further analyzed the gene expression profile of silymarin-treated liver by DNA microarray to identify the novel mechanisms of silymarin. In comparison with mock, 420 transcripts were upregulated and 439 transcripts were downregulated by 2-fold by CCl_4. In comparison with CCl_4, the expressions of 67 transcripts, including 2 upregulated and 65 downregulated transcripts, were altered with fold changes $\geqslant 2.0$ or $\leqslant -2.0$ by silymarin. These genes were further selected for pathway classification. Table 1 shows that 34 pathways were significantly altered by silymarin ($p < 0.01$). The half of pathways was associated with metabolism, while others were related to regulation of cellular process and signal transduction. TGF-β-associated pathways, including TGF-β signaling pathway, TGF-β-induced apoptosis and TGF-β-mediated pathway, were significantly regulated by silymarin. Because

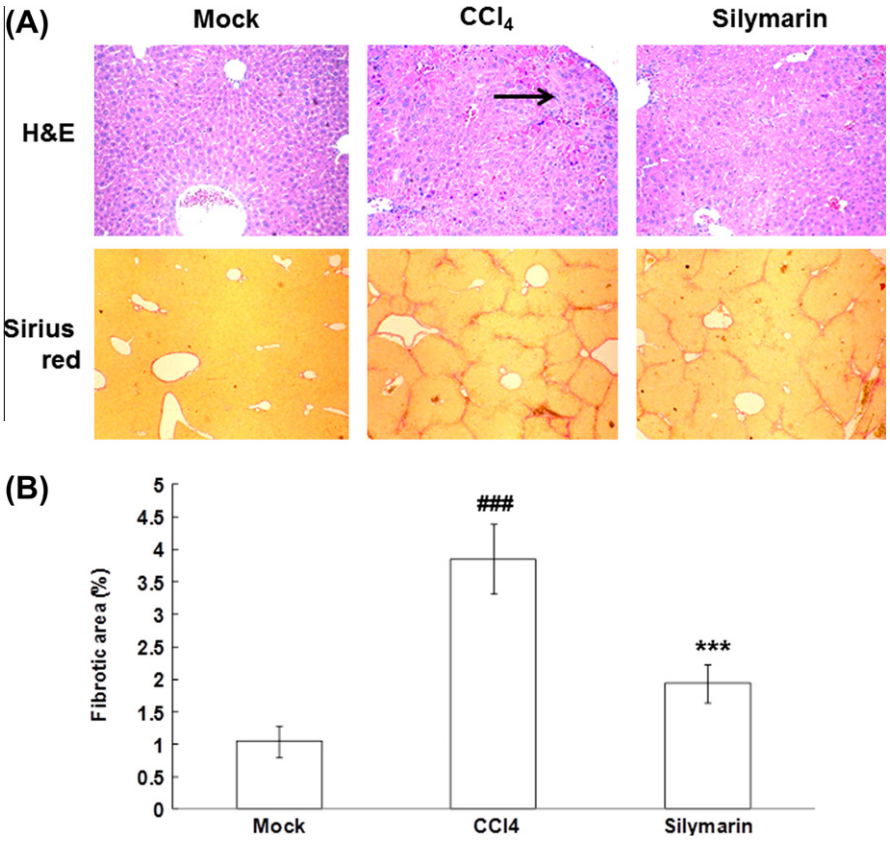

Fig. 3. Histological examination of liver by H&E and Sirius red staining. (A) Histological examination. Transgenic mice were administered with CCl_4 and/or silymarin. Twelve weeks later, mice were sacrificed, livers were excised, and sections were stained with H&E (100× magnification) or Sirius red (40× magnification). Photos are representative images ($n = 8$). (B) Quantification of liver fibrosis by Sirius red stain. Results are expressed as fibrotic area (%), which was calculated as areas occupied with red color/area of whole tissue. Values are mean ± standard error (8 sections/group and 10 fields/section). ###$p < 0.001$, compared with mock. $^{***}p < 0.001$, compared with CCl_4.

TGF-β1 plays a pivotal role in the progression of liver fibrosis, alteration of TGF-β-related pathways might contribute to the improvement of CCl_4-induced liver fibrosis by silymarin. Silymarin downregulated the expression levels of 65 genes in the CCl_4-treated liver. The genes with fold changes $\leqslant -4.0$ are shown in Table 2. The half of silymarin-downregulated genes was associated with cytoskeleton organization and muscle contraction, while three genes, including Cox6a2, Cox7a2 and Cox8b genes, were related to mitochondrion electron-transport chain. These findings suggested that silymarin might improve the CCl_4-induced liver fibrosis via regulation the expression of genes involved in cytoskeleton organization and electron transport.

3.4. Verification of expression levels of novel silymarin-regulated genes by qPCR

Microarray data showed that the expression of mitochondrial respiratory chain-related genes, including Cox6a2, Cox7a1 and Cox8b genes, were downregulated by silymarin. We further applied qPCR to validate the transcriptional expression levels of these genes. As shown in Table 3, the expression levels of Cox6a2, Cox7a1, and Cox8b genes in CCl_4 group were 496.21-, 21.36-, and 240.38-fold higher, respectively, as compared with mock group. However, CCl_4-upregulated gene expression was downregulated by silymarin, and the expression levels of Cox6a2, Cox7a1, and Cox8b genes in silymarin group were 9.84-, 0.72-, and 0.7-fold, respectively, as compared with mock group. The consistent data from qPCR and microarray indicated that silymarin downregulated the CCl_4-induced expression of Cox6a2, Cox7a1, and Cox8b genes.

4. Discussion

In this study, we found that silymarin exhibited a steady decrease of CCl_4-induced NF-κB activity in the liver, and the decrease of NF-κB activity by silymarin in the liver was correlated with the improvement of liver fibrosis. During a steady decrease of CCl_4-induced NF-κB-dependent luminescence by silymarin, microarray analysis of liver showed that silymarin altered the TGF-β-mediated pathways. Moreover, we newly identified that novel target genes like Cox genes were downregulated by silymarin, which was evidenced by NF-κB bioluminescence imaging-guided transcriptomic analysis. Bioluminescence imaging is a sensitive and noninvasive technique for real-time reporting disease progression and quantifying therapy efficacies in living animals. This technique has been used for monitoring tumor cell trafficking, tumor targeting, and host-biomaterial interaction (Contag and Bachmann, 2002; Ho et al., 2007; Ottobrini et al., 2005; Xiong et al., 2005). It has also been used to predict hepatic tumor burden in mice (Sarraf-Yazdi et al., 2004). In previous studies, we have constructed the transgenic mice carrying the NF-κB-driven luciferase gene and demonstrated the feasibility of NF-κB-dependent bioluminescent imaging for assessing the host-biomaterials interaction, elucidating the host response to ionizing radiation, evaluating the therapeutic effects of vanillin in inflammatory bowel diseases, and analyzing the anti-inflammatory effects of *Antrodia camphorata* (Chang et al., 2011; Ho et al., 2007; Hseu et al., 2010; Wu et al., 2009). In this study, we applied bioluminescent imaging to evaluate the progression of CCl_4-induced liver damages. Liver injury induced by CCl_4 is the best-characterized mechanism of xenobiotic-induced

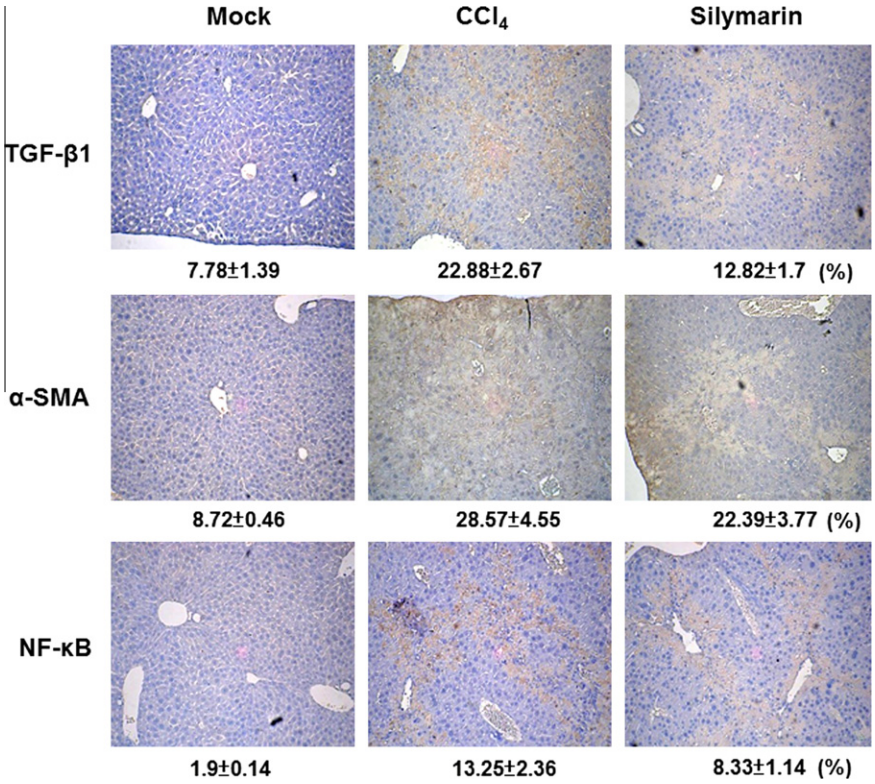

Fig. 4. Immunohistochemical examination of liver. Transgenic mice were administered with CCl_4 and/or silymarin. Twelve weeks later, mice were sacrificed, livers were excised, and sections were immunostained with antibodies against TGF-β1, α-SMA, and p65 (100× magnification). Quantification of TGF-β1, α-SMA, and p65-positive areas (%) was shown at the bottom. Values are mean ± standard error (8 sections/group and 3 fields/section). Photos are representative images ($n = 8$).

hepatotoxicity and a commonly used model for the screening of anti-hepatotoxic and/or hepatoprotective drugs (Weber et al., 2003). CCl_4 is metabolized by cytochrome p450 system and converted to trichloromethyl and trichloromethyl peroxy radicals. The free radicals of CCl_4 bind covalently to macromolecules and cause lipid peroxidation, which results in the fatty infiltration of hepatocytes and the sequential liver damage and fibrosis (Comporti et al., 2009). CCl_4 has been used extensively to induce liver injury in various animal models for decades. The experimentally induced cirrhotic response by CCl_4 in rats and mice are similar to liver cirrhosis in human (Weiler-Normann et al., 2007). Traditionally, liver injury and liver fibrosis induced by hepatotoxic substances can be evaluated by histological changes and concentrations of alanine aminotransferase, aspartate aminotransferase, alkaline phosphatase, and γ-glutamyl transpeptidase in sera (Nanji et al., 2001; Sun et al., 2010; Tacke et al., 2005). Because the sustained hepatic inflammation induced by various etiologies leads to liver fibrosis, and NF-κB plays a critical role in regulating inflammatory responses (Luedde and Schwabe, 2011), we tried to apply NF-κB transgenic mice to report the liver fibrosis induced by CCl_4. CCl_4 induced the NF-κB-dependent luminescence in the liver with specificity and the NF-κB activation was correlated with liver fibrosis, judged by Sirius red staining and immunohistochemical analysis. These findings indicated the feasibility of NF-κB bioluminescent imaging on the reporting of liver fibrosis induced by CCl_4.

Silymarin is a well-known hepatoprotective agent for the treatment of liver diseases (Abenavoli et al., 2010). It possesses antioxidative, antilipid peroxidative, antifibrotic, membrane stabilizing, immunomodulatory, and liver regenerating activities (Polyak et al., 2007; Saller et al., 2001; Shaker et al., 2010). Silymarin offers a good protection in various models of experimental liver diseases. It has also been applied clinically for alcoholic liver diseases, liver cirrhosis, Amanita mushroom poisoning, and drug-induced liver diseases (Pradhan and Girish, 2006). In this study, bioluminescent imaging showed that oral administration of silymarin reduced the CCl_4-induced NF-κB-dependent luminescent intensity in the liver with specificity. The correlation of the decreased NF-κB activity and the improved liver fibrosis by silymarin, suggesting the feasibility of NF-κB-dependent bioluminescent imaging for the evaluation of therapeutic effect of silymarin *in vivo*.

NF-κB bioluminescent imaging-guided transcriptomic analysis was further applied for the evaluation of novel targets and mechanisms of silymarin-mediated protection in the liver. Previous studies indicated that the anti-fibrotic and anti-inflammatory effects of silymarin are associated with TGF-β1 pathway (Ai et al., 2010). Silymarin suppresses the expression of profibrotic procollagen-α and TIMP-1 via downregulation of TGF-β1 mRNA in rats with biliary fibrosis (Jia et al., 2001). Moreover, genes associated with oxidative stress, cell cycle, cytoskeletal network, cell-cell adhesion, extracellular matrix, inflammation, and apoptosis are altered by silymarin in pyrogallol-exposed liver (Upadhyay et al., 2010). In this study, microarray data showed that silymarin altered the TGF-β1-associated pathways, including TGF-β signaling pathway, TGF-β-induced apoptosis and TGF-β-mediated pathway, in CCl_4-induced liver fibrosis, which were in agreement with previous reports. Furthermore, we newly identified that silymarin downregulated the expression levels of cytoskeleton organization genes and mitochondrion electron-transfer chain genes. It has been known that CCl_4 treatment induces the reorganization of cytoskeleton and, in turn, induces the differentiation of hepatic stellate cells into myofibroblast-like cells (De Minicis et al., 2007). Silymarin downregulated the expression of cytoskeleton component genes, suggesting that silymarin might suppress the transformation of hepatic stellate cells via inhibiting cytoskeleton reorganization and thus ameliorate the fibrosis of liver. Progression of CCl_4-induced liver fibrosis is associated with free radicals pro-

Table 1
Pathway analysis of silymarin-altered genes with fold changes ⩾2.0 or ⩽−2.0.

Pathway	*p* Value[a]
Regulation of cellular process/cell cycle and death	
TGF-β signaling pathway	2.75×10^{-7}
p53-Mediated pathway	0.00171
Tight junction	0.00014
TGF-β-induced apoptosis	0.00261
Adherens junction	0.00494
TGF-β-mediated pathway	0.00976
Metabolism	
Urea cycle and metabolism of amino groups	2.49×10^{-5}
Citrate cycle	2.45×10^{-6}
Arginine and proline metabolism	0.00016
Galactose metabolism	0.00034
Biosynthesis of steroids	0.00049
Glycine, serine and threonine metabolism	0.00070
Glycolysis/gluconeogenesis	0.00100
Butanoate metabolism	0.00098
Folate biosynthesis	0.00218
Pyruvate metabolism	0.00223
Fatty acid metabolism	0.00273
Bile acid biosynthesis	0.00273
Alanine and aspartate metabolism	0.00442
Glutathione metabolism	0.00544
Starch and sucrose metabolism	0.00601
Glycosaminoglycan degradation	0.00799
Glutamate metabolism	0.00921
Signal transduction	
Adipocytokine signaling pathway	8.26×10^{-5}
IL6 signaling pathway	0.00016
PPAR signaling pathway	0.00039
Insulin signaling pathway	0.00047
Vitamin D3 signaling pathway	0.00067
RANKL signaling pathway	0.00548
TNF signaling pathway	0.00629
IGF signaling pathway	0.00655
Chemokine signaling pathway	0.00709
EGF signaling pathway	0.00770
PTH/PTHrP signaling pathway	0.00840

[a] *p* Value was calculated on WebGestalt web site by hypergeometric test.

Table 2
Expression levels of silymarin-downregulated genes in CCl_4-treated liver.

Gene symbol	Description	Fold changes[a]
Acta1	Actin, alpha 1, skeletal muscle	−90.21 ± 0.001
Myl1	Myosin, light polypeptide 1	−77.05 ± 0.001
Tnni2	Troponin I, skeletal, fast 2	−49.39 ± 0.001
Atp2a1	ATPase, Ca^{+2} transporting, cardiac muscle, fast twitch 1	−48.46 ± 0.001
Mylpf	Myosin light chain, phosphorylatable, fast skeletal muscle	−41.90 ± 0.001
Mb	Myoglobin	−35.39 ± 0.002
Cox6a2	Cytochrome c oxidase, subunit VI a, polypeptide 2	−28.43 ± 0.003
Cox8b	Cytochrome c oxidase, subunit VIII b	−18.60 ± 0.004
Eno3	Enolase 3, beta muscle	−8.17 ± 0.009
Tnnt1	Troponin T1, skeletal, slow	−7.60 ± 0.011
Tnnc1	Troponin C, cardiac/slow skeletal	−7.56 ± 0.010
Cox7a1	Cytochrome c oxidase, subunit VIIa 1	−6.67 ± 0.015
Eef1a2	Eukaryotic translation elongation factor 1 alpha 2	−4.64 ± 0.022
EG433229	Predicted gene, EG433229, transcript variant 7	−4.06 ± 0.016

[a] Fold changes are mean ± standard error ($n = 3$).

duction that results in the significant alternations in functional state of mitochondrial respiratory chain (Tanaka et al., 1987). The electron transporters are combined in four complex: NADH reductase, succinate reductase, cytochrome *c* reductase, and Cox (Boyer, 1997). Cox plays a crucial role in oxidative metabolism, acting as

Table 3
Expression levels of Cox6a2, Cox7a1, and Cox8b genes by qPCR.

Sample	Average C_T of target	Average C_T of GAPDH	ΔC_T[a]	$\Delta\Delta C_T$[b]	Relative to mock
Cox6a2					
Mock	35.82 ± 0.40	19.71 ± 0.03	16.11 ± 0.40	0.00 ± 0.40	1.00
CCl_4	25.80 ± 0.05	18.64 ± 0.05	7.16 ± 0.07	−8.96 ± 0.07	496.21
Silymarin	31.17 ± 0.09	18.36 ± 0.01	12.81 ± 0.09	−3.30 ± 0.09	9.84
Cox7a1					
Mock	29.98 ± 0.10	19.71 ± 0.03	10.27 ± 0.11	0.00 ± 0.11	1.00
CCl_4	24.49 ± 0.04	18.64 ± 0.05	5.85 ± 0.07	−4.42 ± 0.07	21.36
Silymarin	29.10 ± 0.11	18.36 ± 0.01	10.74 ± 0.11	0.47 ± 0.11	0.72
Cox8b					
Mock	32.81 ± 0.11	19.71 ± 0.03	13.09 ± 0.12	0.00 ± 0.12	1.00
CCl_4	23.83 ± 0.05	18.64 ± 0.05	5.18 ± 0.07	−7.91 ± 0.07	240.38
Silymarin	31.97 ± 0.29	18.36 ± 0.01	13.61 ± 0.29	0.52 ± 0.29	0.70

[a] The ΔC_T value is determined by subtracting the average GAPDH C_T value from the average target gene C_T value. The standard deviation of the difference is calculated from the standard deviations of the target gene and GAPDH.

[b] The calculation of $\Delta\Delta C_T$ involves subtraction by the ΔC_T calibrator value. This is a subtraction of an arbitrary constant, so the standard deviation of $\Delta\Delta C_T$ is the same as the standard deviation of ΔC_T value.

the terminal component of the mitochondrial electron-transport chain in which electrons are passed from cytochrome *c* to molecular oxygen (Boyer, 1997). Previous studies showed that CCl_4 treatment decreases the activity of NADH reductase and increases the activity of Cox in rats with CCl_4-induced liver fibrosis (Krahenbuhl and Reichen, 1992; Shiryaeva et al., 2008; Tanaka et al., 1987). Our data also showed that the expression levels of Cox genes were elevated by CCl_4. The decrease and damage of NADH reductase results in electron leakage to $\cdot O_2^-$ oxygen and superoxide anion production, which lead to the increased oxygen consumption by the respiratory chain of pathologic mitochondria. Subsequently, the elevated activity of Cox by CCl_4 promotes the transfer of electrons to molecular oxygen and drive the ATP production of the mitochondria (Shiryaeva et al., 2008). In contrast, previous study indicated that silymarin inhibits the oxygen consumption in mitochondria isolated from rats and increases the iron-reduced NADH reductase activity to the basal level (Chavez and Bravo, 1988; Pietrangelo et al., 2002). Moreover, our data showed that silymarin reduced the CCl_4-induced expression levels of Cox genes to the basal levels as compared to mock. These findings suggested that silymarin might counteract the mitochondrion electron-transfer chain alteration by CCl_4, which might be associated with the improvement of CCl_4-induced liver fibrosis by silymarin.

5. Conclusions

In conclusion, we applied for the first time the *in vivo* NF-κB bioluminescent imaging and microarray analysis for the evaluation and identification of the therapeutic potentials and novel mechanisms of silymarin in CCl_4-induced liver fibrosis. The correlation of NF-κB bioluminescence and liver fibrosis suggested the feasibility of NF-κB bioluminescent imaging on the evaluation of therapeutic potentials of drugs for the treatment of liver fibrosis. Moreover, we newly identified that silymarin exhibited anti-fibrotic effects *in vivo* via regulating TGF-β-mediated pathways and altering the expression of genes involved in cytoskeleton organization and mitochondrion electron-transfer chain.

Conflict of Interest

The authors declare that there are no conflicts of interest.

Acknowledgments

This work was supported by grants from National Science Council, Committee on Chinese Medicine and Pharmacy at Department of Health (CCMP100-RD-048), and China Medical University (CMU100-S-16, CMU100-S-34, and CMU100-TS-14).

References

Abenavoli, L., Capasso, R., Milic, N., Capasso, F., 2010. Milk thistle in liver diseases: past, present, future. Phytother. Res. 24, 1423–1432.

Ai, W., Zhang, Y., Tang, Q.Z., Yan, L., Bian, Z.Y., Liu, C., Huang, H., Bai, X., Yin, L., Li, H., 2010. Silibinin attenuates cardiac hypertrophy and fibrosis through blocking EGFR-dependent signaling. J. Cell Biochem. 110, 1111–1122.

Baeuerle, P.A., Baichwal, V.R., 1997. NF-κB as a frequent target for immunosuppressive and anti-inflammatory molecules. Adv. Immunol. 65, 111–137.

Baldwin Jr., A.S., 1996. The NF-κB and IκB proteins: new discoveries and insights. Annu. Rev. Immunol. 14, 649–683.

Basiglio, C.L., Sanchez Pozzi, E.J., Mottino, A.D., Roma, M.G., 2009. Differential effects of silymarin and its active component silibinin on plasma membrane stability and hepatocellular lysis. Chem. Biol. Interact 179, 297–303.

Bataller, R., Brenner, D.A., 2005. Liver fibrosis. J. Clin. Invest. 115, 209–218.

Baur, J.A., Pearson, K.J., Price, N.L., Jamieson, H.A., Lerin, C., Kalra, A., Prabhu, V.V., Allard, J.S., Lopez-Lluch, G., Lewis, K., Pistell, P.J., Poosala, S., Becker, K.G., Boss, O., Gwinn, D., Wang, M., Ramaswamy, S., Fishbein, K.W., Spencer, R.G., Lakatta, E.G., Le Couteur, D., Shaw, R.J., Navas, P., Puigserver, P., Ingram, D.K., de Cabo, R., Sinclair, D.A., 2006. Resveratrol improves health and survival of mice on a high-calorie diet. Nature 444, 337–342.

Bonizzi, G., Karin, M., 2004. The two NF-κB activation pathways and their role in innate and adaptive immunity. Trends Immunol. 25, 280–288.

Boyer, P.D., 1997. The ATP synthase – a splendid molecular machine. Annu. Rev. Biochem. 66, 717–749.

Chandan, B.K., Saxena, A.K., Shukla, S., Sharma, N., Gupta, D.K., Singh, K., Suri, J., Bhadauria, M., Qazi, G.N., 2008. Hepatoprotective activity of Woodfordia fruticosa Kurz flowers against carbon tetrachloride induced hepatotoxicity. J. Ethnopharmacol. 119, 218–224.

Chang, C.T., Lin, H., Ho, T.Y., Li, C.C., Lo, H.Y., Wu, S.L., Huang, Y.F., Liang, J.A., Hsiang, C.Y., 2011. Comprehensive assessment of host responses to ionizing radiation by nuclear factor-κB bioluminescence imaging-guided transcriptomic analysis. PLoS One 6, e23682.

Chavez, E., Bravo, C., 1988. Silymarin-induced mitochondrial Ca^{2+} release. Life Sci. 43, 975–981.

Cheng, H.M., Li, C.C., Chen, C.Y., Lo, H.Y., Cheng, W.Y., Lee, C.H., Yang, S.Z., Wu, S.L., Hsiang, C.Y., Ho, T.Y., 2010. Application of bioactivity database of Chinese herbal medicine on the therapeutic prediction, drug development, and safety evaluation. J. Ethnopharmacol. 132, 429–437.

Comporti, M., Arezzini, B., Signorini, C., Vecchio, D., Gardi, C., 2009. Oxidative stress, isoprostanes and hepatic fibrosis. Histol. Histopathol. 24, 893–900.

Contag, C.H., Bachmann, M.H., 2002. Advances in *in vivo* bioluminescence imaging of gene expression. Annu. Rev. Biomed. Eng. 4, 235–260.

De Minicis, S., Seki, E., Uchinami, H., Kluwe, J., Zhang, Y., Brenner, D.A., Schwabe, R.F., 2007. Gene expression profiles during hepatic stellate cell activation in culture and *in vivo*. Gastroenterology 132, 1937–1946.

Dothager, R.S., Flentie, K., Moss, B., Pan, M.H., Kesarwala, A., Piwnica-Worms, D., 2009. Advances in bioluminescence imaging of live animal models. Curr. Opin. Biotechnol. 20, 45–53.

Hellerbrand, C., Stefanovic, B., Giordano, F., Burchardt, E.R., Brenner, D.A., 1999. The role of TGFβ1 in initiating hepatic stellate cell activation *in vivo*. J. Hepatol. 30, 77–87.

Ho, T.Y., Chen, Y.S., Hsiang, C.Y., 2007. Noninvasive nuclear factor-κB bioluminescence imaging for the assessment of host-biomaterial interaction in transgenic mice. Biomaterials 28, 4370–4377.

Hseu, Y.C., Huang, H.C., Hsiang, C.Y., 2011. *Antrodia camphorata* suppresses lipopolysaccharide-induced nuclear factor-κB activation in transgenic mice evaluated by bioluminescence imaging. Food Chem. Toxicol. 48, 2319–2325.

Hsiang, C.Y., Chen, Y.S., Ho, T.Y., 2009. Nuclear factor-κB bioluminescence imaging-guided transcriptomic analysis for the assessment of host-biomaterial interaction *in vivo*. Biomaterials 30, 3042–3049.

Jia, J.D., Bauer, M., Cho, J.J., Ruehl, M., Milani, S., Boigk, G., Riecken, E.O., Schuppan, D., 2001. Antifibrotic effect of silymarin in rat secondary biliary fibrosis is mediated by downregulation of procollagen alpha1(I) and TIMP-1. J. Hepatol. 35, 392–398.

Jimenez, W., Pares, A., Caballeria, J., Heredia, D., Bruguera, M., Torres, M., Rojkind, M., Rodes, J., 1985. Measurement of fibrosis in needle liver biopsies: evaluation of a colorimetric method. Hepatology 5, 815–818.

Karin, M., Ben-Neriah, Y., 2000. Phosphorylation meets ubiquitination: the control of NF-κB activity. Annu. Rev. Immunol. 18, 621–663.

Krahenbuhl, S., Reichen, J., 1992. Adaptation of mitochondrial metabolism in liver cirrhosis. Different strategies to maintain a vital function. Scand. J. Gastroenterol. Suppl. 193, 90–96.

Lamb, J., Crawford, E.D., Peck, D., Modell, J.W., Blat, I.C., Wrobel, M.J., Lerner, J., Brunet, J.P., Subramanian, A., Ross, K.N., Reich, M., Hieronymus, H., Wei, G., Armstrong, S.A., Haggarty, S.J., Clemons, P.A., Wei, R., Carr, S.A., Lander, E.S., Golub, T.R., 2006. The Connectivity Map: using gene-expression signatures to connect small molecules, genes, and disease. Science 313, 1929–1935.

Lopez-De Leon, A., Rojkind, M., 1985. A simple micromethod for collagen and total protein determination in formalin-fixed paraffin-embedded sections. J. Histochem. Cytochem. 33, 737–743.

Lotersztajn, S., Julien, B., Teixeira-Clerc, F., Grenard, P., Mallat, A., 2005. Hepatic fibrosis: molecular mechanisms and drug targets. Annu. Rev. Pharmacol. Toxicol. 45, 605–628.

Luedde, T., Schwabe, R.F., 2011. NF-κB in the liver–linking injury, fibrosis and hepatocellular carcinoma. Nat. Rev. Gastroenterol Hepatol. 8, 108–118.

Montaner, D., Tarraga, J., Huerta-Cepas, J., Burguet, J., Vaquerizas, J.M., Conde, L., Minguez, P., Vera, J., Mukherjee, S., Valls, J., Pujana, M.A., Alloza, E., Herrero, J., Al-Shahrour, F., Dopazo, J., 2006. Next station in microarray data analysis: GEPAS. Nucleic Acids Res. 34, W486–W491.

Nanji, A.A., Jokelainen, K., Tipoe, G.L., Rahemtulla, A., Dannenberg, A.J., 2001. Dietary saturated fatty acids reverse inflammatory and fibrotic changes in rat liver despite continued ethanol administration. J. Pharmacol. Exp. Ther. 299, 638–644.

Ottobrini, L., Lucignani, G., Clerici, M., Rescigno, M., 2005. Assessing cell trafficking by noninvasive imaging techniques: applications in experimental tumor immunology. Q. J. Nucl. Med. Mol. Imaging 49, 361–366.

Pietrangelo, A., Montosi, G., Garuti, C., Contri, M., Giovannini, F., Ceccarelli, D., Masini, A., 2002. Iron-induced oxidant stress in nonparenchymal liver cells: mitochondrial derangement and fibrosis in acutely iron-dosed gerbils and its prevention by silybin. J. Bioenerg. Biomembr. 34, 67–79.

Polyak, S.J., Morishima, C., Shuhart, M.C., Wang, C.C., Liu, Y., Lee, D.Y., 2007. Inhibition of T-cell inflammatory cytokines, hepatocyte NF-κB signaling, and HCV infection by standardized Silymarin. Gastroenterology 132, 1925–1936.

Pradhan, S.C., Girish, C., 2006. Hepatoprotective herbal drug, silymarin from experimental pharmacology to clinical medicine. Ind. J. Med. Res. 124, 491–504.

Sakaida, I., Terai, S., Yamamoto, N., Aoyama, K., Ishikawa, T., Nishina, H., Okita, K., 2004. Transplantation of bone marrow cells reduces CCl_4-induced liver fibrosis in mice. Hepatology 40, 1304–1311.

Saller, R., Meier, R., Brignoli, R., 2001. The use of silymarin in the treatment of liver diseases. Drugs 61, 2035–2063.

Sarraf-Yazdi, S., Mi, J., Dewhirst, M.W., Clary, B.M., 2004. Use of *in vivo* bioluminescence imaging to predict hepatic tumor burden in mice. J. Surg. Res. 120, 249–255.

Shaker, E., Mahmoud, H., Mnaa, S., 2010. Silymarin, the antioxidant component and *Silybum marianum* extracts prevent liver damage. Food Chem. Toxicol. 48, 803–806.

Shiryaeva, A., Baidyuk, E., Arkadieva, A., Okovityy, S., Morozov, V., Sakuta, G., 2008. Hepatocyte mitochondrion electron-transport chain alterations in CCl_4 and alcohol induced hepatitis in rats and their correction with simvastatin. J. Bioenerg. Biomembr. 40, 27–34.

Siebenlist, U., Franzoso, G., Brown, K., 1994. Structure, regulation and function of NF-κB. Annu. Rev. Cell Biol. 10, 405–455.

Sun, H., Che, Q.M., Zhao, X., Pu, X.P., 2010. Antifibrotic effects of chronic baicalein administration in a CCl_4 liver fibrosis model in rats. Eur. J. Pharmacol. 631, 53–60.

Suter, L., Babiss, L.E., Wheeldon, E.B., 2004. Toxicogenomics in predictive toxicology in drug development. Chem. Biol. 11, 161–171.

Tacke, F., Wustefeld, T., Horn, R., Luedde, T., Srinivas Rao, A., Manns, M.P., Trautwein, C., Brabant, G., 2005. High adiponectin in chronic liver disease and cholestasis suggests biliary route of adiponectin excretion *in vivo*. J. Hepatol. 42, 666–673.

Tanaka, A., Morimoto, T., Wakashiro, S., Ikai, I., Ozawa, K., Orii, Y., 1987. Kinetic alterations of cytochrome *c* oxidase in carbon tetrachloride induced cirrhotic rat liver. Life Sci. 41, 741–748.

Upadhyay, G., Tiwari, M.N., Prakash, O., Jyoti, A., Shanker, R., Singh, M.P., 2010. Involvement of multiple molecular events in pyrogallol-induced hepatotoxicity and silymarin-mediated protection: evidence from gene expression profiles. Food Chem. Toxicol. 48, 1660–1670.

Weber, L.W., Boll, M., Stampfl, A., 2003. Hepatotoxicity and mechanism of action of haloalkanes: carbon tetrachloride as a toxicological model. Crit. Rev. Toxicol. 33, 105–136.

Weiler-Normann, C., Herkel, J., Lohse, A.W., 2007. Mouse models of liver fibrosis. Z. Gastroenterol. 45, 43–50.

Wells, R.G., 2005. The role of matrix stiffness in hepatic stellate cell activation and liver fibrosis. J. Clin. Gastroenterol. 39, S158–S161.

Wu, S.L., Chen, J.C., Li, C.C., Lo, H.Y., Ho, T.Y., Hsiang, C.Y., 2009. Vanillin improves and prevents trinitrobenzene sulfonic acid-induced colitis in mice. J. Pharmacol. Exp. Ther. 330, 370–376.

Xiong, Y.Q., Willard, J., Kadurugamuwa, J.L., Yu, J., Francis, K.P., Bayer, A.S., 2005. Real-time *in vivo* bioluminescent imaging for evaluating the efficacy of antibiotics in a rat Staphylococcus aureus endocarditis model. Antimicrob Agents Chemother. 49, 380–387.

Food and Chemical Toxicology xxx (2012) xxx–xxx

Contents lists available at SciVerse ScienceDirect

Food and Chemical Toxicology

journal homepage: www.elsevier.com/locate/foodchemtox

Genipin inhibits lipopolysaccharide-induced acute systemic inflammation in mice as evidenced by nuclear factor-κB bioluminescent imaging-guided transcriptomic analysis

Chia-Cheng Li [a,1], Chien-Yun Hsiang [b,1], Hsin-Yi Lo [a], Fu-Tzu Pai [a], Shih-Lu Wu [c], Tin-Yun Ho [a,d,*]

[a] Graduate Institute of Chinese Medicine, China Medical University, Taichung 40402, Taiwan
[b] Department of Microbiology, China Medical University, Taichung 40402, Taiwan
[c] Department of Biochemistry, China Medical University, Taichung 40402, Taiwan
[d] Department of Nuclear Medicine, China Medical University Hospital, Taichung 40447, Taiwan

ARTICLE INFO

Article history:
Received 20 September 2011
Accepted 30 May 2012
Available online xxxx

Keywords:
Genipin
Systemic inflammation
Nuclear factor-κB
Bioluminescent imaging
DNA microarray

ABSTRACT

Genipin is a natural blue colorant in food industry. Inflammation is correlated with human disorders, and nuclear factor-κB (NF-κB) is the critical molecule involved in inflammation. In this study, the anti-inflammatory effect of genipin on the lipopolysaccharide (LPS)-induced acute systemic inflammation in mice was evaluated by NF-κB bioluminescence-guided transcriptomic analysis. Transgenic mice carrying the NF-κB-driven luciferase genes were administered intraperitoneally with LPS and various amounts of genipin. Bioluminescent imaging showed that genipin significantly suppressed LPS-induced NF-κB-dependent luminescence *in vivo*. The suppression of LPS-induced acute inflammation by genipin was further evidenced by the reductions of cytokine levels in sera and organs. Microarray analysis of these organs showed that the transcripts of 79 genes were differentially expressed in both LPS and LPS/genipin groups, and one third of these genes belonged to chemokine ligand, chemokine receptor, and interferon (IFN)-induced protein genes. Moreover, network analysis showed that NF-κB played a critical role in the regulation of genipin-affected gene expression. In conclusion, we newly identified that genipin exhibited anti-inflammatory effects in a model of LPS-induced acute systemic inflammation via downregulation of chemokine ligand, chemokine receptor, and IFN-induced protein productions.

1. Introduction

The fruit of *Gardenia jasminoides* Ellis is a medicinal herb that has been used for the treatment of inflammation, jaundice, and hepatic disorders in traditional Chinese medicine (Tseng et al., 1995). Genipin is the aglycon of geniposide found in gardenia fruit (He et al., 2006). Genipin has been used as a blue colorant in food industry (Fujikawa et al., 1987). It also has been used as the cross-linking agent for biological tissue fixation (Sung et al., 1998). Genipin possesses a variety of pharmacological activities, such as anti-microbial, hepatoprotective, and neurotrophic effects (Yamamoto et al., 2000; Yamazaki and Chiba, 2008). Anti-topical inflammatory potentials of genipin have also been reported (Koo et al., 2004, 2006); however, the therapeutic effect and mechanism of genipin on systemic inflammation *in vivo* remain to be clarified.

A wide range of human disorders, such as pneumonia, asthma, rheumatic arthritis, neurodegenerative diseases and obesity, correlates with inflammation (Amor et al., 2010; Thaler and Schwartz, 2010). Moreover, epidemiological studies have identified chronic infections and inflammation as major risk factors for various types of cancers (Karin, 2006). The development of inflammation is controlled by various cytokines, such as interleukin-1β (IL-1β), tumor necrosis factor-α (TNF-α) and interferon-γ (IFN-γ) (Hanada and Yoshimura, 2002). The production of cytokine is further controlled by the transcription factor, nuclear factor-κB (NF-κB) (Baldwin, 1996). NF-κB is an inducible nuclear transcription factor that consists of heterodimers of RelA (p65), c-Rel, RelB, p50/NF-κB1, and

Abbreviations: BCR, B-cell receptor; CCL, chemokine (C–C motif) ligand; CXCL, chemokine (C–X–C motif) ligand; ELISA, enzyme-linked immunosorbent assay; GAPDH, glyceraldahyde-3-phosphate dehydrogenase; GO, gene ontology; Ifi202, IFN-activated gene 202B; IFN, interferon; IL-1β, interleukin-1β; LAPTM5, lysosomal-associated protein transmembrane 5; LPS, lipopolysaccharide; MTT, methylthiazolyldiphenyl-tetrazolium bromide; NF-κB, nuclear factor-κB; Nrarp, Notch-regulated ankyrin repeat protein; PBS, phosphate-buffered saline; qPCR, quantitative real-time polymerase chain reaction; RLU, relative luciferase unit; SNF, sucrose nonfermenting protein; TNF-α, tumor necrosis factor-α.

* Corresponding author at: Graduate Institute of Chinese Medicine, China Medical University, 91 Hsueh-Shih Road, Taichung 40402, Taiwan. Tel.: +886 4 22053366 3302; fax: +886 4 22053764.
E-mail address: cyhsiang@mail.cmu.edu.tw (T.-Y. Ho).

[1] These authors contributed equally to this work.

0278-6915/$ - see front matter © 2012 Published by Elsevier Ltd.
http://dx.doi.org/10.1016/j.fct.2012.05.054

p52/NF-κB2. NF-κB activity is induced by a large variety of signals, such as bacteria, viruses, necrotic cell products, and inflammatory cytokines. When stimulated, NF-κB binds to the NF-κB-responsive element present in the promoter of inflammatory genes, leading to the induction of gene expression. Accordingly, NF-κB is a critical molecule involved in the regulation of inflammatory cytokine production and inflammation (Bonizzi and Karin, 2004).

We have previously applied NF-κB bioluminescent imaging to assess the host inflammatory responses to *Antrodia camphorata*, vanillin, and biomaterials *in vivo* (Ho et al., 2007; Hseu et al., 2010; Hsiang et al., 2009; Wu et al., 2009). Transgenic mice carrying the NF-κB-driven luciferase genes were used to monitor the host inflammatory responses, and the anti-inflammatory mechanism was further analyzed by transcriptomic tools. In this study, we applied such a platform to evaluate the anti-inflammatory potential of genipin in an *in vivo* model of lipopolysaccharide (LPS)-induced acute systemic inflammation. Our findings showed that genipin exhibited systemic anti-inflammatory effects *in vivo* via inhibiting the expressions of chemokine ligand, chemokine receptor, and IFN-induced protein genes.

2. Materials and methods

2.1. Materials

LPS was purchased from Sigma (St. Louis, MO) and dissolved in phosphate-buffered saline (PBS) (137 mM NaCl, 1.4 mM KH_2PO_4, 4.3 mM Na_2HPO_4, 2.7 mM KCl, pH 7.2). Genipin was purchased from Wako (Osaka, Japan). Methylthiazolyldiphenyl-tetrazolium bromide (MTT) was purchased from Sigma (St. Louis, MO) and dissolved in PBS at 5 mg/ml. D-Luciferin was purchased from Xenogen (Hopkinton, MA) and dissolved in PBS at 15 mg/ml. Mouse monoclonal antibodies against IL-1β and TNF-α were purchased from Santa Cruz (Santa Cruz, CA).

2.2. Cell culture and genipin treatment

Recombinant HepG2/NF-κB cells, which contained the luciferase genes driven by NF-κB-responsive elements, were constructed as described previously (Ho et al., 2007). HepG2/NF-κB cells were maintained in Dulbecco's modified Eagle's medium supplemented with 10% fetal bovine serum. For genipin treatment, cells were cultured in 96-well plates at 37 °C. Twenty-four hours later, cells were treated with 100 ng/ml LPS and various amounts of genipin for an additional 24 h.

2.3. Luciferase assay and cell viability assay

Luciferase assay was performed as described previously (Ho et al., 2007). Relative NF-κB activity was calculated by dividing the relative luciferase unit (RLU) of treated cells by the RLU of untreated cells. Cell viability was monitored by MTT colorimetric assay as described previously (Ho et al., 2007). Cell viability (%) was calculated by (OD of genipin-treated cells/ OD of solvent-treated cells).

2.4. Animal experiments

Mouse experiments were conducted under ethics approval from the China Medical University Animal Care and Use Committee (Ethics Approval Number 97–28N). Transgenic mice, carrying the luciferase genes driven by NF-κB-responsive elements, were constructed as described previously (Ho et al., 2007). All transgenic mice were crossed with wild-type F1 mice to yield NF-κB-*luc* heterozygous mice with the FVB genetic background.

A total of 25 transgenic mice (female, 6 to 8 weeks old) were randomly divided into five groups of five mice: (1) mock, no treatment; (2) LPS (4 mg/kg), (3) LPS plus genipin (1 mg/kg), (4) LPS plus genipin (10 mg/kg), and (5) LPS plus genipin (100 mg/kg). Mice were challenged intraperitoneally with LPS and then with genipin 10 min later. Four hours later, mice were imaged for the luciferase activity, and subsequently sacrificed for *ex vivo* imaging, RNA extraction, and immunohistochemical staining.

2.5. In vivo and ex vivo imaging of luciferase activity

For *in vivo* imaging, mice were anesthetized with isoflurane and injected intraperitoneally with 150 mg/kg luciferin. Ten minutes later, mice were placed face up in the chamber and imaged for 1 min with the camera set at the highest sensitivity by IVIS Imaging System® 200 Series (Xenogen, Hopkinton, MA). Photons emitted from tissues were quantified using Living Images® software (Xenogen, Hopkinton, MA). For *ex vivo* imaging, mice were anesthetized and injected with luciferase intraperitoneally. Ten minutes later, mice were sacrificed and tissues were rapidly removed. Tissues were placed in the IVIS system and imaged with the same setting used for *in vivo* studies. Signal intensity was quantified as the sum of all detected photon counts per second from tissues and presented as photon/s.

2.6. Cytokine enzyme-linked immunosorbent assay (ELISA)

IL-1β and TNF-α were quantified by ELISA with the OptEIA™ mouse IL-1β and TNF-α sets (Pharmingen, San Diego, CA). Sera were placed into wells that were coated with monoclonal antibody against IL-1β or TNF-α. After three washes with 0.05% Tween 20 in PBS, peroxidase-conjugated avidin, biotinylated antibody against IL-1β or TNF-α, and chromogenic substrate were added to each well in that order. The absorbance at 450 nm was measured in an ELISA plate reader.

2.7. Immunohistochemical staining

Parafilm-embedded organs were cut into 5-μm sections, deparaffinized in xylene, and then rehydrated in graded alcohol. Endogenous peroxidase was quenched with 3% hydrogen peroxide in methanol for 15 min and the nonspecific binding was blocked with 1% bovine serum albumin at room temperature for 1 h. Sections were incubated with mouse monoclonal antibody against IL-1β or TNF-α at 1:50 dilution overnight at 4 °C and then incubated with biotinylated secondary antibody (Zymed Laboratories, South San Francisco, CA) at room temperature for 20 min. Finally, slides were incubated with avidin–biotin complex reagent and stained with 3,3′-diaminobenzidine according to manufacturer's protocol (Histostain®-Plus Kit, Zymed Laboratories, South San Francisco, CA). IL-1β- and TNF-α-positive areas were measured using Image-Pro Plus (Media Cybernetics, Bethesda, MD) to quantify the expression levels of IL-1β and TNF-α. The proportions of IL-1β- and TNF-α-positive areas (%) were calculated as areas occupied with brown color/area of whole tissue.

2.8. Microarray analysis

Total RNA was extracted from brain, heart, liver, or kidney using the RNeasy Mini kit (Qiagen, Valencia, CA). Total RNA was quantified and evaluated as described previously (Cheng et al., 2010). Microarray analysis was performed as described previously (Cheng et al., 2010). Briefly, fluorescence-labeled RNA targets were prepared from 5 μg of total RNA using MessageAmp™ aRNA kit (Ambion, Austin, TX) and Cy5 dye (Amersham Pharmacia, Piscataway, NJ). Fluorescent targets were hybridized to the Mouse Whole Genome OneArray™ (Phalanx Biotech Group, Hsinchu, Taiwan), and the slides were scanned by an Axon 4000 scanner (Molecular Devices, Sunnyvale, CA). Number of replicates was three. The Cy5 fluorescent intensity of each spot was analyzed by genepix 4.1 software (Molecular Devices, Sunnyvale, CA). The signal intensity of each spot was corrected by subtracting background signals in the surrounding. We filtered out spots that signal-to-noise ratio was less than 0 or control probes. Spots that passed these criteria were normalized by the limma package of the R program. Normalized data were tested for differential expression using the Gene Expression Pattern Analysis Suite v3.1 (Montaner et al., 2006). Genes with fold changes >2.0 or <−2.0 were selected and analyzed by gene ontology (GO) on Gene Ontology Tree Machine (http://bioinfo.vanderbilt.edu/gotm/) (Zhang et al., 2004). We used the WebGestalt tool to test significant GO terms. The hierarchical clustering analysis of differential expressed genes was further performed and displayed using the TIGR Multiexperiment Viewer (http://www.tm4.org/index.html). Furthermore, we constructed the interaction networks of differential expressed genes using BiblioSphere Pathway Edition software (Genomatix Applications, http://www.genomatix.de/index.html). Microarray data are MIAME compliant and the raw data have been deposited in a MIAME compliant database (Gene Expression Omnibus, accession number GSE35934).

2.9. Quantitative real-time polymerase chain reaction (qPCR)

The expression levels of IFN-induced protein genes, including IFN-inducible GTPase (ligp1) and IFN-activated gene 202B (Ifi202) genes, in the brains of three mice per group were validated by qPCR. RNA samples were reverse-transcribed for 2 h at 37 °C with High Capacity cDNA Reverse Transcription kit (Applied Biosystems, Foster City, CA). qPCR was performed using 1 μl of cDNA, 2× SYBR Green PCR Master Mix (Applied Biosystems, Foster City, CA), and 200 nM of forward and reverse primers. The reaction condition was followed: 10 min at 95 °C, and 40 cycles of 15 s at 95 °C, 1 min at 60 °C. Each assay was run on an Applied Biosystems 7300 Real-Time PCR system in triplicates. Primer sets used in this study were designed using Primer3 program (http://frodo.wi.mit.edu/primer3/). The specificities of primer sets were analyzed by nucleotide BLAST (http://blast.ncbi.nlm.nih.gov/Blast.cgi). Each primer set was able to amplify a target DNA fragment from the respective gene with specificity. The primer set for each gene is followed: ligp1 forward, 5′-CTTGACATGGTGACTGAGGATG-3′; ligp1 reverse, 5′-AGGTGGATAAAGCCCGAATAAC-3′; Ifi202 forward, 5′-AAGGCTGGTTGATGGAGAG-3′; Ifi202 reverse, 5′-GTCAATTCAAAGCAGACAAGTC-3′; glyceraldahyde-3-phosphate dehydrogenase (GAPDH) forward, 5′-TCACCCACACTGTGCCCATCTATGA-3′; GAPDH reverse, 5′-GAGGAAGAGGATGCGGCAGTGG-3′.

Please cite this article in press as: Li, C.-C., et al. Genipin inhibits lipopolysaccharide-induced acute systemic inflammation in mice as evidenced by nuclear factor-κB bioluminescent imaging-guided transcriptomic analysis. Food Chem. Toxicol. (2012), http://dx.doi.org/10.1016/j.fct.2012.05.054

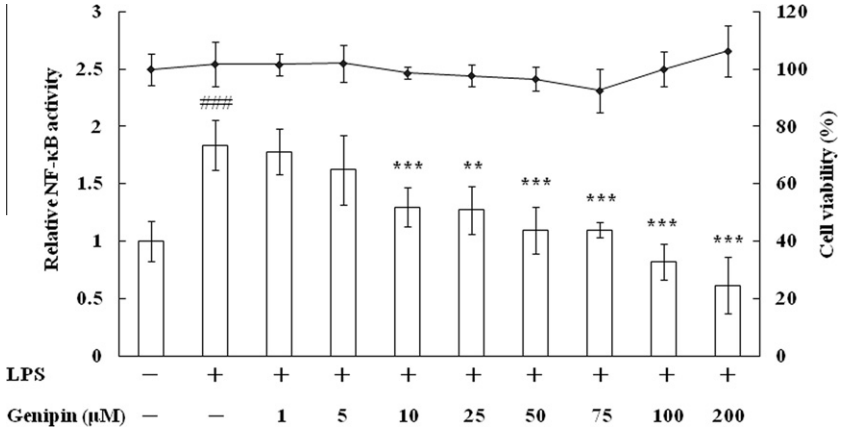

Fig. 1. Effect of genipin on the LPS-induced NF-κB activation in HepG2/NF-κB cells. HepG2/NF-κB cells were exposed to 100 ng/ml LPS and/or various concentrations of genipin. After a 24-h incubation at 37 °C, NF-κB activity and cell viability were measured by luciferase assay and MTT assay, respectively. Bars represent relative NF-κB activity, which is presented as the comparison with RLU relative to solvent-treated cells. Line represents cell viability, which is presented as the comparison with the OD relative to solvent-treated cells. Values are mean ± standard error of triplicate assays. $^{###}p < 0.001$, compared with mock. $^{**}p < 0.01$, $^{***}p < 0.001$, compared with LPS.

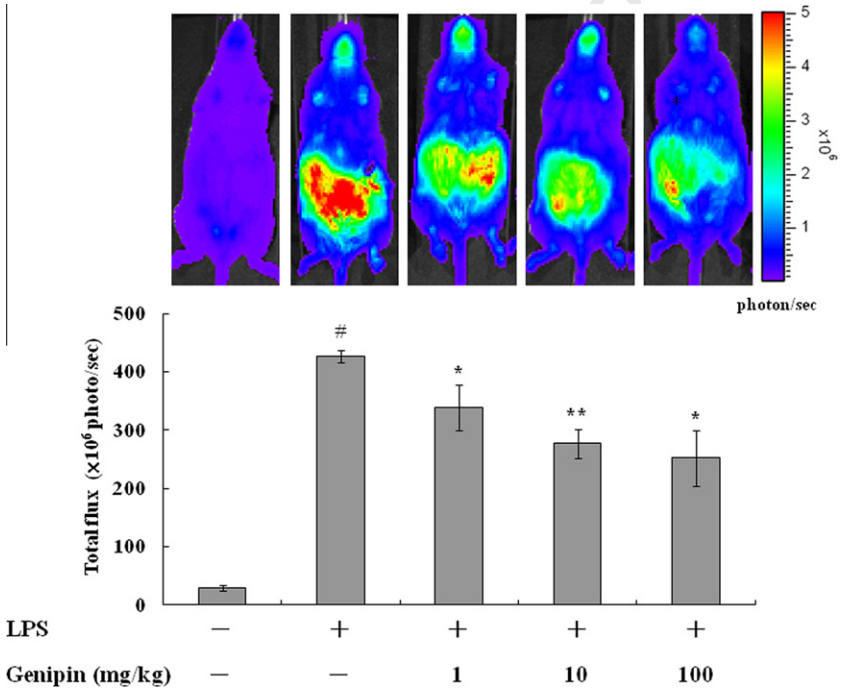

Fig. 2. NF-κB-dependent bioluminescence in living mice. Transgenic mice were intraperitoneally administered with 4 mg/kg LPS and/or various amounts of genipin. Four hours later, mice were injected intraperitoneally with D-luciferin and imaged for 1 min. *In vivo* imaging is shown on the top. The color overlay on the image represents the photon/s emitted from the animals, as indicated by the color scale. Photos are representative images ($n = 5$/group). Quantification of photon emission from the whole body is shown on the bottom. Values are mean ± standard error. $^{#}p < 0.05$, compared with mock. $^{*}p < 0.05$, $^{**}p < 0.01$ compared with LPS.

2.10. Statistical analysis

Data were presented as mean ± standard error. Data were analyzed by one-way ANOVA and post hoc LSD test using PASW Statistics (SPSS) version 12. A p value less than 0.05 was considered as statistically significant.

3. Results

3.1. Genipin suppressed LPS-induced NF-κB activities in vitro and in vivo

To evaluate the effect of genipin on the LPS-induced NF-κB activity, we first treated recombinant HepG2/NF-κB cells with LPS and various amounts of genipin. LPS significantly induced NF-κB activity by 1.8-fold, while genipin significantly inhibited LPS-induced NF-κB activation in a dose-dependent manner (Fig. 1). No cytotoxicity was observed during treatment. These findings indicated that genipin suppressed LPS-induced NF-κB activity *in vitro*.

Next, we treated mice with LPS and various amounts of genipin, and NF-κB-driven luciferase activity was evaluated by *in vivo* imaging 4 h later. As shown in Fig. 2, LPS induced an approximately 14.7-fold increase of NF-κB-driven luminescent intensity in mice. Strong luminescent signals were emitted from the abdominal region of LPS group. However, genipin significantly suppressed the LPS-induced luminescence *in vivo*, and the inhibition displayed a dose-dependent manner (1, 10, and 100 mg/kg). These findings indicated that genipin suppressed LPS-induced NF-κB activity

Please cite this article in press as: Li, C.-C., et al. Genipin inhibits lipopolysaccharide-induced acute systemic inflammation in mice as evidenced by nuclear factor-κB bioluminescent imaging-guided transcriptomic analysis. Food Chem. Toxicol. (2012), http://dx.doi.org/10.1016/j.fct.2012.05.054

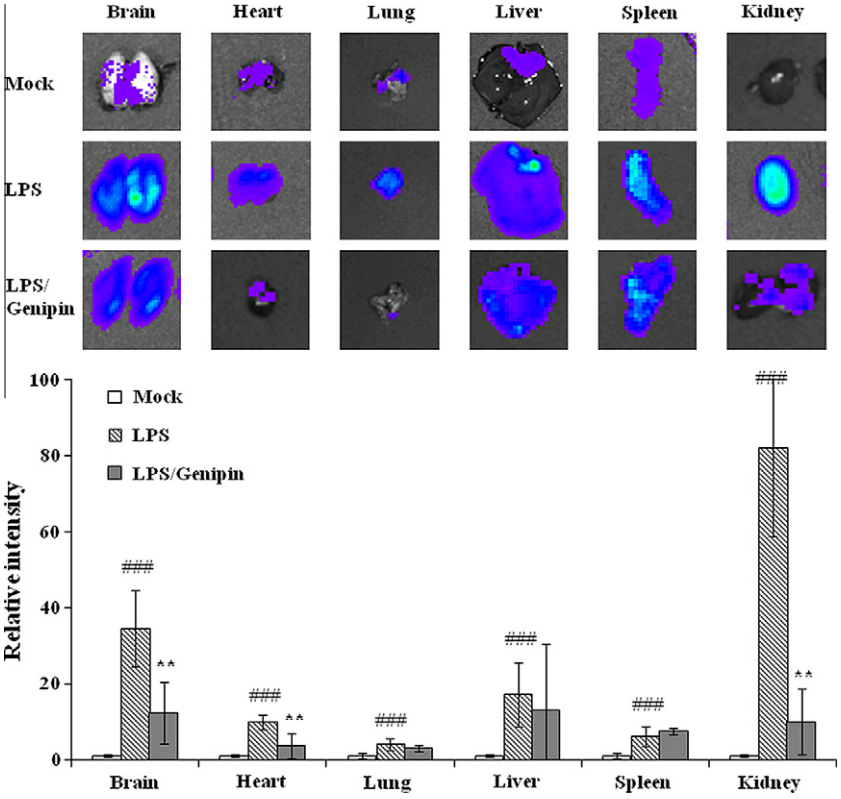

Fig. 3. NF-κB-dependent luminescence in individual organs. Transgenic mice were administered with 4 mg/kg LPS and/or 100 mg/kg genipin. Four hours later, mice were injected intraperitoneally with D-luciferin. Five minutes later, mice were sacrificed, and organs were excised rapidly and subjected to image. Photos ate representative images ($n = 5$/group). Quantification of photon emission from organs is shown at the bottom. Results are expressed as relative intensity, which is presented as the comparison with the luminescence relative to mock. Values are mean ± standard error. $^{###}p < 0.001$, compared with mock. $^{***}p < 0.001$, compared with LPS.

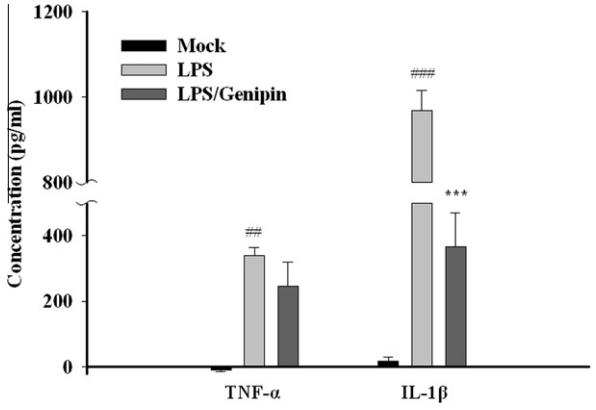

Fig. 4. Effect of genipin on the LPS-induced IL-1β and TNF-α productions. Transgenic mice were intraperitoneally injected with 4 mg/kg LPS and/or 100 mg/kg genipin. The levels of IL-1β and TNF-α in sera were measured by ELISA. Values are mean ± standard error ($n = 5$/group). $^{##}p < 0.01$, $^{###}p < 0.001$, compared with mock. $^{***}p < 0.001$, compared with LPS.

in vivo, and we chose 100 mg/kg genipin for further experiments. Since our previous study has demonstrated that NF-κB-driven bioluminescence is correlated with inflammatory responses, these data suggested that genipin suppressed LPS-induced acute systemic inflammation *in vivo*.

3.2. Genipin suppressed LPS-induced NF-κB activities in various organs

We performed *ex vivo* imaging to elucidate the target organs that genipin acted on. As shown in Fig. 3, LPS significantly enhanced the NF-κB-dependent luminescence in brain, heart, lung, liver, spleen, and kidney. Administration of genipin reduced LPS-induced bioluminescent intensities in brain, heart, liver, and kidney. The induction of genipin in brain, heart, and kidney displayed significant differences. Therefore, we analyzed the cytokine productions by ELISA and immunohistochemical staining, and collected RNA samples from these organs for DNA microarray analysis.

3.3. Genipin suppressed LPS-induced IL-1β and TNF-α productions

IL-1β and TNF-α are proinflammatory cytokines that initiate the acute-phase responses and lead to inflammation (Hanada and Yoshimura, 2002). We further analyzed the productions of IL-1β and TNF-α by ELISA and immunohistochemical staining to validate whether genipin inhibited systemic inflammation. As shown in Fig. 4, the concentrations of IL-1β and TNF-α in sera from LPS-given mice were 969 ± 47 and 339 ± 25 pg/ml, respectively. However, administration of genipin decreased the levels of IL-1β and TNF-α productions. Immunohistochemical staining with antibodies against IL-1β and TNF-α revealed that, in comparison with mock, there were many brown IL-1β- or TNF-α-reactive cells in LPS-treated organs, and the proportions of brown areas were significantly increased by LPS (Fig. 5). However, the proportions of IL-1β- or TNF-α-reactive areas were significantly decreased by genipin in these organs. Genipin decreased the levels of IL-1β and TNF-α in sera and organs, suggesting that genipin suppressed LPS-induced systemic inflammation via the inhibition of proinflammatory cytokine production.

Please cite this article in press as: Li, C.-C., et al. Genipin inhibits lipopolysaccharide-induced acute systemic inflammation in mice as evidenced by nuclear factor-κB bioluminescent imaging-guided transcriptomic analysis. Food Chem. Toxicol. (2012), http://dx.doi.org/10.1016/j.fct.2012.05.054

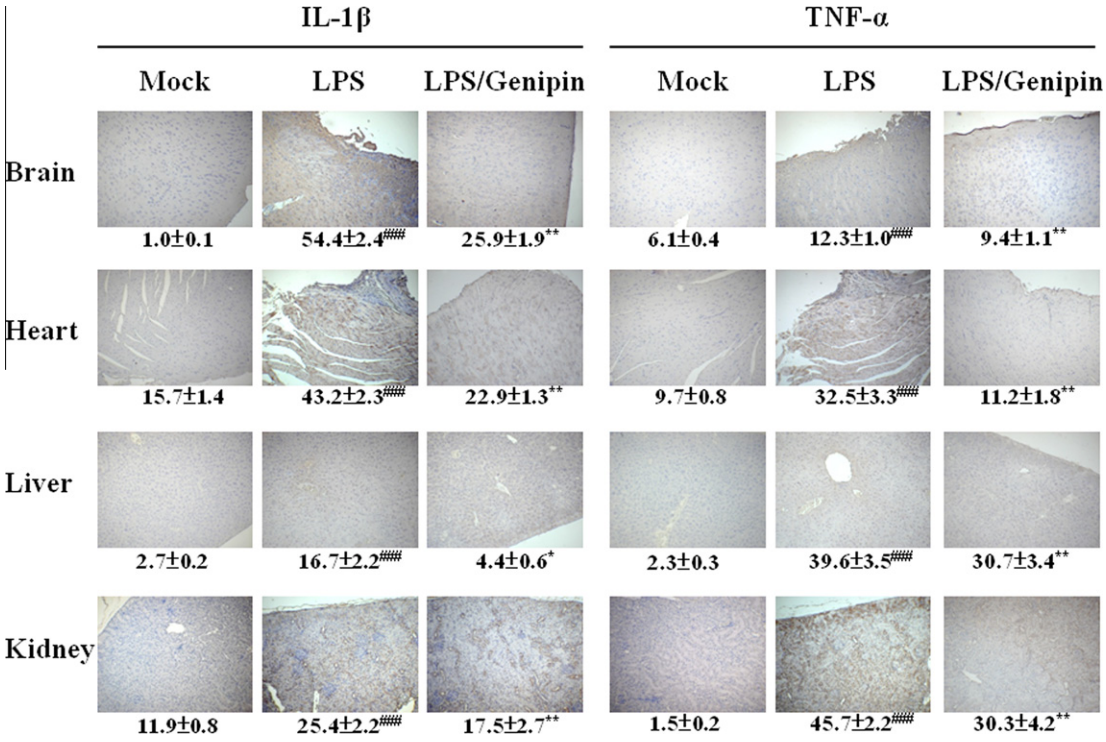

Fig. 5. Immunohistochemical staining of brain, heart, liver, and kidney. Transgenic mice were intraperitoneally injected with 4 mg/kg LPS and/or 100 mg/kg genipin. The sections were stained by immunohistochemistry using antibody for IL-1β or TNF-α (100× magnification). Photos are representative images (n = 5/group). Quantification of IL-1β- and TNF-α-positive areas (%) was shown at the bottom. Values are mean ± standard error (n = 5/group). $^{###}p < 0.001$, compared with mock. $^{*}p < 0.05$, $^{**}p < 0.01$, compared with LPS.

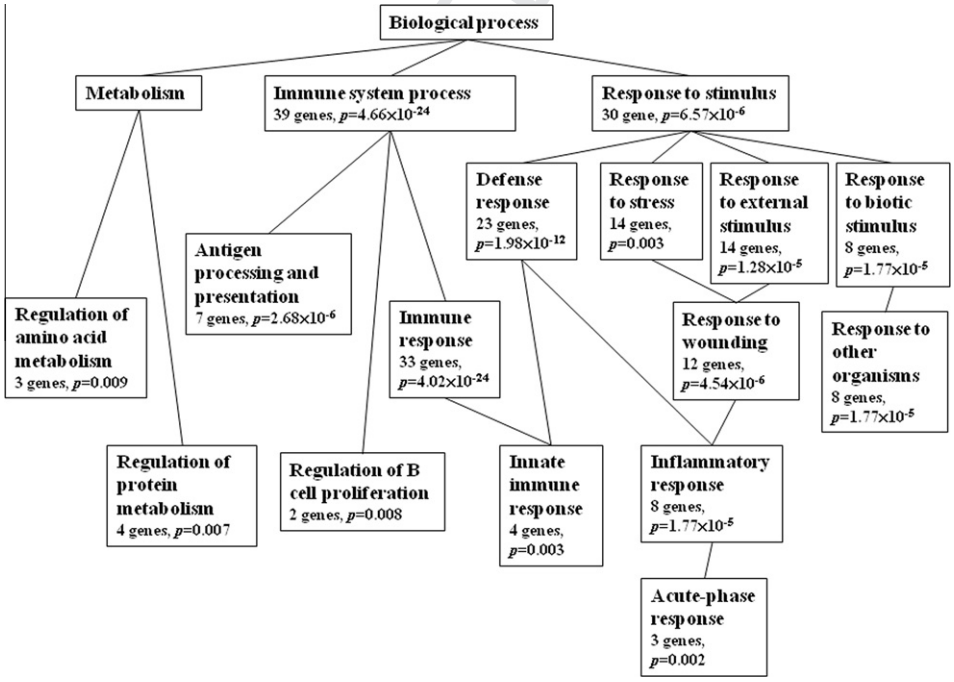

Fig. 6. GO analysis of differential expressed genes in brain, heart, kidney, and liver in both LPS and LPS/genipin groups. Differentially expressed genes were organized using Gene Ontology Tree Machine. The enriched GO categories ($p < 0.01$ and at least two genes) are shown.

3.4. Microarray analysis of genipin-regulated gene expression profile

Microarray data were analyzed by Gene Expression Pattern Analysis Suite v3.1 to test for the differential expressed genes in brain, heart, liver, and kidney treated with LPS and/or genipin. In a total of 30,968 genes, the transcripts of 79 genes were differentially expressed in both LPS and LPS/genipin groups. We further used the WebGestalt tool to annotate these genes and to get an

Please cite this article in press as: Li, C.-C., et al. Genipin inhibits lipopolysaccharide-induced acute systemic inflammation in mice as evidenced by nuclear factor-κB bioluminescent imaging-guided transcriptomic analysis. Food Chem. Toxicol. (2012), http://dx.doi.org/10.1016/j.fct.2012.05.054

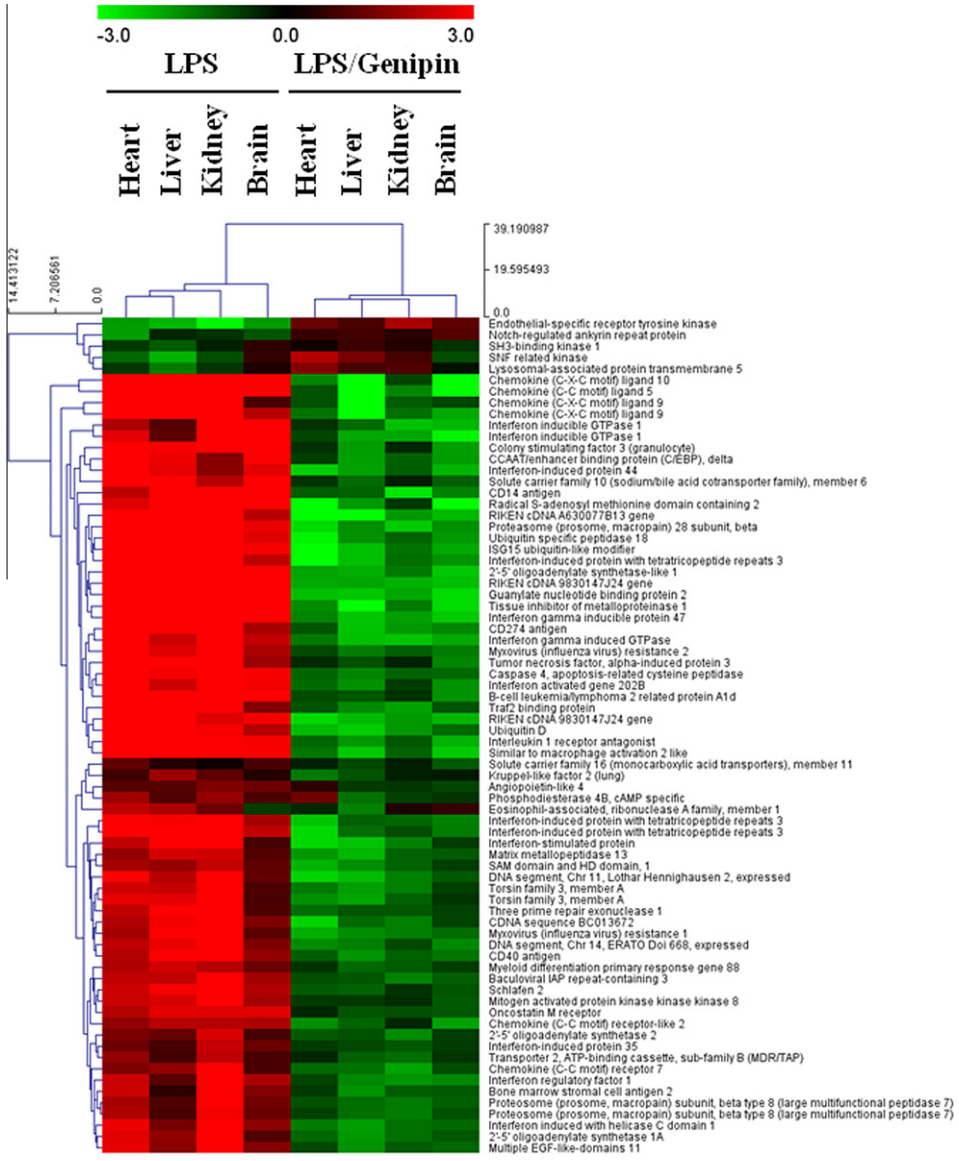

Fig. 7. Hierarchical clustering analysis of differential expressed genes in brain, heart, kidney, and liver in both LPS and LPS/genipin groups. Normalized $\log_2$ expression values are color-coded according to the legend on the top. Increased transcript levels are colored red and decreased levels are colored green. (For interpretation of the references to color in this figure legend, the reader is referred to the web version of this article.)

overview of cellular physiological status altered by genipin in these organs. GO categories were considered if they contained at least two genes and their p values were below 0.01. As shown in Fig. 6, most differential expressed genes were grouped into immunity-related GO categories, such as antigen processing and presentation, regulation of B cell proliferation, inflammatory responses, and acute-phase response. Only few genes were associated with metabolism.

The expression patterns of these genes were further assessed by hierarchical clustering analysis and visualized by TIGR Multiexperiment Viewer. It was interesting to find that the expression levels of LPS-affected genes were reversed by genipin in these organs (Fig. 7). LPS activated the expressions of most genes, while genipin downregulated the LPS-induced gene expression. Only 5 genes, including endothelial-specific receptor tyrosine kinase, Notch-regulated ankyrin repeat protein (Nrarp), SH3-binding kinase 1, sucrose nonfermenting protein (SNF)-related kinase and lysosomal-associated protein transmembrane 5 (LAPTM5) genes, were downregulated by LPS, while genipin activated the LPS-repressed expressions of these genes. Additionally, about one third of genes belonged to chemokine ligand, chemokine receptor, and IFN-induced protein genes. These findings suggested that genipin suppressed LPS-induced inflammation by downregulation of chemokine ligands, chemokine receptors, and IFN-induced proteins.

The relationship between differential expressed genes was further analyzed by Genomatix Applications software based on knowledgebase. Genes were correlated based on the literatures, the Genomatix Knowledge Base, and the promoter DNA sequence analysis. Interestingly, most genes were directly connected to NF-κB and NF-κB seemed to be in the central part of the network (Fig. 8). These findings suggested that NF-κB may play a central role in the regulation of genipin-affected gene expression network.

3.5. Verification of expression levels of novel genipin-regulated genes by qPCR

Microarray analysis showed that one third of differentially expressed genes belonged to chemokine ligand, chemokine receptor, and IFN-induced protein genes, so we validated microarray data by qPCR analysis. We quantified the expression levels of IFN-induced

Please cite this article in press as: Li, C.-C., et al. Genipin inhibits lipopolysaccharide-induced acute systemic inflammation in mice as evidenced by nuclear factor-κB bioluminescent imaging-guided transcriptomic analysis. Food Chem. Toxicol. (2012), http://dx.doi.org/10.1016/j.fct.2012.05.054

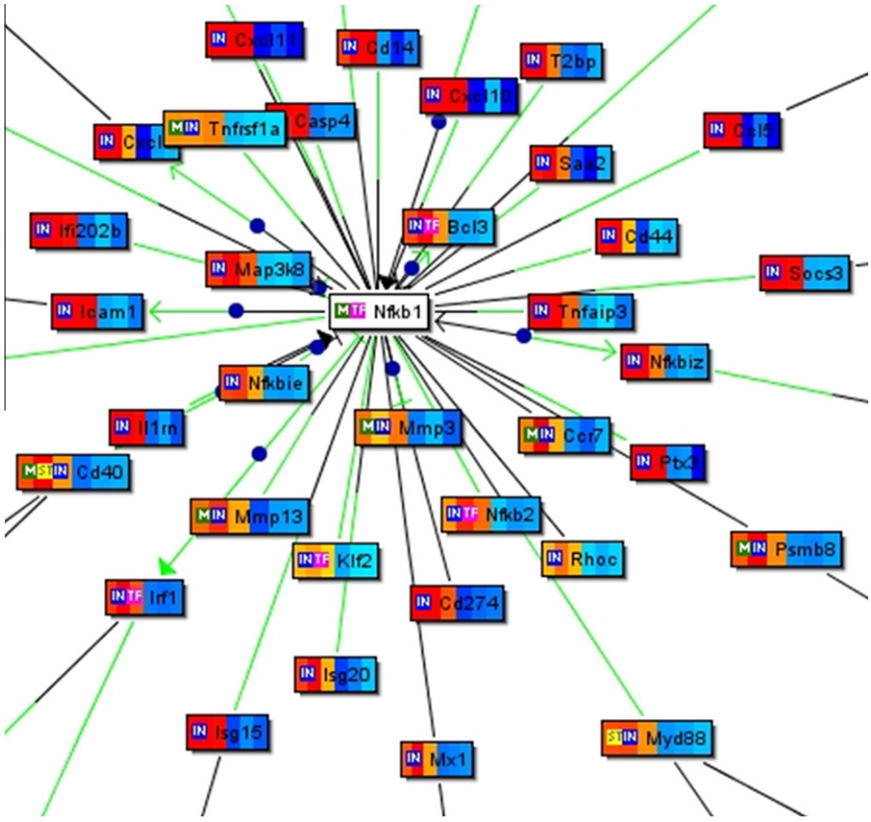

Fig. 8. Network analysis of differentially expressed genes in brain, heart, kidney, and liver in both LPS and LPS/genipin groups. Input genes are marked with IN. Gene that codes for a transcription factor is marked with TF. The product of the gene marked with ST is part of a Genomatix signal transduction pathway. If a gene that codes for a transcription factor is connected to a gene that is known to contain a binding site for this transcription factor in its promoter, the connecting line is colored green over half of its length near the gene containing the binding site. (For interpretation of the references to color in this figure legend, the reader is referred to the web version of this article.)

Table 1
Expression levels of Iigp1 and Ifi202 genes by qPCR.

Sample	Average C_T of target	Average C_T of GAPDH	ΔC_T[a]	$\Delta\Delta C_T$[b]	Relative to mock
Iigp1					
Mock	26.10 ± 0.04	17.13 ± 0.05	8.96 ± 0.06	0.00 ± 0.06	1.00
LPS	23.31 ± 0.05	17.07 ± 0.02	6.24 ± 0.06	−2.72 ± 0.06	6.62
LPS/Genipin	23.84 ± 0.07	17.25 ± 0.01	6.59 ± 0.08	−2.37 ± 0.08	5.17
Ifi202					
Mock	32.11 ± 0.11	17.13 ± 0.05	14.97 ± 0.12	0.00 ± 0.12	1.00
LPS	26.25 ± 0.04	17.07 ± 0.02	9.18 ± 0.05	−5.79 ± 0.05	55.40
LPS/Genipin	27.40 ± 0.02	17.25 ± 0.01	10.15 ± 0.02	−4.82 ± 0.02	28.33

[a] The ΔC_T value is determined by subtracting the average C_T value of GAPDH gene from the average C_T value of target gene. The standard deviation of the difference is calculated from the standard deviations of the target gene and GAPDH gene.
[b] The calculation of $\Delta\Delta C_T$ involves subtraction by the ΔC_T calibrator value. This is a subtraction of an arbitrary constant, so the standard deviation of $\Delta\Delta C_T$ is the same as the standard deviation of ΔC_T value.

protein genes, including Iigp1 and Ifi202 genes, by qPCR because the expressions of these genes were directly regulated by NF-κB in the network analysis. As shown in Table 1, the expression levels of Iigp1 and Ifi202 genes in LPS group were 6.62- and 55.4-fold, respectively, as compared with mock group. However, LPS-upregulated gene expression was downregulated by genipin, and the expression levels of Iigp1 and Ifi202 genes in LPS/genipin group were 5.17- and 28.33-fold, respectively, as compared with mock group. The consistency of qPCR data and microarray analysis indicated that genipin downregulated the LPS-induced expression of Iigp1 and Ifi202 genes.

4. Discussion

Genipin is a natural iridoid compound and an aglycon of geniposide found in gardenia fruit. It has been used as a natural blue colorant for staining food. Several reports have shown that genipin exhibits anti-inflammatory effects in cell models, such as LPS-treated brain microglial cells, LPS-stimulated murine macrophages, intact human erythroleukemia cells, and intact rat adrenal pheochromocytoma cells (Nam et al., 2010; Park et al., 2010). Additionally, previous studies indicated that genipin possesses significant topical anti-inflammatory effects by inhibiting carrageenan-in-

Please cite this article in press as: Li, C.-C., et al. Genipin inhibits lipopolysaccharide-induced acute systemic inflammation in mice as evidenced by nuclear factor-κB bioluminescent imaging-guided transcriptomic analysis. Food Chem. Toxicol. (2012), http://dx.doi.org/10.1016/j.fct.2012.05.054

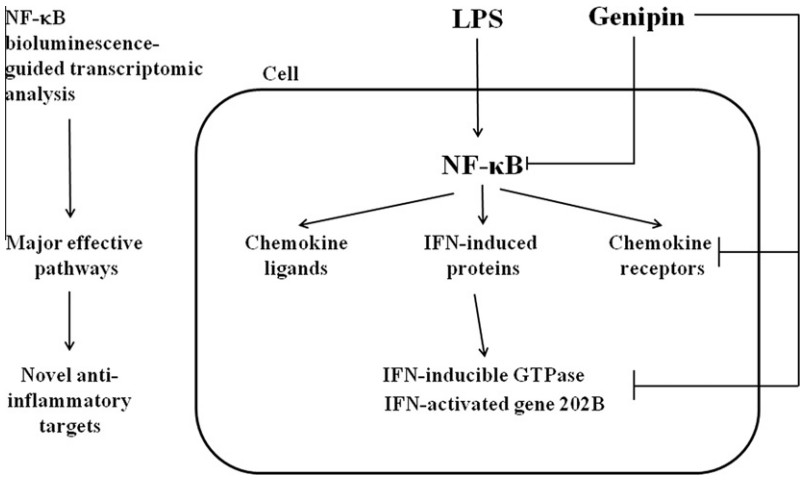

Fig. 9. Schematic diagram illustrates the molecular mechanism of anti-inflammatory effects of genipin in the LPS-induced acute systemic inflammation. Anti-inflammatory effect of genipin in mice was evaluated by NF-κB bioluminescence-guided transcriptomic analysis. Genipin suppressed LPS-induced systemic inflammation via the inhibition of inflammatory cytokine production and the downregulation of chemokine ligand, chemokine receptor, and IFN-induced protein genes. Moreover, genipin inhibited the expression of novel anti-inflammatory targets, such as IFN-inducible GTPase, which plays critical roles in mediating innate resistance to intracellular pathogens, and Ifi202, which is an important NF-κB activator in dendritic cells.

duced paw edema in rats, croton oil-induced ear edema in mice, concanavalin A-induced hepatitis in mice, HCl/ethanol-induced gastritis in rats, and LPS-induced brain inflammation in rats (Koo et al., 2006, 2004; Lee et al., 2009; Mase et al., 2010). In this study, we found that intraperitoneal administration of genipin led to the inhibition of LPS-induced NF-κB activities and cytokine productions in many organs. These findings suggested that genipin exhibited not only topical but also systemic anti-inflammatory potential *in vivo*.

In this study, we applied NF-κB-driven bioluminescent imaging to monitor the anti-inflammatory potential of genipin in an *in vivo* model of LPS-induced acute systemic inflammation. LPS is the major integral structural component of the outer membrane of Gram-negative bacteria. Release of LPS from Gram-negative bacteria activates cells, such as macrophages and neutrophils, to produce proinflammatory cytokines. The production of cytokine subsequently leads to the expression of adhesion molecules and the recruitment of inflammatory cells (Andonegui et al., 2003). It has been shown that LPS binds to the Toll-like receptor 4/CD14 complex, activates the NF-κB, and then up-regulates the expressions of proinflammatory cytokine genes, such as TNF-α, IL-1β, and IL-6 (Andonegui et al., 2003). Additionally, previous study has demonstrated that LPS produces its effect largely on pivotal organs, such as liver, kidney, spleen, lung, and heart (Mathison and Ulevitch, 1979). In this study, LPS-induced acute systemic inflammation was evidenced by elevations of cytokine levels in sera and organs. LPS-induced NF-κB-dependent bioluminescence in whole body was consistent with previous observations of NF-κB activation caused by systemic administration of LPS. Moreover, LPS-induced NF-κB activation was observed in heart, liver, spleen, and kidney, which have been known to be the major organs affected by LPS treatment. Therefore, these findings suggested that NF-κB-driven bioluminescent imaging could be used to reflect the real-time inflammatory status *in vivo*. Furthermore, in addition to the previous known organs, LPS also produced its effect on brain.

NF-κB bioluminescent imaging showed that LPS-induced NF-κB activities in brain, heart, liver, and kidney were suppressed by genipin. The gene expression profiles of these organs were further analyzed to elucidate the anti-inflammatory mechanisms of genipin. GO classification showed that differential expressed genes belonged to the immunity-related GO categories. Moreover, it was interesting to find that the expression levels of LPS-affected genes were reversed by genipin. It was noticed that LPS activated the expressions of most genes except endothelial-specific receptor tyrosine kinase, Nrarp, SH3-binding kinase 1, SNF-related kinase, and LAPTM5 genes. LAPTM5 is a lysosomal protein specially expressed in the myeloid and lymphoid lineages. LAPTM5 negatively regulates the cell surface B-cell receptor (BCR) levels and B cell activation by promoting BCR degradation in the lysosomal compartment of mouse cells (Ouchida et al., 2010). Nrarp is a small protein that is transcriptionally regulated by Notch signaling pathway. Previous study has shown that Nrarp specifically inhibits T cell development in the hematopoietic system (Yun and Bevan, 2003). Endothelial-specific receptor tyrosine kinase is a receptor that critically involves in the formation of embryonic vasculature. Previous studies have shown that phosphorylation of endothelial-specific receptor tyrosine kinase recruits and activates A20 binding inhibitor of NF-κB2, leading to the suppression of NF-κB activation (Hughes et al., 2003). LPS downregulated the expressions of endothelial-specific receptor tyrosine kinase, Nrarp, and LAPTM5 genes, suggesting that LPS might promote B cell activation, T cell development, and NF-κB activation. However, genipin might abolish the LPS-induced B cell activation, T cell development, and NF-κB activation via upregulation of these genes.

Among 79 differential expressed genes, 74 genes were upregulated by LPS and downregulated by genipin, and about one third of these genes belonged to chemokine ligand, chemokine receptor, and IFN-induced protein genes. Helper T cell T_H1 attractant genes, such as chemokine (C–X–C motif) ligand 9 (CXCL9), CXCL10 and chemokine (C–C motif) ligand (CCL5), were upregulated by LPS and downregulated by genipin in this study. CXCL9 (also known as monokine induced by IFN-γ) and CXCL10 (also known as IFN-γ-inducible protein 10) stimulate the chemotaxis of activated CXCR3-positive T cells and natural killer cells *in vitro*. They are also pivotal for T cell migration in infectious and chronic inflammatory diseases (Ellis et al., 2010). CCL5 (also known as RANTES) generally produces later in immune responses and contributes to augmentation of the adaptive immune responses (O'Sullivan et al., 2010). In addition to these chemokines, some IFN-induced proteins were affected by LPS. For examples, IFN-inducible GTPase and IFN-γ-inducible protein 47 belong to immunity-related GTPases, which play critical roles in mediating innate resistance to intracellular pathogens (MacMicking, 2004). IFN-activated gene 202B (Ifi202) belong to the IFN-inducible 200-protein family. Ifi202 is an important NF-κB activator in dendritic cells and involved in IL-12 production in BWF1 mice (Yamauchi et al., 2007). IFN induced with helicase C domain 1 serves as a cytoplasmic sensor for virus infec-

Please cite this article in press as: Li, C.-C., et al. Genipin inhibits lipopolysaccharide-induced acute systemic inflammation in mice as evidenced by nuclear factor-κB bioluminescent imaging-guided transcriptomic analysis. Food Chem. Toxicol. (2012), http://dx.doi.org/10.1016/j.fct.2012.05.054

tions and activates the antiviral immune responses (Balan et al., 2006).

5. Conclusions

In conclusion, previous studies indicated that genipin possesses topical anti-inflammatory potential by suppressing cytokine and nitric oxide productions, or by inhibiting lipid peroxidation (Amor et al., 2010; Nam et al., 2010; Park et al., 2010). Additionally, genipin enhances the anti-inflammatory capacity via upregulation of heme oxygenase-1 in macrophages (Jeon et al., 2011). In this study, we found that genipin exhibited systemic anti-inflammatory effects in the LPS-induced acute systemic inflammation model. Moreover, genipin suppressed LPS-induced inflammation via newly identified mechanisms, including downregulation of chemokine ligand, chemokine receptor, and IFN-induced protein productions (Fig. 9). These findings suggested that genipin could be a potent candidate for the treatment of systemic inflammation.

Conflict of Interest

The authors declare that there are no conflicts of interest.

Acknowledgments

This work was supported by grants from National Science Council, Committee on Chinese Medicine and Pharmacy at Department of Health (CCMP100-RD-048 and CCMP101-RD-103), and China Medical University (CMU100-S-16, CMU100-S-34, and CMU100-TS-14).

References

Amor, S., Puentes, F., Baker, D., van der Valk, P., 2010. Inflammation in neurodegenerative diseases. Immunology 129, 154–169.

Andonegui, G., Bonder, C.S., Green, F., Mullaly, S.C., Zbytnuik, L., Raharjo, E., Kubes, P., 2003. Endothelium-derived Toll-like receptor-4 is the key molecule in LPS-induced neutrophil sequestration into lungs. J. Clin. Invest. 111, 1011–1020.

Balan, V., Nelson, D.R., Sulkowski, M.S., Everson, G.T., Lambiase, L.R., Wiesner, R.H., Dickson, R.C., Garcia, A., Moore, P.A., Yu, R., Subramanian, G.M., 2006. Modulation of interferon-specific gene expression by albumin-interferon-α in interferon-α-experienced patients with chronic hepatitis C. Anti viral ther. 11, 901–908.

Baldwin Jr., A.S., 1996. The NF-κB and IκB proteins: new discoveries and insights. Annu. Rev. Immunol. 14, 649–683.

Bonizzi, G., Karin, M., 2004. The two NF-κB activation pathways and their role in innate and adaptive immunity. Trends Immunol. 25, 280–288.

Cheng, H.M., Li, C.C., Chen, C.Y., Lo, H.Y., Cheng, W.Y., Lee, C.H., Yang, S.Z., Wu, S.L., Hsiang, C.Y., Ho, T.Y., 2010. Application of bioactivity database of Chinese herbal medicine on the therapeutic prediction, drug development, and safety evaluation. J. Ethnopharmacol. 132, 429–437.

Ellis, S.L., Gysbers, V., Manders, P.M., Li, W., Hofer, M.J., Muller, M., Campbell, I.L., 2010. The cell-specific induction of CXC chemokine ligand 9 mediated by IFN-γ in microglia of the central nervous system is determined by the myeloid transcription factor PU.1. J. Immunol. 185, 1864–1877.

Fujikawa, S., Fukui, Y., Koga, K., Kumada, J., 1987. Brilliant skyblue pigment formation from gardenia fruits. J. Fermentation Technol. 65, 419–424.

Hanada, T., Yoshimura, A., 2002. Regulation of cytokine signaling and inflammation. Cytokine Growth Factor Rev. 13, 413–421.

He, M.L., Cheng, X.W., Chen, J.K., Zhou, T.S., 2006. Simultaneous determination of five major biologically active ingredients in different parts of *Gardenia jasminoides* fruits by HPLC with diode-array detection. Chromatographia 64, 713–717.

Ho, T.Y., Chen, Y.S., Hsiang, C.Y., 2007. Noninvasive nuclear factor-κB bioluminescence imaging for the assessment of host-biomaterial interaction in transgenic mice. Biomaterials 28, 4370–4377.

Hseu, Y.C., Huang, H.C., Hsiang, C.Y., 2010. *Antrodia camphorata* suppresses lipopolysaccharide-induced nuclear factor-κB activation in transgenic mice evaluated by bioluminescence imaging. Food Chem. Toxicol. 48, 2319–2325.

Hsiang, C.Y., Chen, Y.S., Ho, T.Y., 2009. Nuclear factor-κB bioluminescence imaging-guided transcriptomic analysis for the assessment of host-biomaterial interaction *in vivo*. Biomaterials 30, 3042–3049.

Hughes, D.P., Marron, M.B., Brindle, N.P., 2003. The antiinflammatory endothelial tyrosine kinase Tie2 interacts with a novel nuclear factor-κB inhibitor ABIN-2. Circ. Res. 92, 630–636.

Jeon, W.K., Hong, H.Y., Kim, B.C., 2011. Genipin up-regulates heme oxygenase-1 via PI3-kinase-JNK1/2-Nrf2 signaling pathway to enhance the anti-inflammatory capacity in RAW264.7 macrophages. Arch. Biochem. Biophy. 512, 119–125.

Karin, M., 2006. Nuclear factor-κB in cancer development and progression. Nature 441, 431–436.

Koo, H.J., Lim, K.H., Jung, H.J., Park, E.H., 2006. Anti-inflammatory evaluation of gardenia extract, geniposide and genipin. J. Ethnopharmacol. 103, 496–500.

Koo, H.J., Song, Y.S., Kim, H.J., Lee, Y.H., Hong, S.M., Kim, S.J., Kim, B.C., Jin, C., Lim, C.J., Park, E.H., 2004. Antiinflammatory effects of genipin, an active principle of gardenia. Eur. J. Pharmacol. 495, 201–208.

Lee, J.H., Lee, D.U., Jeong, C.S., 2009. *Gardenia jasminoides* Ellis ethanol extract and its constituents reduce the risks of gastritis and reverse gastric lesions in rats. Food Chem. Toxicol. 47, 1127–1131.

MacMicking, J.D., 2004. IFN-inducible GTPases and immunity to intracellular pathogens. Trends Immunol. 25, 601–609.

Mase, A., Makino, B., Tsuchiya, N., Yamamoto, M., Kase, Y., Takeda, S., Hasegawa, T., 2010. Active ingredients of traditional Japanese (kampo) medicine, inchinkoto, in murine concanavalin A-induced hepatitis. J. Ethnopharmacol. 127, 742–749.

Mathison, J.C., Ulevitch, R.J., 1979. The clearance, tissue distribution, and cellular localization of intravenously injected lipopolysaccharide in rabbits. J. Immunol. 123, 2133–2143.

Montaner, D., Tarraga, J., Huerta-Cepas, J., Burguet, J., Vaquerizas, J.M., Conde, L., Minguez, P., Vera, J., Mukherjee, S., Valls, J., Pujana, M.A., Alloza, E., Herrero, J., Al-Shahrour, F., Dopazo, J., 2006. Next station in microarray data analysis: GEPAS. Nucleic Acids Res. 34, W486–W491.

Nam, K.N., Choi, Y.S., Jung, H.J., Park, G.H., Park, J.M., Moon, S.K., Cho, K.H., Kang, C., Kang, I., Oh, M.S., Lee, E.H., 2010. Genipin inhibits the inflammatory response of rat brain microglial cells. Int. Immunopharmacol. 10, 493–499.

O'Sullivan, J.B., Ryan, K.M., Harkin, A., Connor, T.J., 2010. Noradrenaline reuptake inhibitors inhibit expression of chemokines IP-10 and RANTES and cell adhesion molecules VCAM-1 and ICAM-1 in the CNS following a systemic inflammatory challenge. J. Neuroimmunol. 220, 34–42.

Ouchida, R., Kurosaki, T., Wang, J.Y., 2010. A role for lysosomal-associated protein transmembrane 5 in the negative regulation of surface B cell receptor levels and B cell activation. J. Immunol. 185, 294–301.

Park, K.S., Kim, B.H., Chang, I.M., 2010. Inhibitory potencies of several iridoids on cyclooxygenase-1, cyclooxygnase-2 enzymes activities, tumor necrosis factor-α and nitric oxide production *in vitro*. Evid. Based Complement. Alternat. Med. 7, 41–45.

Sung, H.W., Huang, R.N., Huang, L.L., Tsai, C.C., Chiu, C.T., 1998. Feasibility study of a natural crosslinking reagent for biological tissue fixation. J. Biomed. Mater. Res. 42, 560–567.

Thaler, J.P., Schwartz, M.W., 2010. Minireview: inflammation and obesity pathogenesis: the hypothalamus heats up. Endocrinology 151, 4109–4115.

Tseng, T.H., Chu, C.Y., Huang, J.M., Shiow, S.J., Wang, C.J., 1995. Crocetin protects against oxidative damage in rat primary hepatocytes. Cancer Lett. 97, 61–67.

Wu, S.L., Chen, J.C., Li, C.C., Lo, H.Y., Ho, T.Y., Hsiang, C.Y., 2009. Vanillin improves and prevents trinitrobenzene sulfonic acid-induced colitis in mice. J. Pharmacol. Exp. Ther. 330, 370–376.

Yamamoto, M., Miura, N., Ohtake, N., Amagaya, S., Ishige, A., Sasaki, H., Komatsu, Y., Fukuda, K., Ito, T., Terasawa, K., 2000. Genipin, a metabolite derived from the herbal medicine Inchin-ko-to, and suppression of Fas-induced lethal liver apoptosis in mice. Gastroenterology 118, 380–389.

Yamauchi, M., Hashimoto, M., Ichiyama, K., Yoshida, R., Hanada, T., Muta, T., Komune, S., Kobayashi, T., Yoshimura, A., 2007. Ifi202, an IFN-inducible candidate gene for lupus susceptibility in NZB/W F1 mice, is a positive regulator for NF-kappaB activation in dendritic cells. Int. Immunol. 19, 935–942.

Yamazaki, M., Chiba, K., 2008. Genipin exhibits neurotrophic effects through a common signaling pathway in nitric oxide synthase-expressing cells. Eur. J. Pharmacol. 581, 255–261.

Yun, T.J., Bevan, M.J., 2003. Notch-regulated ankyrin-repeat protein inhibits Notch1 signaling: multiple Notch1 signaling pathways involved in T cell development. J. Immunol. 170, 5834–5841.

Zhang, B., Schmoyer, D., Kirov, S., Snoddy, J., 2004. GOTree Machine (GOTM): a web-based platform for interpreting sets of interesting genes using Gene Ontology hierarchies. BMC Bioinformatics 5, 16.

Please cite this article in press as: Li, C.-C., et al. Genipin inhibits lipopolysaccharide-induced acute systemic inflammation in mice as evidenced by nuclear factor-κB bioluminescent imaging-guided transcriptomic analysis. Food Chem. Toxicol. (2012), http://dx.doi.org/10.1016/j.fct.2012.05.054